

CHLORINE-36 PRODUCTION RATE  
CALIBRATION USING  
SHORELINES FROM PLEISTOCENE  
LAKE BONNEVILLE, UTAH

Shasta McGee Marrero

Submitted in partial fulfillment of a

Master of Science Degree in Hydrology

Department of Earth and Environmental Science

New Mexico Institute of Mining and Technology

May 2009

## **ABSTRACT**

Due to the increasing use of cosmogenic nuclides in the fields of geochronology and geomorphology, it is important to have a consistent set of methods for comparing and interpreting the results. The NSF-funded project, CRONUS-Earth (Cosmic-Ray prOduced NUclide Systematics on Earth), was designed to address these issues by unifying the cosmogenic user community by providing a common interpretation platform as well as recommendations for the best scaling schemes, sampling procedures, production rate parameters, and reporting methods for the community. As part of this project, the use of geological calibration sites will provide better individual production rates and intercomparisons between nuclides than those of previous studies.

The production rates for chlorine-36 are a large source of uncertainty in the calibration of chlorine-36 systematics. Production rates have been published by several research groups, with the most commonly cited rates from Phillips, Stone, and Swanson. However, there are significant discrepancies among these published rates, leading to age differences of greater than 20% in some cases. Most people in the cosmogenic community are aware of the existence of these differences; however, no quantitative analysis of the differences has been performed on a surface of known age in order to compare these rates. A quantitative study performed on

Pleistocene Lake Bonneville shorelines in two locations, Tabernacle Hill and Promontory Point, clearly illustrated the discrepancies between the production rates.

The results showed that the Phillips production rate matched both sites the best out of the published rates. The Stone rate was also a good fit at Tabernacle Hill, although it did not fit the independent age constraints at Promontory Point. However, the Swanson rate did not produce ages that were geologically reasonable at either site. Using the samples collected for this study, a new production rate was calculated. The results are  $67.1 \pm 2.3$  atoms  $^{36}\text{Cl}$  (gram Ca\* yr) $^{-1}$  for calcium,  $158 \pm 11$  atoms  $^{36}\text{Cl}$  (gram K\* yr) $^{-1}$  for potassium, and  $638 \pm 27$  neutrons (gram\*yr) $^{-1}$  for  $P_f(0)$ , a parameter for the thermal neutron absorption pathway. The value for the potassium production rate falls between the published rates of Phillips and Stone. The value for  $P_f(0)$  is very similar to the lowest of the previously published values, but this was expected based on the Promontory Point samples that constrained this pathway. These production rates are not intended to be used as new production rates for chlorine-36, but are only intended to look at the general trends of the production rates based on these new samples. These preliminary rates will be revised later as more samples representing a wider geographic distribution as well as varying lithologies are added to the calibration dataset in the continuation of this study.

## ACKNOWLEDGEMENTS

I would like to thank my advisor, Fred Phillips, for all his help and especially his patience. During this process, I have grown as both a writer and a scientist. I also appreciate the expertise, advice, and encouragement of my other committee members, Rob Bowman and Nelia Dunbar. John Stone (University of Washington) and Brian Borchers have helped me in various ways to understand the intricacies and mathematical details of cosmogenic nuclides. I would like to thank Marc Caffee (PRIME Lab) for the AMS analyses and the rearranging of schedules to make my samples work on time. Marek Zreda and Mark Kurz have been especially generous in letting me use their unpublished results. For funding, I would like to thank the NSF and the CRONUS-Earth project (EAR-0345949). I would like to thank Patrick Ostrye and Natalie Thomas-Earthman for keeping me from drowning under the endless labwork. Although I had no other cosmogenic students to talk to, many other E&ES students have let me talk through my problems and have offered valuable advice and most importantly, friendship and support. My grandparents, Bob and Barbara, and my parents, Jack and Ruth, have always supported me in whatever goals I have wanted to achieve and I appreciate all their loving encouragement. Thanks to my sister, Whitney, for listening to all the stories of

my obstacles and triumphs of grad school (and for being foolish enough to follow suit).

Finally, I would not have finished if it weren't for my husband, Nico, and my dog, Kasha.

Thank you both for hugs, smiles, and my sanity.

## TABLE OF CONTENTS

1	INTRODUCTION .....	1
1.1	CRONUS-Earth (Cosmic-Ray prOduced NUclide Systematics on Earth) .....	3
2	BACKGROUND .....	5
2.1	Cosmogenic Nuclide Concepts .....	5
2.1.1	Cosmic rays.....	5
2.1.2	Production of <i>In Situ</i> Terrestrial Cosmogenic Nuclides .....	7
2.1.3	Accumulation.....	21
2.1.4	Scaling, Shielding, and Other Correction Factors .....	22
2.1.5	Factors affecting nuclide accumulation in rock .....	36
2.1.6	Uncertainties .....	44
2.2	Production Rate Discrepancies.....	45
2.2.1	Possible Sources of Discrepancy .....	45
2.2.2	Production Rates in the Literature .....	48
3	METHODS .....	53
3.1	Cosmogenic Nuclide Calibration Site Requirements.....	53
3.2	Individual Sample Requirements .....	54
3.3	Lake Bonneville Chronology .....	55
3.3.1	Radiocarbon constraints on the Bonneville and Provo Shorelines .....	59
3.4	Promontory Point Site Description .....	66
3.5	Tabernacle Hill Site Description .....	72
3.6	Chemical Processing .....	78
3.7	Interpretation of the AMS results – CHLOE .....	80
3.8	Calculations of New Production Rates.....	82
3.9	Reduced Chi-Squared Calculation .....	83
3.10	Blank Correction.....	84
4	RESULTS .....	89
4.1	Discussion of Reproducibility .....	90
4.2	Tabernacle Hill Results .....	94
4.3	Promontory Point Results.....	98

5	DISCUSSION .....	101
5.1	Tabernacle Hill .....	101
5.1.1	Chlorine-36 Interlaboratory Comparison .....	101
5.1.2	Helium-3 Comparison .....	104
5.2	Promontory Point .....	105
5.3	Production rate comparison .....	107
5.3.1	Tabernacle Hill Production Rate Comparison .....	108
5.3.2	Promontory Point Production Rate Comparison .....	109
5.3.3	Insights from Other Nuclides .....	111
5.4	Preliminary Production Rates .....	113
5.4.1	Sensitivity Analysis for Preliminary Production Rates .....	117
5.4.2	Discussion .....	122
6	CONCLUSIONS .....	126
7	REFERENCES .....	130
8	APPENDIX 1: SAMPLE CHLORINE-36 INFORMATION .....	136
8.1	Promontory Point Data .....	136
8.2	Tabernacle Hill Data .....	139
9	APPENDIX 2: FIELD SAMPLE PHOTOS AND FIELD SKETCHES .....	143
9.1	Tabernacle Hill photos and field data .....	143
9.1.1	05TAB01 .....	143
9.1.2	05TAB02 .....	146
9.1.3	05TAB03 .....	146
9.1.4	05TAB04 .....	149
9.1.5	05TAB05 .....	152
9.1.6	05TAB06 .....	155
9.1.7	05TAB07 .....	157
9.2	Promontory Point Samples .....	159
9.2.1	05PPT01 .....	159
9.2.2	05PPT02 .....	161
9.2.3	05PPT03 .....	163

9.2.4	05PPT04.....	165
9.2.5	05PPT05.....	167
9.2.6	05PPT08.....	169
10	APPENDIX 3: CHLORINE-36 SAMPLE PREPARATION PROCEDURE .....	172
11	APPENDIX 4: OTHER NUCLIDE DATA.....	200
12	APPENDIX 5: BLANK INFORMATION .....	201

# List of Figures

Figure 1-Absolute production from each pathway for a basalt sample from Tabernacle Hill, UT. The graph on the left shows the production with depth on a linear scale, while the graph on the right shows the log of the production with depth. The production due to muons is less than 1 on the log graph so muon production is not visible. The production vs depth was calculated using CHLOE (PHILLIPS and PLUMMER, 1996). Chemistry information for these samples can be found in the appendix in section 8.2. Production pathways are: Ps –spallation, Pth – thermal neutrons, Peth – epithermal neutrons, Pm – muons, Ptotal – sum of all production pathways. .... 10

Figure 2 - (a) The sample on a horizontal surface is bombarded by cosmic rays (shown by arrows) from all directions. (b) When the sample is on a slope, only some of the cosmic rays reach the sample while others are blocked by the hill (self-shielding). In both cases, the larger arrow represents the vertical incident angle of the majority of the cosmic rays..... 24

Figure 3 - Illustration of the angle nomenclature for shielding calculations (GOSSE and PHILLIPS, 2001). Note that the geologic term “strike” is not equivalent to the direction of dip ( $\theta_n$ ) of the surface..... 25

Figure 4-(a) The incoming cosmic rays only penetrate a specific distance into the rock. When the angle of this rock changes (b), the apparent attenuation length also changes, causing the overall penetration depth perpendicular to the rock surface to decrease. The black lines perpendicular to the surface show the decrease in apparent attenuation length from case (a) to case (b). .... 27

Figure 5 - The effective attenuation length as a function of the slope of the dipping sample surface (GOSSE and PHILLIPS, 2001). The degree markings indicate the horizon angle, assumed to be uniform, of the topographic shielding. .... 27

Figure 6-Lal’s spatial scaling factor plotted against geomagnetic latitude. The numbered contour lines indicate elevation in km (figure from GOSSE and PHILLIPS, 2001; based on data in LAL, 1991). .... 30

Figure 7-The SINT-800 paleointensity record showing the last 800,000 years (GUYODO and VALET, 1999). The number of records for each interval is shown at top while the stacked data are shown on the bottom. The dashed line shows the minimum value below which geomagnetic excursions (short-lived periods of decreased magnetic field intensity) have been observed..... 32

Figure 8-(left) A map of Utah with a box showing where the more detailed study area map is located (MERRIAM-WEBSTER, 2001). (right) Map of the current Great Salt Lake showing Bonneville extent. Modified from Digital Geology of Idaho, Idaho State University (IDAHO STATE UNIVERSITY, 2006). The two sample locations are shown by red circles and arrows..... 56

Figure 9-Shoreline curve for Lake Bonneville (modified from OVIATT et al., 1992). The ages given here do not correspond to the ages provided in the table due to the use of carbon-14 ages here and the use of cal years in the table. This curve is designed to show the relative shoreline curve for the history of the lake. The labels represent the named shorelines and the major flood event. .... 57

Figure 10-Calendar year probability distributions for the radiocarbon ages used in the Bonneville flood age analysis (Balco, pers. comm., 2005). The numbers correspond to the radiocarbon dates in Table 5. The probability density functions were created using Calib 5.0 (STUIVER et al., 2005). The y-axis is probability and the x-axis is calendar age BP. Sample numbers 1-10 postdate the flood and sample numbers 11-19 predate the flood event. .... 63

Figure 11-Probability density for the maximum likelihood function for the Bonneville flood age (Borchers, personal communication, 2005). .... 63

Figure 12-Carbon-14 chronology for the Lake Bonneville shoreline using the 19 data points shown in Table 5. The Blue line connects the samples that are at the lake level. The ages correspond to the calendar year ages shown in Table 5. .... 64

Figure 13-Foreground shows the wavecut bench where samples were taken. Background shows other wavecut benches (Photo by Nishiizumi, 2005). .... 67

Figure 14-Promontory Point map showing the approximate outline of the remaining cliff (the base of which is shown in black on the far right), the approximate lake edge of the wavecut bench (shown in

blue on the far left), and the approximate transect along which samples were collected to make sure that the samples were not being influenced by inheritance or other factors dependent on position in relation to the cliffs. Samples plotted using Google Earth (GOOGLE, 2008).....	67
Figure 15-Promontory Point sample locations (yellow dots) shown on a geomorphic surface map (Mapping by F. M. Phillips, 2005).....	70
Figure 16-Photo showing Promontory Point sample positions relative to each other (Photo by Nishiizumi, 2005).....	70
Figure 17-Marc Caffee Sampling Promontory Point quartzite bedrock outcrop (Photo by F. M. Phillips, 2008). Note: person sampling is standing on wave-polished surface.....	71
Figure 18-Tabernacle Hill basalt flow (satellite image from Google Earth) (GOOGLE, 2008). The sample area is indicated by a box and details are shown in Figure 20. Coordinates shown across the top represent the approximate location of the top corners. ....	73
Figure 19-Geologic map of Tabernacle Hill basalt flow showing faults, basaltic tuffs (vt), basalt (vb), and lacustrine/eolian deposits (le), and scoriaceous cinders (vc) (OVIATT and NASH, 1989). The dashed line is the 1445 m contour line. ....	74
Figure 20-Locations of samples on the basalt flow. Other important features, such as tufa and the wave platform, are labeled. The area that looks stippled is the basalt while the surrounding, uniform terrain is the surrounding plains (Mapping by F. M. Phillips, 2005). ....	74
Figure 21-Tufa encrustation on Tabernacle Hill basalt flow (Photo by F. M. Phillips, 2005). ....	77
Figure 22-(left) Tabernacle Hill basalt tumulus and (right) using a rock saw to collect a sample. ....	78
Figure 23-Reproducibility of TAB and PPT samples using the Phillips production rate. A 1:1 line is plotted for reference. ....	91
Figure 24-Varying age with different erosion rates for the best reproducible samples for Tabernacle Hill. 96	
Figure 25-Tabernacle Hill sample results using the Phillips production rate (PHILLIPS et al., 2001) and 0.9mm/kyr erosion rate. Trial one and trial two are the duplicates of the same set of samples. The upper bound (Bonneville flood age of 17.4 cal ka ) and lower bound (carbon-14 date on tufa at 16.6 cal ka ) are also shown for comparison with the results. Duplicate samples of 05TAB04 plot on top of each other. Y-axis error bars represent the 1 sigma errors calculated from the original PRIME Lab reported errors. The reproducible samples are 05TAB01 through 05TAB04 and 05TAB07. ....	97
Figure 26-Varying age due to different erosion rates for the best reproducible samples from Promontory Point. These results are calculated using the Phillips production rate. ....	99
Figure 27 - Promontory Point data calculated using the Phillips production rate (PHILLIPS et al., 2001)and with an erosion rate of 0.56 mm/kyr. Trial one and trial two are the duplicates of the same set of samples. The upper (carbon-14 date of 18.9 cal ka ) and lower (Bonneville flood age of 17.4 cal ka ) carbon-14 bounds are also shown for comparison with the results. Duplicate samples of 05PPT04 and 05PPT08 plot on top of each other. Y-axis error bars represent the 1 sigma errors calculated from the original PRIME Lab-reported errors. The reproducible samples are all samples except 05PPT03. ....	100
Figure 28-Comparison of chlorine-36 Tabernacle Hill results from Zreda (personal communication, 2006) and Phillips/Marrero. The Phillips/Marrero results assume an erosion rate of 0.9mm/kyr. Y-direction error bars represent the 1-sigma errors calculated from the original PRIME Lab-reported errors. All ages calculated using the Phillips production rates. ....	102
Figure 29-Tabernacle Hill data from our laboratory (chlorine-36, trial 1 &2) compared to Helium-3 results from the Isotope Geochemistry Facility at WHOI, under the supervision of Mark Kurz (personal communication, 2006). Y-direction error bars on the chlorine-36 samples represent the 1 sigma errors calculated from the original PRIME Lab reported errors. Kurz' ages and error bars are shown as he reported them. ....	104
Figure 30-Promontory Point results showing both the chlorine-36 analysis performed in our laboratory and the beryllium-10 results from three different laboratories reported anonymously to CRONUS-Earth. The ages for the Be-10 data were calculated using the Be-10 web calculator (BALCO, 2007). The scaling scheme for the Be-10 is Lal/Stone (time-dependent)(LAL, 1991; STONE, 2000), while the scaling scheme for the <sup>36</sup> Cl data is Lal (LAL, 1991). Y-direction error bars on the chlorine-36 data	

represent the 1 sigma errors calculated from the AMS-reported errors. Upper and lower bounds refer to carbon-14 bounding ages. ....	106
Figure 31-TAB results comparing production rates of Phillips (PHILLIPS et al., 2001), Stone (EVANS et al., 1997), and Swanson (SWANSON and CAFFEE, 2001) at 0.9mm/kyr erosion. The graph shows only the first four samples because these are the reproducible samples with the best results. Y-direction error bars represent the 1 sigma errors from the AMS measurement. ....	108
Figure 32-Ages calculated using all three production rates (Phillips, Stone, and Swanson) for Promontory Point samples. Only the best samples, 05PPT01, 05PPT02, 05PPT04, and 05PPT05, were used in this calculation. These ages are calculated for zero erosion. ....	109
Figure 33-Comparison of all the production rates for Chlorine-36 with the Helium-3 data for Tabernacle Hill reproducible samples close to the C-14 bounds. 0.9 mm/kyr erosion rate. ....	111
Figure 34-Comparison of results from Be-10 and Chlorine-36 production rates for Promontory Point samples. These results are calculated for zero erosion. ....	112
Figure 35-Tabernacle Hill results using the new production rates. ....	116
Figure 36-Promontory Point ages calculated using the new production rates. ....	116
Figure 37- $P_i(0)$ production rate sensitivity study looking at PPT erosion rate, TAB erosion rate, and TAB exposure age. ....	118
Figure 38- Potassium production rate sensitivity study looking at PPT erosion rate, TAB erosion rate, and TAB exposure age. ....	118
Figure 39-Calcium production rate sensitivity study looking at PPT erosion rate, TAB erosion rate, and TAB exposure age. ....	119
Figure 40-Depth profiles for sample 05PPT08 for varying erosion rates. ....	121
Figure 41-Depth profiles for sample 05TAB03 for varying erosion rates. ....	121
Figure 42-Official CRONUS field note sketch. ....	143
Figure 43- Same sketch for samples 05TAB01 & 05TAB02 (Kurz, personal communication, 2005). ....	144
Figure 44-05TAB01 prior to sample collection. ....	144
Figure 45-05TAB01 prior to sample collection. ....	145
Figure 46-The horizon for 05TAB01. ....	145
Figure 47-Sample 05TAB01 after sample collection. ....	145
Figure 48-Sample 05TAB02 after collection. ....	146
Figure 49-Sketch of 05TAB03 (Kurz, personal communication, 2005). ....	146
Figure 50-Location of sample 05TAB03 at top of basalt tumulus. ....	147
Figure 51-Collection of sample 05TAB03. ....	147
Figure 52-Sample location for 05TAB03. ....	148
Figure 53-Horizon view for 05TAB03. ....	148
Figure 54-The sample location and sample 05TAB03 after collection. ....	148
Figure 55-Sample 05TAB03 after sample collection. ....	149
Figure 56-Official CRONUS field notes. ....	149
Figure 57-Sample sketch of 05TAB04 (Kurz, personal communication, 2005). ....	150
Figure 58-Sample location for 05TAB04. ....	150
Figure 59-Sample location for sample 05TAB04. ....	151
Figure 60-Sample 05TAB04 after collection. ....	151
Figure 61-Sample 05TAB04 after collection. ....	152
Figure 62-Sample sketch for 05TAB05 (Kurz, personal communication, 2005). ....	152
Figure 63-Sample location for 05TAB05 at the top of the tumulus. ....	153
Figure 64-05TAB05 prior to sample collection. ....	153
Figure 65-05TAB05 prior to sample collection. ....	154
Figure 66-Horizon for sample 05TAB05. ....	154
Figure 67-Sample 05TAB05 after cutting but prior to collection. ....	154
Figure 68-The sample location and sample 05TAB05 after collection. ....	155
Figure 69-Sketch for both 05TAB06 & 05TAB07 (Kurz, personal communication, 2005). ....	155
Figure 70-Sample location for 05TAB06. ....	156
Figure 71-Sample location for 05TAB06. ....	156

Figure 72-Sample location for 05TAB06. ....	157
Figure 73-Horizon for samples 05TAB06 & 05TAB07. ....	157
Figure 74-Sample location for 05TAB06 after sample collection. ....	157
Figure 75-Left side is the 05TAB06 while the right side is 05TAB07. ....	158
Figure 76-Sample location for 05TAB07. ....	158
Figure 77-Chipped out sample (in place) for 05TAB07. ....	159
Figure 78-Official CRONUS field sketch. ....	159
Figure 79-05PPT01 before sampling. ....	160
Figure 80-05PPT01 in profile before sampling. ....	160
Figure 81-05PPT01 after sampling. ....	161
Figure 82-Official CRONUS field sketch. ....	161
Figure 83-05PPT02 before sampling. ....	162
Figure 84-05PPT02 after sampling. ....	162
Figure 85-Official CRONUS field sketch. ....	163
Figure 86-05PPT03 before sampling. ....	163
Figure 87-05PPT03 before sampling. Note blocky appearance of outcrop. ....	164
Figure 88-05PPT03 after sampling. ....	164
Figure 89-CRONUS field notes. ....	165
Figure 90-05PPT04 before sampling. ....	165
Figure 91-05PPT04 before sampling in profile. ....	166
Figure 92-Panorama around 05PPT04. ....	166
Figure 93-05PPT04 after sampling. ....	166
Figure 94-Sketch of samples 05PPT05 and 05PPT06 (not used in this study) (Kurz, personal communication, 2005). ....	167
Figure 95-05PPT05 before sampling. ....	168
Figure 96-05PPT05 before sampling. Note profile of outcrop. ....	168
Figure 97-05PPT05 after sampling. 05PPT05 and 05PPT06 were taken at the same location. 05PPT05 is the center piece while 05PPT06 was taken from an edge to examine edge effects. ....	169
Figure 98-Official CRONUS field sketch. ....	169
Figure 99-05PPT08 before sampling. ....	170
Figure 100-05PPT08 in profile before sampling. ....	170
Figure 101-05PPT08 panorama from sample. ....	171
Figure 102-05PPT08 after sampling. ....	171

# LIST OF TABLES

Table 1-Major reactions producing Chlorine-36, modified from Gosse and Phillips (2001) and Fabryka-Martin (1988). Percentage ranges for contribution of each reaction type to production of chlorine-36 within the top 100 g/cm <sup>2</sup> of common terrestrial rocks (such as granites and carbonates) at sea level and high geomagnetic latitudes (modified from ZREDA, 1994).....	9
Table 2 - Scaling scheme summary describing the differences in input parameters and time-dependence (modified from BALCO, 2007).....	34
Table 3-Elemental properties used in calculation of rock properties. $A_i$ –atomic weight of element in gram/mole, $\xi_i$ –average log decrement of energy per neutron collision with element $i$ , $\sigma_{sc,i}$ – neutron scattering cross-section of element $i$ , $\sigma_{th,i}$ – thermal neutron absorption cross-section of element $i$ , $I_{a,i}$ – dilute resonance integral for element $i$ , $S_i$ – mass stopping power of element $i$ for alpha particle of a given energy, $Yn, iU$ – neutron yield of element $i$ per ppm U in radioequilibrium, $Yn, iTh$ – neutron yield of element $i$ per ppm Th in radioequilibrium, $K_m$ – conversion from ppm to atom/gram. ....	40
Table 4-Production rates from various research groups for chlorine-36 (EVANS et al., 1997; PHILLIPS et al., 2001; STONE et al., 1996; STONE et al., 1998; SWANSON and CAFFEE, 2001). The values for Ca and K include are spallation values only. Units for production rates are Ca: [atoms <sup>36</sup> Cl (g Ca) <sup>-1</sup> yr <sup>-1</sup> ], K: [atoms <sup>36</sup> Cl (g K) <sup>-1</sup> yr <sup>-1</sup> ], secondary neutron production ( $P_f(0)$ ): [neutron <sup>36</sup> Cl (g air) <sup>-1</sup> yr <sup>-1</sup> ]. *These values originally reported as total production values for muon and spallation production. Original values for total production from Ca: 91±5, K: 228±18.....	50
Table 5-Radiocarbon information for ages used in Bonneville flood calculations (modified from OVIATT and MILLER, 2005). ....	62
Table 6-Production rate parameters varied in CHLOE for each production rate scheme. The research group references are as follows: Phillips (PHILLIPS et al., 2001), Stone (EVANS, 2001; EVANS et al., 1997; STONE et al., 1996; STONE et al., 1998), and Swanson (SWANSON and CAFFEE, 2001). ....	81
Table 7-Results table showing all results from (a) Tabernacle Hill and (b) Promontory Point. The chloride concentration (ppm), the R/S ratio ( <sup>36</sup> Cl/tot Cl x 10 <sup>-15</sup> ), and the atoms of <sup>36</sup> Cl in the sample all refer to the values for the rock and not the spiked sample. The unit of ppm is used in lieu of mg/kg due to its use as the conventional unit in cosmogenic nuclide research. ....	90
Table 8-Calculated age for Tabernacle Hill using Phillips chlorine-36 production rates with varying erosion. The reproducible samples are 05TAB01-04, and 05TAB07. The best samples, those reproducible samples closest to the C-14 bounds, are 05TAB01-04 only. ....	97
Table 9-Weighted mean ages for Promontory Point samples calculated using the Phillips production rates and varying erosion rates. The reproducible samples are all those except 05PPT03. The best samples, those closest to the carbon-14 bounds, are all the samples except 05PPT03 and 05PPT08. ....	100
Table 10-Weighted mean ages using Phillips, Stone, and Swanson chlorine-36 production rates for the Tabernacle Hill samples. Only samples 05TAB01-04 have been used in these calculations for reasons discussed previously. This is calculated for different erosion rates. The most reasonable erosion rate is 0.9 mm/kyr. The carbon-14 bounds are 16.6 ka – 17.4 ka. Reduced chi-squared values are shown in parentheses next to the age. ....	109
Table 11-Comparison of production rates at Promontory Point using only samples 05PPT01-02 and 05PPT04-05. These ages are shown for varying erosion rates. The carbon-14 bounds are 17.4 ka for the lower bound and 18.9 ka for the upper bound. ....	110
Table 12-Production rates for chlorine-36 pathways listed by research group. Swanson rates have been adjusted to show only spallation pathways in order to be comparable to the other rates. ....	110
Table 13-Preliminary production rates calculated from the reproducible samples in the Tabernacle Hill and Promontory Point datasets. These are preliminary numbers only and are not intended to be used in lieu of published rates at this point in time. The rates highlighted in dark blue are lower than the rates calculated here, while rates highlighted in light pink are higher than those calculated here. ....	115

Table 14-Reduced chi-squared for each of the production rate sets, including the new production rate calculated in this study. The number in parentheses next to the site name is the preferred erosion rate at that site in mm/kyr.....	116
Table 15-Chemical data for Chlorine-36 Promontory Point samples. ....	136
Table 16-Position and other data for Promontory Point samples. ....	137
Table 17-Promontory Point sample information – trial 1. ....	138
Table 18- Promontory Point sample information – trial 2. ....	138
Table 19-Chemical data for Cl-36 Tabernacle Hill samples. ....	139
Table 20-Position and other data for Tabernacle Hill. ....	141
Table 21- Tabernacle Hill sample information – trial 1. ....	141
Table 22- Tabernacle Hill sample information – trial 2. ....	142
Table 23- Original data from other laboratories for chlorine-36, helium-3, and beryllium-10. All results are shown in ka. The Phillips/Marrero data (no erosion) is shown for comparison. The Helium-3 analysis was performed at the Isotope Geochemistry Facility, under the supervision of Mark Kurz, at Woods Hole Oceanographic Institute. The Be-10 data is from the anonymous intercalibration study by CRONUS. The CRONUS Web calculator (BALCO, 2007) was used to calculate the results of the Be-10 data and the Lal (not time dependent) scaling was reported along with the external uncertainty. Be Lab 3 was not used in any analysis because the results were anomalous and probably due to incorrect calculation of age by the laboratory. ....	200
Table 24-Blank data for blanks run with the CRONUS samples. The R/S ratio is the Cl-36/total chloride ( $\times 10^{-15}$ ) and the S/S ratio is the Cl-35/Cl-37 ratio. Both the R/S and S/S are from the PRIME Lab. The blanks are labeled with the month and year they were started (BS0805 was the Blank Sample from August of 2005). ....	201
Table 25-Composition of Week's Island Halite solution from the analysis done by Thomas (2005). All values shown are in ppm. ....	201

# 1 INTRODUCTION

Cosmogenic nuclides are commonly used to date the exposure age of erosional or aggradational features. As a geomorphic tool, cosmogenic exposure dating is a beneficial technique and is quite different when compared to techniques that can only date the formation age of the rock (such as U-Th/He) or other techniques that only indirectly date the feature (such as radiocarbon). This unique capability allows the technique to be applied in the fields of geochronology and geomorphology.

As a rock at the earth's surface is exposed to cosmic rays, a number of different types of reactions take place. Some of these reactions produce byproducts of specific nuclides called cosmogenic nuclides. These particular nuclides become useful in scientific applications when the naturally occurring concentrations of the nuclide within the rocks are very low, allowing measurements of the cosmogenically formed nuclides. Longer periods of exposure lead to greater amounts of nuclide accumulation within a sample. The accumulated concentration of the nuclide can be measured and, using the production rate, an exposure age calculated. The details of the theory and calculations are shown explicitly in the background section, chapter 0.

Chlorine-36 is a particularly useful cosmogenic nuclide because it can be applied to almost any lithology, which is not possible with other cosmogenic isotopes. Compared

to other cosmogenic nuclide techniques, the sample processing is also relatively simple. For these reasons, among others, chlorine-36 has become widely used. While the theory and calculations are similar for all cosmogenically-produced nuclides, this study focused primarily on chlorine-36.

Along with the increase in cosmogenic nuclide applications has come the need for increased accuracy of the technique. The current 10-15% accuracy in cosmogenic ages (PHILLIPS et al., 1997) is no longer sufficient to answer many of the scientific questions now being posed. In order to increase accuracy, specifically for chlorine-36, the fundamentals of cosmogenic nuclides must be agreed upon by researchers working in the field. In this case, there is a clearly identified discrepancy among the published production rates for chlorine-36. Three different research groups have proposed three different sets of production rates. I identify these groups as follows: Phillips (PHILLIPS et al., 2001), Stone (EVANS, 2001; EVANS et al., 1997; STONE et al., 1996; STONE et al., 1998), and Swanson (SWANSON and CAFFEE, 2001). Each research group has proposed a set of chlorine-36 production rates based on their own geologic calibration at a site or sites of independently-dated age. However, these three rate sets are not in agreement with one another. Although the problem is recognized throughout the community, nobody has been able to identify the exact cause(s) of the discrepancies. In fact, these three production rates have never been quantitatively compared on a single surface of known age.

The purpose of this research was to attempt to quantify the differences among the published production rates and propose possible methods for discovering the reasons for the differences. This project has evaluated the accuracy of the current chlorine-36

production rate parameters by examining two sites of known age. By measuring the amount of chlorine-36 in the samples and then using the various production rates to calculate the age, the discrepancies among the production rates were clearly identified. Some of the main discrepancies may lie in the laboratory method, the scaling scheme, or the assumptions made by the research groups. Using the results from two specific sites at the well-dated Lake Bonneville geological calibration site, the listed possible reasons for the discrepancies, as well as other possibilities, were qualitatively assessed. The results for other cosmogenic nuclides analyzed from the same samples were used to further compare the chlorine-36 production rates.

Another way to examine the validity of the published rates was to calculate a new set of production rate parameters using the new data from the independently dated site. The results were quantitatively compared to the published rates to gain even more insight into the differences among them. Although new preliminary production rates were calculated, these are not intended to be used in lieu of the other published production rates. This project was only the initial step in the process of developing a more accurate set of chlorine-36 production rate parameters.

### **1.1 *CRONUS-Earth (Cosmic-Ray prOduced NUclide Systematics on Earth)***

The CRONUS-Earth project is a National Science Foundation (NSF)-funded cooperative venture with over 13 collaborating universities, labs, and investigators in the United States and abroad. The objective of the project is to provide the cosmogenic community with all the tools needed to use cosmogenic nuclides in the sciences at a high level of accuracy and precision in all of the commonly used nuclide systems. This effort involves several concurrent investigations into the production rates of each nuclide via

geologic calibrations, scaling systems, geomagnetic field variations, and cosmic-ray fluxes. There is a sister project called CRONUS-EU, the European Union's independent project, which is working in tandem with CRONUS-Earth to contribute to the overall CRONUS project goals.

## 2 BACKGROUND

### 2.1 *Cosmogenic Nuclide Concepts*

Cosmogenic nuclides are being applied to an increasing number of topics in the geosciences, with even more opportunities available as the accuracy of the technique grows. Several nuclides are commonly used, including aluminum-26 ( $^{26}\text{Al}$ ), beryllium-10 ( $^{10}\text{Be}$ ), carbon-14 ( $^{14}\text{C}$ ), chlorine-36 ( $^{36}\text{Cl}$ ), and helium-3 ( $^3\text{He}$ ). The theory describing the production of cosmogenic nuclides is similar for all the nuclides, however, this study dealt mainly with chlorine-36, so special attention was given to that nuclide. The next section presents a thorough background, beginning with initial production and including factors that may affect accumulation within samples.

#### 2.1.1 **Cosmic rays**

Galactic cosmic radiation (GCR) initially consists of 90% protons, 8% helium nuclei, and some electrons and heavier nuclei. GCR originates mainly from within the Milky Way galaxy although other sources include the sun and energetic phenomena outside our galaxy (GAISSER, 1990; GOSSE and PHILLIPS, 2001; LIFTON et al., 2005). Incoming particles interact with the magnetic field of the earth as they approach the planet. The strength and orientation of the earth's magnetic field can affect the intensity

of the cosmic-ray flux that reaches the earth's surface (PIGATI and LIFTON, 2004; ZREDA, 1994). Not all particles approaching the planet have sufficient momentum or an approach trajectory appropriate to penetrate the magnetic field and thus reach the atmosphere.

Whether a particle is allowed access or not depends on its rigidity and its incidence angle (PIGATI and LIFTON, 2004). A particle's rigidity ( $\mathfrak{R}$ ) is defined as the product of the radius of curvature ( $R$ ) due to the deflection of a charged particle through a magnetic field (GOSSE and PHILLIPS, 2001). This can also be formulated as:

**Equation 1 (GOSSE and PHILLIPS, 2001; O'BRIEN, 1979)**

$$\mathfrak{R} = BR = pc/q$$

Where:  $p$  – momentum,  $c$  – speed of light,  $B$  – magnitude of intensity of the magnetic field, and  $q$  – particle charge

For any particular location and incidence angle, an incoming particle must exceed a minimum threshold value of rigidity, called the cutoff rigidity, in order to finally penetrate the magnetic field and interact with the earth's atmosphere (PIGATI and LIFTON, 2004). In cosmogenic calculations, vertical cutoff rigidity, or the rigidity that is determined by particle path tracing of vertically incident anti-protons, is typically used (GOSSE and PHILLIPS, 2001; PIGATI and LIFTON, 2004). The earth has a dipole geomagnetic field which means that the highest values of the cutoff rigidity are at the magnetic equator where the magnetic field lines are parallel to the earth's surface. At higher latitudes, the magnetic field lines become almost perpendicular to the earth's surface, requiring a lower rigidity to penetrate the magnetic field. The cutoff rigidity decreases towards the poles due to the changing interaction with the magnetic field until the cutoff rigidity finally falls to a level below the lowest rigidity present in the incoming cosmic rays at latitudes greater than  $58^\circ$ , thereby allowing all cosmic rays to reach the top

of the atmosphere near the poles (GOSSE and PHILLIPS, 2001; PIGATI and LIFTON, 2004). The latitude at which this effect occurs decreases at higher elevations (ZREDA, 1994). In general, a stronger magnetic field will result in fewer cosmic rays reaching the earth and therefore lower production rates.

When the cosmic-ray particles reach the top of the atmosphere, the primary GCR particles are involved in numerous inelastic interactions with atmospheric nuclei that produce a shower of secondary cosmic-ray particles. Secondary particles may be very energetic, in some cases almost indistinguishable from the energetic primary particles. Primary and secondary particles continue to interact with the nuclei of atmospheric gas atoms as they progress through the atmosphere, and as they do so the composition of the main component of the flux evolves from principally protons to principally neutrons. This series of events produces cosmogenic nuclides in the atmosphere. Although cosmogenic nuclides are produced in the atmosphere, this project focuses on terrestrially produced cosmogenic nuclides, i.e. those produced within rocks on the earth's surface, the production of which will be detailed below.

### **2.1.2 Production of *In Situ* Terrestrial Cosmogenic Nuclides**

Once they reach the earth's surface, cosmic rays interact with atomic nuclei in rocks to form *in situ* terrestrial cosmogenic nuclides. The study of the accumulation of these nuclides within rocks can provide valuable information in many fields of science. In this particular study, the interactions will be described in detail for the reactions producing chlorine-36.

A generalized equation that describes the production of a specific nuclide at a specific location in a sample of defined thickness is shown below in Equation 2 (GOSSE and PHILLIPS, 2001).

**Equation 2**

$$P_{t,m} = S_{el}S_T(Q_sP_{s,m} + S_{L,th}Q_{th}P_{th,m} + S_{L,eth}Q_{eth}P_{eth,m}) + S_{\mu}S_{T,\mu}Q_{\mu}P_{\mu,m}$$

Where:

- $P_{x,m}$  – Production rate of nuclide, m, for the reaction, x;
- X - Reaction type corresponding to the following types: total (t), fast/spallation (s), thermal/absorption (th), epithermal/absorption (eth), and muon ( $\mu$ ) [atoms  $^{36}\text{Cl}$ / g sample/ year]
- $S_{el}$  – Scaling factor for elevation and latitude for the nucleonic component [unitless]
- $S_{\mu}$  – Scaling factor for elevation and latitude for the muonic component [unitless]
- $S_T$  – Scaling factor for shielding from nucleonic component of cosmic radiation (topography and rock geometry) [unitless]
- $S_{T,\mu}$  – Scaling factor for shielding from muonic component of cosmic radiation [unitless]
- $S_{L,x}$  – Net diffusion of neutrons for different reactions [unitless]
- $Q_x$  – Accounts for integration of production over the sample thickness [unitless]

The production rate equation above includes the production rates for reactions from spallation (s), thermal neutrons (th), epithermal neutrons (eth), as well as those formed through muonic pathways ( $\mu$ ). All the major production pathways for chlorine-36 are summarized below in Table 1. Other minor reactions are discussed in section 2.1.2.5. Spallation reactions are the result of fast neutrons (> 10 MeV) interacting with elemental nuclei. The spallation reactions that produce chlorine-36 occur when fast neutrons interact with several specific nuclei, primarily the nuclei of either calcium-40 or potassium-39 (GOSSE and PHILLIPS, 2001). Technically, the reaction of a neutron with potassium-39 is slightly below the spallation energy range; however, the reaction is still significantly above the epithermal energy range and is therefore conventionally termed “spallation” despite the energy difference. Thermal neutrons produce chlorine-36

through the absorption of a thermal neutron ( $< 0.5$  eV) by a chlorine-35 nucleus (GOSSE and PHILLIPS, 2001). Epithermal neutrons, those with energies between 0.5 eV and  $\sim 0.1$  MeV, move in a diffusive manner, similar to thermal neutrons and also produce chlorine-36 through absorption by a chlorine-35 nucleus. Finally, muons interact with potassium and calcium nuclei through negative muon capture to form chlorine-36 (GOSSE and PHILLIPS, 2001). The relative contributions from each pathway can be seen in Figure 1.

**Table 1-Major reactions producing Chlorine-36, modified from Gosse and Phillips (2001) and Fabryka-Martin (1988). Percentage ranges for contribution of each reaction type to production of chlorine-36 within the top 100 g/cm<sup>2</sup> of common terrestrial rocks (such as granites and carbonates) at sea level and high geomagnetic latitudes (modified from ZREDA, 1994).**

<b>Reaction</b>	<b>Type</b>	<b>% of total <sup>36</sup>Cl production</b>
$^{40}\text{Ca}(n,2n,3p)^{36}\text{Cl}$	Spallation	16-80
$^{39}\text{K}(n,\alpha)^{36}\text{Cl}$	Spallation	16-80
$^{35}\text{Cl}(n,\gamma)^{36}\text{Cl}$	Thermal neutron absorption	11-80
$^{39}\text{K}(\mu^-, p2n)^{36}\text{Cl}$	Negative muon capture	0-10
$^{40}\text{Ca}(\mu^-, \alpha)^{36}\text{Cl}$	Negative muon capture	0-10

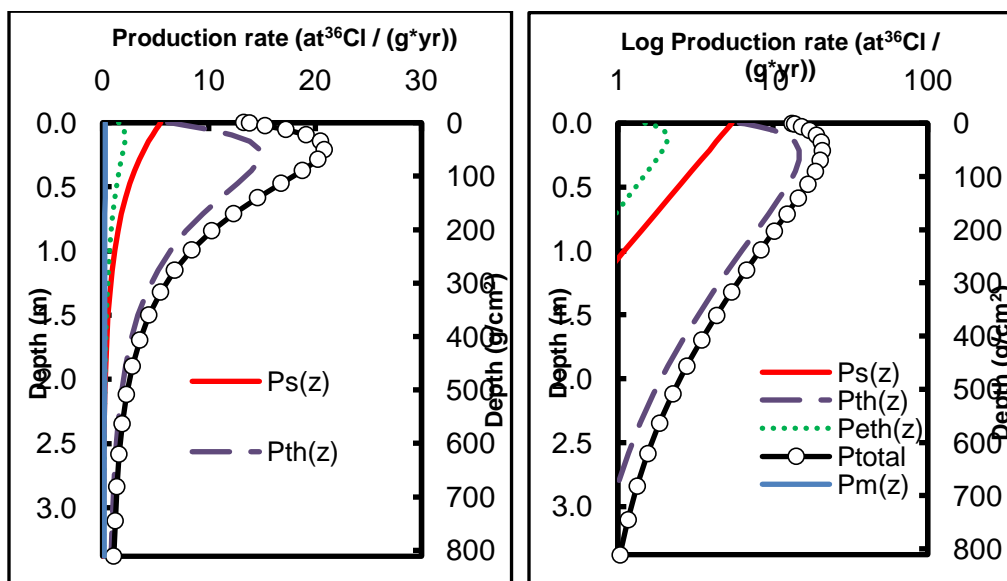


Figure 1-Absolute production from each pathway for a basalt sample from Tabernacle Hill, UT. The graph on the left shows the production with depth on a linear scale, while the graph on the right shows the log of the production with depth. The production due to muons is less than 1 on the log graph so muon production is not visible. The production vs depth was calculated using CHLOE (PHILLIPS and PLUMMER, 1996). Chemistry information for these samples can be found in the appendix in section 8.2. Production pathways are: Ps –spallation, Pth – thermal neutrons, Peth – epithermal neutrons, Pm – muons, Ptotal – sum of all production pathways.

### 2.1.2.1 Fast Neutron/Spallation

Incoming high energy nucleons participate in spallation reactions, which occur when a neutron (or other nucleon) hits a target nucleus (such as potassium-40) and impacts with sufficient energy to break nuclear bonds and fragment the nucleus into a lighter element (e.g. chlorine-36) and other lighter particles released during the reaction (such as alpha particles). The rate of spallation reactions with depth is only dependent on the density of the particles in the target medium through which the cosmic rays must pass. The density is measured in units of mass length,  $Z$ , ( $\text{g}/\text{cm}^2$ ) as shown in Equation 3 (GOSSE and PHILLIPS, 2001):

**Equation 3**

$$Z(z) = \int_0^z \rho(z) dz$$

Where:  $z$  - ordinary linear distance [cm],  $\rho$  – density [ $\text{g}/\text{cm}^3$ ]

The rate of interception of fast nucleons will be proportional to the flux of particles passing through a medium as described by Equation 4 (GOSSE and PHILLIPS, 2001):

**Equation 4**

$$\frac{dF}{dZ} = -\frac{F}{\Lambda_{f,p}}$$

Where:  $F$  - cosmic-ray flux intensity [particles /( $\text{cm}^2\text{s}$ )]

$\Lambda_{f,p}$  - particle attenuation length [ $\text{g}/\text{cm}^2$ ]

The particle attenuation length is the passage length through the medium required to attenuate the original intensity by a factor of  $e^{-1}$  (GOSSE and PHILLIPS, 2001). When Equation 4 is solved using a known reference point ( $F = F_{\text{ref}}$  at some point), it becomes (GOSSE and PHILLIPS, 2001):

**Equation 5**

$$F = F_{\text{ref}} \exp\left(-\frac{Z}{\Lambda_{f,p}}\right)$$

In order to use this equation, the cosmic-ray flux must be integrated over the entire sky, which yields (GOSSE and PHILLIPS, 2001):

**Equation 6**

$$\Phi_f(Z) = \Phi_f(0) \exp\left(-\frac{Z}{\Lambda_f}\right)$$

With  $\Phi_f(Z)$  - integrated annual cosmic-ray flux for entire sky as a function of mass depth [particles/ ( $\text{cm}^2 * \text{yr}$ )]

$\Phi_f(0)$  - integrated cosmic-ray flux at land surface [particles/ ( $\text{cm}^2 * \text{yr}$ )]

$\Lambda_f$  - apparent attenuation length for energetic cosmic-ray particles [ $\text{g}/\text{cm}^2$ ]

The apparent attenuation length,  $\Lambda_f$ , is calculated from the flux-weighted integral (over the exposure angles) of the average particle attenuation length,  $\Lambda_{f,p}$ , and this relationship is expressed by Equation 7 (GOSSE and PHILLIPS, 2001):

**Equation 7**

$$\Lambda_f = \frac{\int_0^{\pi/2} z_p(\phi) \cos^{2.3} \phi \sin \phi d\phi}{\int_0^{\pi/2} \cos^{2.3} \phi \sin \phi d\phi} = \frac{3.3}{4.3} \Lambda_{f,p}$$

With  $z_p$  - vertical penetration depth =  $\Lambda_{f,p} \cos \phi$

$\phi$  - angle of incidence (degrees)

The values for the apparent attenuation length,  $\Lambda_f$ , for fast nucleonic particles range from 121 to  $>170 \text{ g}/\text{cm}^2$  (DUNAI, 2000). For materials of known densities, the apparent attenuation length can be translated to actual depth. Common examples of typical attenuation lengths translated to linear distance include granite (61.5 cm) and water (160 cm) (GOSSE and PHILLIPS, 2001). The apparent attenuation length is an important parameter because it quantifies the depth to which the nucleonic component can penetrate and cause production within a sample.

The production rate of a cosmogenic nuclide due to spallation of the target element is proportional to three things: 1) the cosmic-ray flux, 2) the cross section of the target element for the production of the nuclide, and 3) the abundance of the target element in the matrix (GOSSE and PHILLIPS, 2001). Based on this, the following equation summarizes the production, as a function of depth, of a cosmogenic nuclide due to spallation reactions (GOSSE and PHILLIPS, 2001):

**Equation 8**

$$P_{s,m}(Z) = \psi_{m,k}(0)C_k \exp\left(-\frac{Z}{\Lambda_f}\right)$$

Where:  $\psi_{m,k}(0)$  - production rate of nuclide m by spallation of element k, per unit mass of target element k, at land surface, sea level, and high latitude [atoms / (g target \* year)]

$C_k$  - concentration of element k [g of k/(g material)]

**2.1.2.2 Epithermal Neutrons**

Epithermal neutrons contribute to the production of *in-situ* cosmogenic nuclides through absorption reactions. Because these particles have low energies (0.5 eV to around 1 MeV), they are assumed to be moving in a Brownian fashion and so they behave in a diffusive or quasi-diffusive manner (GOSSE and PHILLIPS, 2001). The particles originate from secondary neutrons and some primary cosmic rays that have lost energy due to other reactions. The fate of epithermal neutrons is either absorption by a nucleus or transferral to the thermal energy range due to loss of energy through elastic collisions (GOSSE and PHILLIPS, 2001). The epithermal neutron absorption is governed by different mechanisms than the spallation reactions and is given by (GOSSE and PHILLIPS, 2001):

**Equation 9**

$$P_{eth,m,ss} = f_{eth,m,ss} \Gamma_{eth,m,ss} = \frac{f_{eth,m,ss}}{\Lambda_{eth,ss}} \Phi_{eth,ss}$$

Where:

**Equation 10**

$$f_{eth,m,ss} = \frac{N_{k,ss} I_{a,k}}{I_{eff,ss}}$$

$f_{eth,m,ss}$  - fraction of total epithermal neutrons absorbed that are used

by the target element to produce nuclide m [unitless]

$N_{k,ss}$  - atomic concentration of element k in subsurface [at/g]

$I_{a,k}$  - dilute resonance integral for absorption of epithermal neutrons by element k [barns]

$I_{eff,ss}$  – effective/macroscopic resonance integral for absorption of epithermal neutrons in subsurface [ $\text{cm}^{-2}\text{g}^{-1}$ ]

$\Gamma_{eth,m,ss}$  - total rate of epithermal neutron absorption in subsurface [ $\text{n}/(\text{g yr})$ ]

$\Lambda_{eth,ss}$  - effective epithermal neutron attenuation length in subsurface [ $\text{g}/\text{cm}^2$ ]

$\Phi_{eth,ss}$  - epithermal neutron flux in subsurface [ $\text{n}/(\text{cm}^2 \text{ yr})$ ]

The epithermal neutron flux,  $\Phi_{eth,ss}$ , can be described using a diffusion equation that accounts for both the creation of the epithermal neutrons from the high energy source flux as well as the loss to the thermal energy range or loss by absorption (GOSSE and PHILLIPS, 2001). The epithermal neutron flux is assumed to be in temporal equilibrium with the high-energy cosmic-ray flux from which it is derived (GOSSE and PHILLIPS, 2001). The equation must describe the diffusion of epithermal neutrons at the air/rock interface due to the complex interactions at this boundary (PHILLIPS et al., 2001). When all the appropriate interface equations are solved with appropriate boundary conditions, the result is (GOSSE and PHILLIPS, 2001):

**Equation 11**

$$\Phi_{eth,i}(Z) = \Phi_{eth,i}^* \exp\left(-\frac{Z}{\Lambda_f}\right) + (F\Delta\Phi)_{eth,i}^* \exp\left(-\frac{|Z|}{L_{eth,i}}\right)$$

Where:

$\Phi_{eth,i}$  - epithermal neutron flux in environment i [ $\text{n}/(\text{cm}^2 \text{ yr})$ ]

$L_{eth,i}$  – Epithermal neutron diffusion length in medium i [ $\text{g}/\text{cm}^2$ ]

**Equation 12**

$$(F\Delta\phi)_{eth,i}^* = \frac{\left(\frac{D_{eth,j}}{L_{eth,j}}\right)\Delta\Phi_{eth,i}^* - \left(\frac{D_{eth,ss}}{\Lambda_f}\right)\Delta\Phi_{eth,a}^{**}}{\left(\frac{D_{eth,a}}{L_{eth,a}}\right) + \left(\frac{D_{eth,ss}}{L_{eth,ss}}\right)}$$

Where:

$D_{eth,j}$  – Diffusion coefficient for epithermal neutrons in medium j [ $\text{g}/\text{cm}^2$ ]

$L_{eth,j}$  – Diffusion length for epithermal neutrons [ $\text{g}/\text{cm}^2$ ]

$\Delta\Phi_{eth,a}^{**}$  - Difference between the fluxes in the air and the subsurface [ $\text{n}/(\text{cm}^2 \text{ yr})$ ]

**Equation 13**

$$\Delta\Phi_{eth,i}^* = \Phi_{eth,j}^* - \Phi_{eth,i}^*$$

**Equation 14**

$$\Delta\Phi_{eth,a}^{**} = \Phi_{eth,ss}^* - \frac{D_{eth,a}}{D_{eth,ss}}\Phi_{eth,a}^*$$

Where i is the particular environment of interest (subsurface or ss) and j is the other environment (air or a).  $\Phi_{eth,ss}^*$  is the epithermal neutron flux that would be observed at the land surface if the properties of the medium did not change and were identical to the subsurface.  $\Delta\Phi_{eth}^*$  represents the difference between the equilibrium flux in the air and the equilibrium flux in the subsurface.  $(F\Delta\Phi)_{eth,i}$  is the difference between the actual flux and the flux that would be at  $Z = 0$  if all materials were medium i. When Equation 11 is substituted into the epithermal neutron production equation, Equation 9, the total epithermal neutron production for nuclide m is obtained.

**2.1.2.3 Thermal Neutrons**

Thermal neutrons have even lower energies than epithermal energies ( $< 0.5 \text{ eV}$ ) and so are also considered to behave in a diffusive manner due to Brownian motion (GOSSE and PHILLIPS, 2001). These particles are derived from the epithermal neutron

flux as the higher energy neutrons lose energy due to collisions. The only possible fate of thermal neutrons is absorption by a nuclide since they are already at low energy (GOSSE and PHILLIPS, 2001). In this study, following Gosse and Phillips (2001), thermal and epithermal neutrons are treated as distinct energy categories, rather than an energy continuum, in order to enable the use of analytical solutions for their vertical fluxes. The equation for production of cosmogenic nuclides by thermal neutrons is analogous to that for production by epithermal neutrons shown in Equation 9.

**Equation 15**

$$P_{th,m} = f_{th,m} \Gamma_{th,m} = \frac{f_{th,m}}{\Lambda_{th}} \Phi_{th}(Z)$$

Where:  $P_{th,m}$  - production of nuclide m by thermal neutrons [atoms/ (g \* yr)]

**Equation 16**

$$f_{th,m} = \frac{\sigma_{th,k} N_k}{\Sigma_{th}}$$

$f_{th,m}$  - fraction of thermal neutrons absorbed by target k that are ultimately used to form cosmogenic nuclide m [unitless]

$\sigma_{th,k}$  - Elemental thermal neutron cross-section [barns]

$\Sigma_{th}$  - macroscopic neutron absorption cross section [cm<sup>2</sup>/g]

$\Gamma_{th,m}$  - total rate of thermal neutron absorption [n/(g yr)]

$\Lambda_{th}$  - effective thermal neutron attenuation length [g/cm<sup>2</sup>]

$\Phi_{th}(Z)$  - thermal neutron flux at depth Z [n/(cm<sup>2</sup> yr)]

To develop the thermal neutron flux term, a diffusion equation similar to that for epithermal neutrons is set up, with the epithermal neutrons as the source of the thermal neutrons (GOSSE and PHILLIPS, 2001). Again, the thermal neutrons are assumed to be in

temporal equilibrium with the epithermal neutrons. The solution to the diffusion equation is:

**Equation 17**

$$\Phi_{th,i} = \Phi_{th,i}^* \exp\left(-\frac{z}{\Lambda_f}\right) + (\mathfrak{S}\Delta\Phi)_{eth,i}^* \exp\left(-\frac{|z|}{L_{eth,i}}\right) + (\mathfrak{S}\Delta\Phi)_{th,i}^* \exp\left(-\frac{|z|}{L_{th,i}}\right)$$

Where:

$\Phi_{th,i}^*$  - thermal neutron flux that would be observed at the land surface if the properties of the medium did not change and were identical to the subsurface

$(\mathfrak{S}\Delta\Phi)_{eth,i}^*$  - difference in the thermal neutron profile at the atmosphere/subsurface interface due to the shape of the epithermal neutron profile across the interface

$(\mathfrak{S}\Delta\Phi)_{th,i}^*$  - difference in the profile due to the diffusion of thermal neutrons across the interface

$\Delta\Phi_{th,i}^*$  - difference between the equilibrium thermal neutron flux in the air and the equilibrium flux in the subsurface

**Equation 18**

$\Delta(\mathfrak{S}\Delta\Phi)_{eth,i}^* = (\mathfrak{S}\Delta\Phi)_{eth,j}^* - (\mathfrak{S}\Delta\Phi)_{eth,i}^* =$  difference between the profile deviations of air and the subsurface due to epithermal neutron diffusion across the boundary

Equations for  $(\mathfrak{S}\Delta\Phi)_{eth,i}^*$  and  $(\mathfrak{S}\Delta\Phi)_{th,i}^*$  can be found in Gosse and Phillips (2001). If Equation 17 is substituted into Equation 15, the total production of nuclide m through thermal neutron production pathways will be obtained.

#### 2.1.2.4 Muons

Muons, the lightest electrically-charged particles, are negatively-charged leptons, as are electrons (POVH et al., 2004). These elementary particles are heavier than electrons, although the behavior is similar. Muons, formed by cosmic rays in the atmosphere, can interact with atomic nuclei and produce chlorine-36. Unless the sample is very calcic, the muonic component contributes very little to the total production of chlorine-36 within the first meter of the rock, so it is often not treated individually (ZREDA, 1994). However, in certain geologic situations, such as rapidly eroding limestone, this pathway can contribute as much as 50% of the production in the sample (STONE et al., 1998). In more typical situations, the muonic reaction pathway begins to dominate as the depth below the surface reaches more than 2-3 meters (FABRYKA-MARTIN, 1988; LAL and PETERS, 1967; STONE et al., 1998). This is because muons are tertiary products of the high energy nucleonic flux and have lower energies. Due to the lower energies, they do not react as frequently as the higher energy component and therefore have much longer transport lengths within the sample (GOSSE and PHILLIPS, 2001). Because muons are not in equilibrium with the high energy component of the incoming cosmic-ray flux, it is necessary to use a separate scaling factor for elevation and latitude, different attenuation lengths, and different angular distributions when calculating the contribution of muons (GOSSE and PHILLIPS, 2001). The equation describing all possible contributions to the cosmogenic nuclide inventory from muonic production is shown here (EVANS, 2001; GOSSE and PHILLIPS, 2001; STONE et al., 1998):

**Equation 19**

$$P_{t,\mu} = S_{\mu} S_{t,\mu} Q_{\mu} (P_{\mu} + P_{n,s\mu} + P_{n,f\mu})$$

Where:  $P_{t,\mu}$  - total production by muons [atoms/(g yr)]

$P_{\mu}$  - direct production by slow negative muon capture [atoms/(g yr)]

$P_{n,s\mu}$  - production by absorption of neutrons released during negative muon capture [atoms/(g yr)]

$P_{t,f\mu}$  - production through absorption of neutrons released during photodisintegration reactions initiated by fast muons [atoms/(g yr)]

The most important muonic cosmogenic production pathway is the slow negative muon capture reaction (GOSSE and PHILLIPS, 2001). Due to the domination of this pathway, this is commonly the only reaction used to calculate the muon contribution to cosmogenic production. For chlorine-36, this pathway consists primarily of negative muon capture by calcium-40, but also includes capture by potassium-39 (ZREDA, 1994). These pathways are discussed in more detail in Heisinger et al. (2002). The equation for production via the negative muon capture pathway is shown here (GOSSE and PHILLIPS, 2001):

**Equation 20**

$$P_{\mu,m}(Z) = \sum_k \psi_{\mu^-}(Z) f_{c,k} f_{i,k} f_{d,k} f_{n,k,m} = Y_{\Sigma k,m} \psi_{\mu^-}(Z)$$

Where:  $P_{\mu,m}(Z)$  = total production by slow negative muon capture [atoms/(g yr)]

k – all elements that may produce nuclide m by negative muon capture

$\psi_{\mu^-}(z)$  – muon stopping rate as a function of depth [stopped  $\mu^-$ /(g yr)]

$f_{c,k}$  – fraction of stopped negative muons captured by element k [unitless]

$f_{i,k}$  – abundance of the isotope that produces nuclide m after negative muon capture [unitless]

$f_{d,k}$  – fraction of captured negative muons that are absorbed by the nucleus of element k before they decay [unitless]

$f_{n,k}$  – probability that the nucleus of a particular isotope of element  $k$  will produce nuclide  $m$  after it has absorbed the negative muon [unitless]

$Y_{\Sigma k,m}$  – total production constant for nuclide  $m$  from slow negative muon absorption reactions [composition dependent]

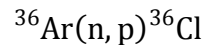
Cosmogenic nuclide production by muons can contribute significantly to the nuclide inventory and must be considered for all sites. For example, pre-exposure to cosmic-rays at a sample site, also known as inheritance, can cause samples to appear too old. If only spallation production is considered, the removal of only a small amount of surface material (a few meters) is needed to provide a fresh, unexposed surface. However, if the effects of muons are incorporated, significantly more material must be removed before the effects of muogenic production is removed entirely (STONE et al., 1998). This is especially important for young surfaces exposed due to shallow excavations, such as short glacial periods (STONE et al., 1998). The advantage of this production at depth is that it may be used to date very heavily eroded surfaces when other nuclides are not applicable (STONE et al., 1998) or to look at long-term limestone erosion rates (STONE et al., 1994).

### **2.1.2.5 Other Cosmogenic Production Pathways**

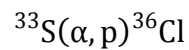
Several other possible cosmogenic production pathways exist for chlorine-36; however, these pathways do not typically contribute significantly to the production of cosmogenic nuclides at the surface. They are mentioned here only for the sake of completeness. These reactions account for a small portion of production, less than 2% in most cases (LICCIARDI et al., 2008). The possible high-energy reactions include spallation of titanium (Ti) and iron (Fe). These reactions may contribute significantly

more than 2% in rocks with high concentrations of the target elements, although this is still being investigated (MASARIK, 2002; STONE, 2005). At this time, these pathways are not constrained enough to be used in this model. Other possible nuclear reactions involve  $^{36}\text{Ar}$  and  $^{36}\text{S}$  (ZREDA, 1994). The nuclear reactions are shown below (FABRYKA-MARTIN, 1988):

**Equation 21**



**Equation 22**



These reactions are commonly disregarded in cosmogenic calculations due to the proportionally small amounts of cosmogenic nuclide produced in rocks of typical compositions (FABRYKA-MARTIN, 1988). Until further research is done on these pathways so the production rates can be defined, it is unclear how much these pathways contribute to the overall production and it is therefore difficult to incorporate in studies at this point. The cosmogenic nuclide produced via these reactions is considered negligible for all calculations herein.

### **2.1.3 Accumulation**

With the production rates quantified in the previous sections, the accumulation of the nuclide within the rock can be quantified as well. The accumulation rate within the rock is described by the production of the nuclide minus the radioactive decay of the element as shown here (ZREDA, 1994):

**Equation 23**

$$\frac{dN_{36}}{dt} = P - \lambda_{36}N_{36}$$

Where:

P – summation of all production pathways of the nuclide as outlined above

$N_{36}$  – abundance of Chlorine-36 [atoms]

$\lambda_{36} = (\ln 2)/t_{1/2}$  – decay constant for Chlorine-36 [1/time]

The solution to this linear first-order differential equation is (modified from DAVIS and SCHAEFFER, 1955; ZREDA, 1994):

**Equation 24**

$$N_{36} = \frac{P}{\lambda_{36}} (1 - e^{-\lambda_{36}t})$$

Where: t - exposure time

If the production rate is assumed to be constant in time, this equation provides the accumulation of chlorine-36 within a rock at the earth's surface through time, accounting for production and decay. The total production reaction, Equation 2, shows the production rates of each pathway along with other scaling factors and corrections needed to account for variations in production under different scenarios.

**2.1.4 Scaling, Shielding, and Other Correction Factors**

Before discussing scaling and shielding of a sample, one must first define an ideal sample situation. For all future discussions, the ideal reference scenario for cosmogenic nuclide samples is assumed to be a sample collected on a horizontal infinite flat plain at sea level and high latitude with no surrounding topography. However, samples are commonly collected on sloping surfaces, in areas with surrounding topography, and in all parts of the world at all elevations. The scaling factors in Equation 2 corrects for these

changes to the standard reference scenario. Each correction/scaling factor will be discussed in detail below.

### 2.1.4.1 Topographic Shielding

The topographic shielding factor,  $S_T$ , is composed of two parts: horizon and slope. The first part, the horizon shielding, is the ratio of the actual radiation flux (based on surrounding topography) to the flux through the surface if it were ideal (i.e. no surrounding topography) (GOSSE and PHILLIPS, 2001). The second part of the scaling factor accounts for the slope of the sample. If the sample is not horizontal, there are several effects that influence the amount or intensity of the incoming cosmic rays. The foreshortening effect decreases the incoming cosmic-ray intensity because the incident angle of most cosmic radiation is vertical. Because a sloped sample rests at an angle, the effective surface area receiving cosmic radiation has been decreased, which decreases the overall incoming radiation. Finally, the upside of the slope blocks a portion of the radiation from reaching the sample. This effect is commonly referred to as self-shielding. A diagram explaining this is shown in Figure 2.

To calculate the topographic shielding factor,  $S_T$ , both horizon and slope effects must be quantified. The topographic component is represented by the ratio of the actual flux through the surface  $\Phi_f(\phi, \theta)$  to the flux that would pass through the surface if it were ideal,  $\Phi_f(max)$ . The equation is shown below (GOSSE and PHILLIPS, 2001):

**Equation 25**

$$S_t = \frac{\Phi_f(\phi, \theta)}{\Phi_f(max)} = \frac{\int_{\theta=0}^{2\pi} \int_{\phi=0}^{\min\{\phi_s, \phi_t(\theta)\}} F_0 \cos^{2.3} \phi \sin \phi \cos \phi d\phi d\theta}{\Phi_f(max)}$$

Where:

**Equation 26**

$$\Phi_f(max) = \frac{2\pi F_0}{m+1}$$

$F_0$  = maximum intensity (vertical) of cosmic radiation

$m$  = constant = 2.3 (NISHIZUMI et al., 1989)

$\phi_s$  = inclination of the surface

$\phi_i(\theta)$  = inclination angle in direction  $\theta$  based on topography

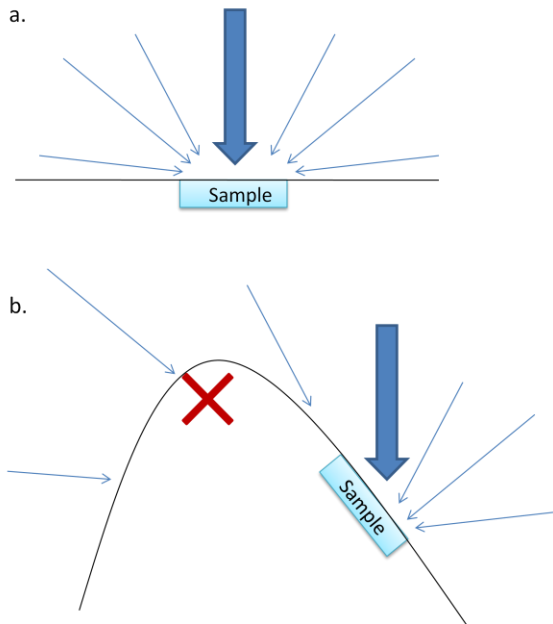


**Figure 2 - (a) The sample on a horizontal surface is bombarded by cosmic rays (shown by arrows) from all directions. (b) When the sample is on a slope, only some of the cosmic rays reach the sample while others are blocked by the hill (self-shielding). In both cases, the larger arrow represents the vertical incident angle of the majority of the cosmic rays.**

The coordinate system used to describe the shielding of a sloping sample is shown below in Figure 3. The angles recorded in the field are direction of dip ( $\theta_n$ ) and dip ( $\phi_d$ ). The sample can be blocked from incoming cosmic rays by topography and/or a sloping surface.

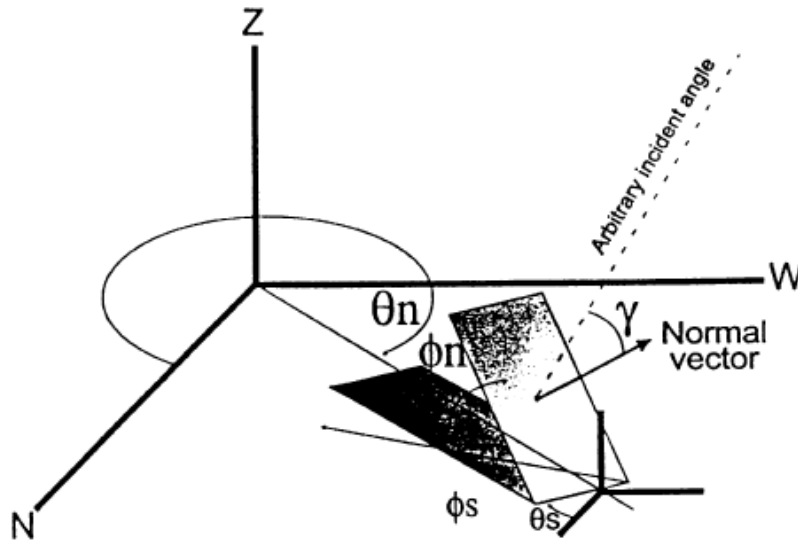


**Figure 3 - Illustration of the angle nomenclature for shielding calculations (GOSSE and PHILLIPS, 2001). Note that the geologic term “strike” is not equivalent to the direction of dip ( $\theta_n$ ) of the surface.**

The equation that describes the energetic component of the cosmic-ray flux through a sloping surface is (GOSSE and PHILLIPS, 2001):

**Equation 27**

$$\Phi_f(\phi, \theta) = \int_{\theta=0}^{2\pi} \int_{\phi=0}^{\min\{\phi_s(\theta), \phi_t(\theta)\}} F_0 \cos^{2.3} \phi \sin \phi \cos(\gamma(\phi, \theta)) d\phi d\theta$$

Where:

$\gamma(\phi, \theta)$  - The difference between the normal vector of the sloping surface and the incident angle of the incoming ray

Combining the previous two equations and using the spherical law of cosines (GOSSE and PHILLIPS, 2001) yields the complete scaling factor for a sample on a sloping surface surrounded by varying topography:

**Equation 28**

$$S_t = \frac{\int_{\theta=0}^{2\pi} \int_{\phi=0}^{\min\{\phi_s(\theta), \phi_t(\theta)\}} F_0 \cos^{2.3} \phi \sin \phi (\cos \phi_n \cos \phi + \sin \phi_n \sin \phi \cos(\theta_n - \theta)) d\phi d\theta}{\Phi_f(\max)}$$

$\phi_n$  - Degrees from horizontal of the dipping surface

$\theta_n$  - Degrees from north of the direction of dip of the surface

In order to completely compensate for a sample on a sloped surface, the attenuation length must be adjusted to reflect the change in the penetration depth of the cosmic rays perpendicular to the sample surface. This adjusted length is referred to as the apparent attenuation length (shown in Figure 4), or the flux-weighted integral of the average attenuation lengths. If a surface has no shielding and is completely horizontal, the apparent attenuation length can be assumed to be constant for all geographic locations (GOSSE and PHILLIPS, 2001). However, as the sample slope increases, an increasing percentage of the cosmic rays strike the sample at oblique angles, reducing the effective attenuation length, or the weighted average of all penetration depths of incoming cosmic rays. Figure 4 illustrates this effect. Topographic shielding, on the other hand, increases the effective attenuation length because it blocks out some of the oblique rays so a larger percentage of the rays are bombarding the rock surface at high angles (GOSSE and PHILLIPS, 2001). Figure 5 illustrates the effect of both slope and topography on effective attenuation length. After accounting for the changes in production due to the changes in effective attenuation length as discussed above, the final equation for the shielding due to topography and slope, is (GOSSE and PHILLIPS, 2001):

**Equation 29**

$$S_T = \frac{\Lambda_f}{\Lambda_{f,e}} S_t$$

Where:  $\Lambda_{f,e}$  = effective attenuation length

$\Lambda_f$  = apparent attenuation length

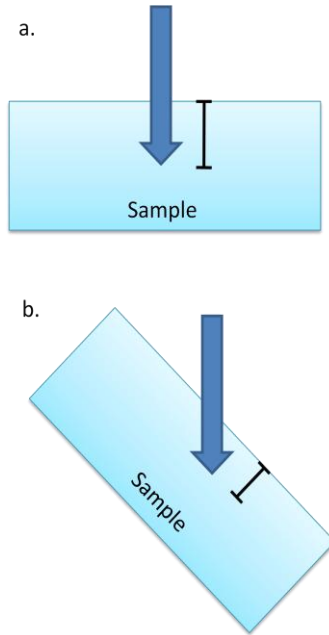


Figure 4-(a) The incoming cosmic rays only penetrate a specific distance into the rock. When the angle of this rock changes (b), the apparent attenuation length also changes, causing the overall penetration depth perpendicular to the rock surface to decrease. The black lines perpendicular to the surface show the decrease in apparent attenuation length from case (a) to case (b).

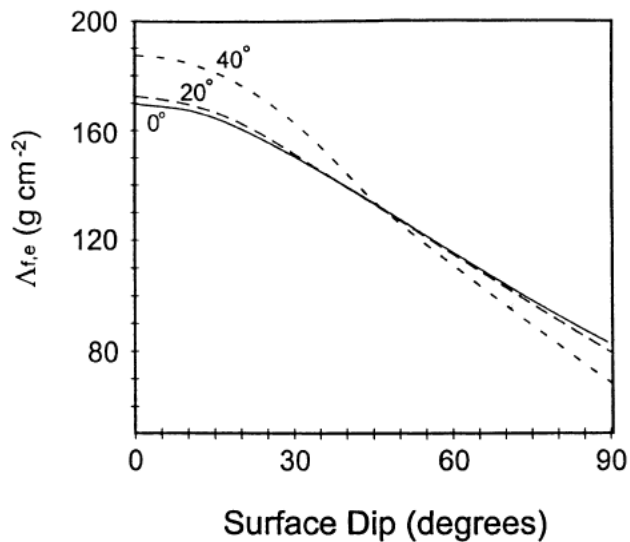


Figure 5 - The effective attenuation length as a function of the slope of the dipping sample surface (GOSSE and PHILLIPS, 2001). The degree markings indicate the horizon angle, assumed to be uniform, of the topographic shielding.

### 2.1.4.2 Thickness Correction

Although the production rates are given only for the surface of the material, they must be applied over the entire thickness of the sample. The thickness correction factor,  $Q_x$ , corrects for the variation of the cosmogenic production rate over the finite sample thickness. This is done by integrating over the actual sample depth and then dividing by the surface production rate. The general equation is shown here (GOSSE and PHILLIPS, 2001):

**Equation 30**

$$Q_{x,m} = \frac{\int_0^{Z_s} P_{x,m} dZ}{Z_s P_{x,m}(0)}$$

Because the production terms are in both the numerator and denominator of the equation, they cancel, leaving the thickness correction dependent on the reaction type and independent of the nuclide. By substituting the production equations for each of the individual pathways (e.g. thermal neutron or spallation production) into the above equation, the appropriate equations for  $Q_i$  can be obtained. There is a correction term for each type of reaction: spallation, thermal, epithermal, and muonic. The full equations can be found in Gosse and Phillips (2001).

### 2.1.4.3 Low-Energy Neutron Leakage

Thermal and epithermal neutrons, both low energy neutrons, behave in a diffusive manner and are therefore subject to diffusion at the atmosphere/rock interface. Because low energy neutrons move only due to Brownian motion, the best way to model the movement is using a diffusion equation. This is accounted for in the original production equation for both thermal and epithermal neutrons. In a flat rock, the diffusion of neutrons out of the sample leads to a maximum nuclide production rate due to low energy

neutron absorption at approximately  $50 \text{ g/cm}^2$  depth instead of at the surface of the sample (GOSSE and PHILLIPS, 2001). However, when dealing with odd geometries or edges, the diffusion may exceed that of a flat surface and must be corrected for using the additional correction factors,  $S_{L,eth}$  and  $S_{L,th}$ , commonly called leakage factors (GOSSE and PHILLIPS, 2001). For example, near the edge of a large basalt crevice, diffusion is greater than in the center of a block of the same material.

The geometry of the material surrounding the sample is also relevant because, in some cases such as the edge of a cliff, the neutron flux can be lower or higher than that of a flat surface depending on location on the cliff face (DUNNE et al., 1999). Spallation reactions are not affected by leakage as much as thermal and epithermal neutrons and the extent of this effect is examined for varying geometries by Masarik and Wieler (2003). However, for most situations fast neutron leakage is neglected. In order to avoid these edge effects and leakage factor corrections entirely, it is recommended that samples be collected at least 30 cm from any edge since the low energy fluxes reach equilibrium approximately 25 cm into the rock (GOSSE and PHILLIPS, 2001).

#### **2.1.4.4 Spatial Scaling**

When production rates are reported, they are typically scaled to sea level and high latitude. However, samples are collected at a variety of elevations and latitudes that have different corrections for atmospheric thickness and magnetic field effects for each location. This necessitates a scaling factor to adjust for the difference between the production rate locations, reported at sea level and high latitude, and the actual sample location. There are currently several proposed scaling schemes to correct for elevation and latitude, although the most commonly used is that of Lal (1991). Lal's scaling

scheme assumed a constant production rate through time and was based mainly on neutron monitor data. If a production rate is known at one location, it can be scaled using simple polynomial relationships to other locations where it can be applied in an area without nearby production rate data (LAL, 1991). Figure 6 illustrates the elevation and latitude dependence of the Lal scaling factors.

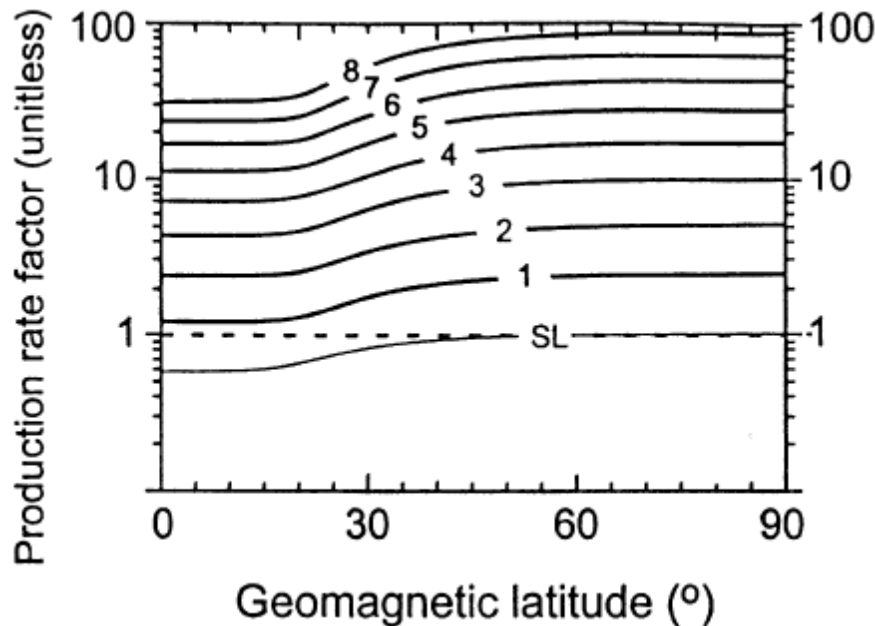


**Figure 6-Lal's spatial scaling factor plotted against geomagnetic latitude. The numbered contour lines indicate elevation in km (figure from GOSSE and PHILLIPS, 2001; based on data in LAL, 1991).**

The original scaling scheme developed by Lal (1991) did not incorporate any temporal variation in the production rate through time or spatial atmospheric variations, although evidence supports the existence of these phenomena (GUYODO and VALET, 1996; STONE, 2000). Other models have been developed to account for these and other spatial changes in production rates. A small revision of the Lal (1991) scaling was made by Stone (2000) to change the original scaling factors to pressure-dependent factors to account for changes in the density of the atmosphere and the subsequent blocking of cosmic rays due to the atmosphere. This is especially important for some areas of the

world where static atmospheric pressure systems have altered the cosmic-ray flux on long-term time scales, such as in Antarctica (STONE, 2000). This modification did not, however, incorporate temporal production rate changes in magnetic field strength through time or the effects of solar modulation.

Production rates are directly dependent on the incoming cosmic-ray flux so when there are changes in the flux due to phenomena such as geomagnetic field strength, the production rate also changes. This flux is known to change in time, even though, for many cosmogenic applications, the flux has been assumed constant and equal to the modern day flux (GOSSE and PHILLIPS, 2001). Although it has been noted that the cosmic-ray flux is not constant, only the most recent scaling models take this into account by using paleomagnetic histories to adjust for paleomagnetic field intensity changes through time (DESILETS and ZREDA, 2003; DUNAI, 2000; LIFTON et al., 2005).

Changes in paleomagnetic field intensity directly affect the time-varying production rate of samples around the world. A paleointensity graph (Figure 7) shows the changes over time of the intensity of the geomagnetic field. There is an inverse relationship between the cosmic-ray flux reaching the earth's surface and the solar activity (CERLING and CRAIG, 1994b). As the intensity of the geomagnetic field increases, the incoming cosmic-ray flux intensity decreases leading to an overall decrease in cosmogenic nuclide production rates. The incoming cosmic-ray flux is dependent on other temporal factors, such as the original galactic cosmic radiation, non-dipole magnetic field effects, solar modulation, and magnetic polar wander, some of which are addressed in the newer scaling models.

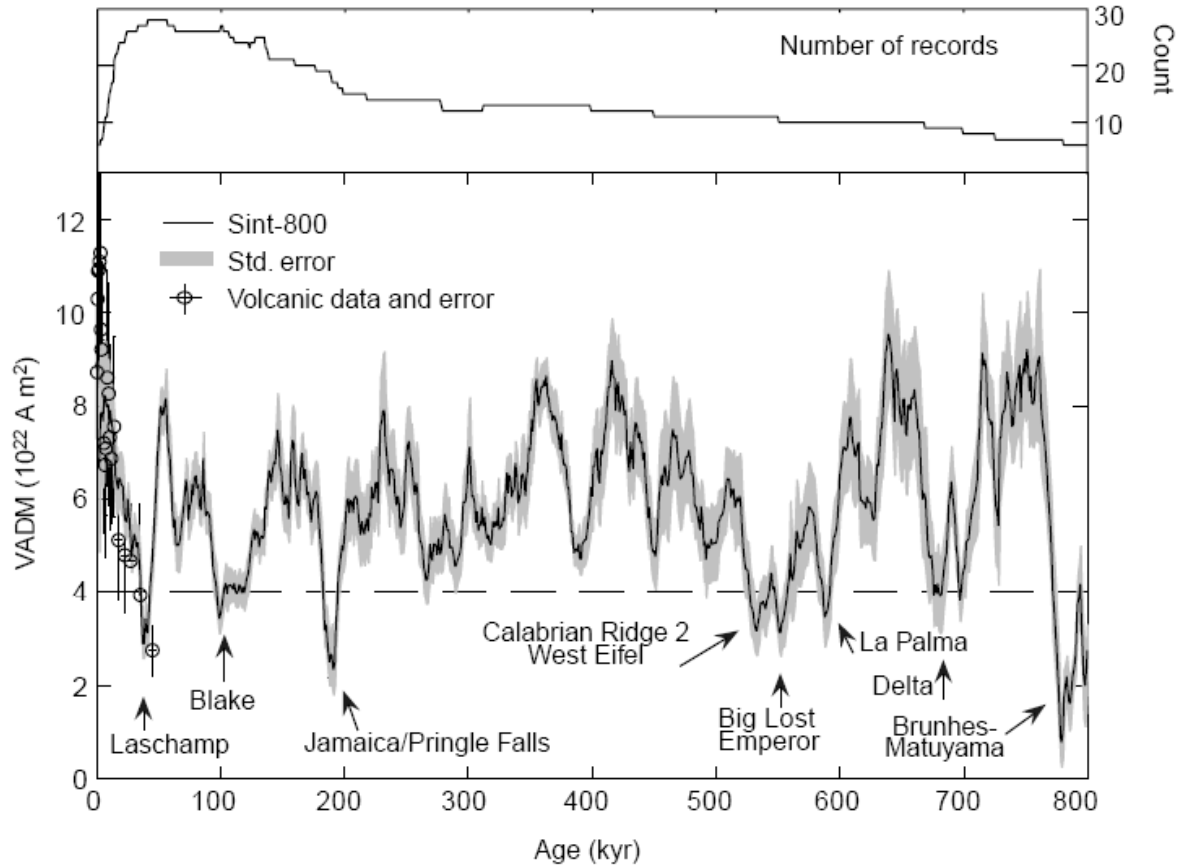


**Figure 7-**The SINT-800 paleointensity record showing the last 800,000 years (GUYODO and VALET, 1999). The number of records for each interval is shown at top while the stacked data are shown on the bottom. The dashed line shows the minimum value below which geomagnetic excursions (short-lived periods of decreased magnetic field intensity) have been observed.

The Dunai (2000) and Desilets (2006b) scaling schemes worked to incorporate magnetic field effects on production rates. Both the Dunai (2000) and Desilets (2006b) schemes used both cutoff rigidity and atmospheric pressure to determine the scaling factor and both were time-dependent based on the changes in the Earth's magnetic field. The Dunai (2000) scheme adjusted for the atmospheric pressure variations, but also included a non-dipole field effect. This resulted in scaling factors that varied between 18% lower (at latitudes between 20°-40°) and 30% higher (high altitudes) than the original Lal scaling (DUNAI, 2000). The Dunai scaling scheme was also different from others due to the method used to calculate the cutoff rigidity. The Dunai cutoff rigidity

values are incompatible with those calculated using trajectory tracing models as discussed in section 2.1.1 (LIFTON et al., 2005).

The Desilets et al. (2006b) scaling scheme modified the typical scaling model by measuring current-day high-cutoff-rigidity locations with neutron monitors and applying these results to extend the scaling model into high-cutoff-rigidity times in the past. The use of the Desilets scaling scheme resulted in deviations of up to 7% in the neutron attenuation length leading to 20% differences for production rates scaled from 4300 m down to sea level (DESILETS and ZREDA, 2001). The Desilets et al. model also implicitly incorporated solar modulation effects and separated scaling schemes for spallogenic reactions, fast muons, and slow muons (DESILETS and ZREDA, 2003; DESILETS et al., 2006b). However, this model did not incorporate any way to deal with global non-dipole field effects (LIFTON et al., 2005).

Another scaling scheme by Lifton et al. (2008; 2005) incorporated the SINT-800 geomagnetic record (GUYODO and VALET, 1996) and a Holocene geomagnetic model (KORTE and CONSTABLE, 2005) to adjust production rates for the changing magnetic field through time as well as altering the scaling factors to include the secondary effects of solar modulation on cosmogenic production. In this scaling scheme, the scaling factor has a dependence on longitude in addition to latitude due to the interaction of the numerous effects mentioned above (LIFTON et al., 2008; PIGATI and LIFTON, 2004). Lifton's model is similar to the other time-varying models in that it is a function of cutoff rigidity and is time-dependent with changes in the magnetic field, but it is different in that it explicitly calculates scaling as a function of solar modulation, incorporates a Holocene geomagnetic model that incorporates non-dipole effects, and uses backwards ray tracing

to examine the effects of the scaling model (LIFTON et al., 2008; LIFTON et al., 2005). The solar modulation component impacts the production rates at sea level and high latitude by up to 10%, depending on the time period over which the solar modulation is averaged (LIFTON et al., 2005).

There are currently five proposed scaling schemes, summarized in Table 2, that all present reasonable solutions to the problem of correcting for the differences in cosmic-ray flux depending on sample location. Most people agree that Lal’s (1991) scaling does not incorporate some of the important factors, such as time-dependent magnetic field effects or atmospheric effects. However, based on the current information and limited calibration samples available, none of the scaling schemes has been eliminated. For the purposes of this study, I used the original Lal (1991) scaling.

**Table 2 - Scaling scheme summary describing the differences in input parameters and time-dependence (modified from BALCO, 2007).**

<b>Scaling Scheme</b>	<b>Input Required</b>	<b>Time-Dependence</b>
Lal (1991)	Latitude, altitude	None
Stone (2000)	Latitude, atmospheric pressure	None
Dunai (2000)	Cutoff rigidity, atmospheric pressure	Global non-dipole effects, Magnetic field changes
Desilets (2006b)	Cutoff rigidity, atmospheric pressure	Local non-dipole effects, Magnetic field changes
Lifton (2005)	Cutoff rigidity, atmospheric pressure, solar modulation parameter	Global non-dipole effects, Magnetic field changes, solar output

#### **2.1.4.5 Sample Coverage**

Materials covering the sample for any period of time, such as snow, ash, peat, soil, till, or plant material, can significantly attenuate the incoming cosmic rays. While snow is the most common (GOSSE and PHILLIPS, 2001), other possible coverage materials may need to be considered depending on the particular history of the sample. For

example, simulations of a dense forest show a decrease in production rate of up to 4% (CERLING and CRAIG, 1994b). The material covering the sample attenuates the energetic component of the cosmic radiation exponentially based on the relationship shown in Equation 31 (GOSSE and PHILLIPS, 2001).

**Equation 31**

$$\Phi_{f,cover} = \Phi_f e^{\left(\frac{-Z_{cover}}{\Lambda_f}\right)}$$

Where:  $Z_{cover}$  - mass of cover per unit area over the rock sampled

The fast neutron attenuation length is important in the coverage calculation because it impacts the flux of cosmic-rays that are able to penetrate the covering material. A longer attenuation length means more incoming cosmic rays reach the sample. In order to reduce the effects of possible sample coverage, it is recommended that samples be taken from topographic highs where the wind is more likely to remove any accumulated cover material quickly (ZREDA, 1994). Sloped surfaces can also offer possibilities of less snow accumulation. If a snow correction is still necessary, snow depths and water content should be measured in order to estimate this shielding factor.

The coverage of a sample can change through time, which, in turn, changes the time-integrated production rate (GOSSE and PHILLIPS, 2001). If a sampled is covered by till, ash, or other material, exhumation over time could contribute to temporal variations in the production rates. An example of these variable production rates is described in detail for a glacial moraine in Zreda and Phillips (1994). A similar process is possible for ash, vegetation, or other materials and must be evaluated on a case-by-case basis.

### **2.1.5 Factors affecting nuclide accumulation in rock**

Factors other than production mechanisms can affect the accumulation of chlorine-36 within the rock. These factors include erosion, radioactive decay, radiogenic production, changes in position, and chemical weathering.

#### **2.1.5.1 Erosion**

Production rates are calculated for a surface experiencing no erosion. If erosion rates can be estimated using geological parameters, such as protrusions due to differential erosion (SWANSON and CAFFEE, 2001), then the changes to the cosmogenic inventory within the sample can be adjusted accordingly. Erosion is a very common factor at many sampling sites and if it goes unrecognized, it can bias the sample age. For spallogenic nuclides, erosion typically makes the sample appear younger than expected due to the removal of the top layers, which contain the highest concentrations of cosmogenic nuclide in the rock. However, for chlorine-36, if there are high chlorine concentrations and low calcium and potassium concentrations, the sample can appear too old if there has been only a small amount of erosion (ZREDA, 1994). This occurs because chlorine-36 production by thermal and epithermal neutron absorption increases down to  $\sim 50 \text{ g/cm}^2$  depth. If more than one cosmogenic nuclide is used, it may become possible to constrain both the age and erosion rate of a surface (LAL, 1991).

A particular case of erosion called spalling or exfoliation, which occurs when the boulders or other rock surfaces are exposed to the freeze-thaw process (or other process) that causes a flake at the surface of the rock to be removed (ZREDA, 1994). Spalling can make it difficult to determine whether or not erosion has occurred due to the clean surface that is left behind (CERLING and CRAIG, 1994b). This form of erosion is also common on pahoehoe structures on lava flows (CERLING and CRAIG, 1994b). For

example, this type of erosion was observed at the Tabernacle Hill basalt flow, described below in section 3.5. Pristine pahoehoe ropes were seen on several surfaces even though there were remaining pieces of a sheet of basalt that had existed above those other surfaces to suggest that a full sheet of the basalt had already been removed (i.e. the surface examined was not the original top of the basalt flow). Erosion effects can usually be minimized by careful selection of the sample surfaces and by taking multiple samples in order to identify outliers.

### **2.1.5.2 Radioactive Decay**

Radioactive decay of chlorine-36 is also occurring in samples during exposure. The half-life of chlorine-36 is  $(3.01 \pm 0.04) \times 10^5$  years and it decays to argon-36 (BENTLEY et al., 1986). The accumulation equation, Equation 24, already includes radioactive decay. Singled out, the equation for radioactive decay is:

**Equation 32**

$$N(t) = N_0 e^{-\lambda t}$$

Where:  $N(t)$  – Nuclide inventory with time,  $N_0$  – Original nuclide inventory

The radioactivity of a nuclide dictates how long it takes to reach a steady state concentration at the surface. For a stable isotope, such as helium-3, steady-state is never reached because it does not decay. However, for radioactive cosmogenic isotopes, it takes approximately 5 half-lives to approach steady-state concentrations (CERLING and CRAIG, 1994b). Surfaces that have reached steady-state, approximately 1 million years for chlorine-36, can be used to determine nuclide production rates as well (EVANS et al., 1997). By assuming steady-state for a surface, a minimum production rate for the nuclide

can be calculated. However, if erosion is acting on a surface, steady-state will be achieved at a younger exposure age.

### **2.1.5.3 Radiogenic Production and Neutron Absorption**

There are other non-cosmogenic processes, such as radiogenic production, that can produce additional chlorine-36 atoms in the subsurface. The radiogenic production is quantified using measured concentrations of uranium and thorium and the method in Fabryka-Martin (1988) and summarized below. The uranium (U) and thorium (Th)  $\alpha$ -decay chain members produce alpha particles ( $\alpha$ ) as they decay. The alpha particles react with light nuclei in the rock matrix to produce neutrons. In turn, the neutrons can react with target elements in the rock in the same way that cosmogenically-produced neutrons react to produce chlorine-36. The equations for calculating this contribution to the total nuclide inventory within a sample are provided in detail in Fabryka-Martin (1988) and are summarized here in Equation 33 through Equation 41.

The production of neutrons as calculated from the concentrations of U and Th is shown below in Equation 33. The elements with the maximum yield of neutrons due to alpha particle reaction are Be, B, F, and Li. However, due to the low concentration of these elements in most rocks, the largest concentrations of neutrons result from targets with larger matrix concentrations, such as Al, Si, Mg, O, and Na. In the samples for this study, the concentrations of the elements listed in Table 3 were measured with the exception of oxygen (O) and hydrogen (H). The concentrations of both O and H were calculated from the oxide measurements performed on the other elements. Although the concentrations of the largest producers of neutrons are the most important elements to quantify, the remaining rock matrix composition must still be quantified in addition to the

elements listed above so that all elements can be used to calculate the stopping power of the rock. In particular, there are several elements, such as boron and gadolinium, that have large neutron cross-sections, meaning that they have a large probability of absorbing neutrons (radiogenically formed and cosmogenically formed neutrons) (FABRYKA-MARTIN, 1988). This decreases the actual amount of chlorine-36 formed within the rock because these other elements intercept the neutrons prior to formation of chlorine-36. The concentrations of all the measured elements are included in these calculations of the properties of the rock. A table of nuclear properties for all the elements included in sample analysis is shown in Table 3.

**Equation 33**

$$(P_n)_\alpha = X[U] + Y[Th]$$

Where:

$(P_n)_\alpha$  - production rate of neutrons from alpha particles [neutrons/g/year]

U & Th - concentrations of the elements [ppm]

X & Y - factors related to the light isotope composition of the rock matrix

**Equation 34**

$$X = \sum_i S_i F_i Y_n^U / \sum_i S_i F_i \quad [\text{neutrons/g/year/ppm U}]$$

Where:

$S_i$  - mass stopping power of element i for alpha particles of given energy

[MeV g<sup>-1</sup> cm<sup>2</sup>]

$F_i$  - fractional abundance of element i [ppm]

$Y_n^U$  - neutron yield of element i per ppm U in equilibrium

**Equation 35**

$$Y = \sum_i S_i F_i Y_n^{Th} / \sum_i S_i F_i \quad [\text{neutrons/g/year/ppm Th}]$$

Where:

$Y_n^{Th}$  - neutron yield of element i per ppm Th in equilibrium

**Table 3-Elemental properties used in calculation of rock properties.**  $A_i$ –atomic weight of element in gram/mole,  $\xi_i$ –average log decrement of energy per neutron collision with element i,  $\sigma_{sc,i}$ – neutron scattering cross-section of element i,  $\sigma_{th,i}$ – thermal neutron absorption cross-section of element i,  $I_{a,i}$ – dilute resonance integral for element i,  $S_i$ – mass stopping power of element i for alpha particle of a given energy,  $Y_{n,i}^U$  – neutron yield of element i per ppm U in radioequilibrium,  $Y_{n,i}^{Th}$  – neutron yield of element i per ppm Th in radioequilibrium,  $K_m$  – conversion from ppm to atom/gram.

<b>i</b>	<b>A<sub>i</sub></b>	<b>ξ<sub>i</sub></b>	<b>σ<sub>sc,i</sub></b>	<b>σ<sub>th,i</sub></b>	<b>I<sub>a,i</sub></b>	<b>S<sub>i</sub></b>	<b>Y<sub>n,i</sub><sup>U</sup></b>	<b>Y<sub>n,i</sub><sup>Th</sup></b>	<b>K<sub>m</sub></b>
<b>O</b>	16	0.12	3.76	0.0002	0.0004	527	0.23	0.079	NA
<b>H</b>	1	1	20.5	0.33	0	-	-	-	NA
<b>C</b>	12	0.158	4.74	0.0034	0.0016	561	0.45	0.18	13.680
<b>Na</b>	23	0.084	3.025	0.53	0.311	456	14.5	6.8	19.420
<b>Mg</b>	24.3	0.08	3.42	0.063	0.038	461	5.8	2.6	14.940
<b>Al</b>	27	0.072	1.41	0.23	0.17	444	5.1	2.6	11.808
<b>Si</b>	28.1	0.07	2.04	0.17	0.127	454	0.69	0.335	10.010
<b>P</b>	31	-	5	0.2	-	433	0	0	8.480
<b>K</b>	39.1	0.05	2.04	2.15	1	414		0.305	12.780
<b>Ca</b>	40.1	0.049	2.53	0.43	0.235	428	0	0	10.730
<b>Ti</b>	47.9	0.041	4.09	6.1	3.1	375	0	0	7.530
<b>Mn</b>	54.9	0.036	2.2	13.3	14	-	-	-	6.924
<b>Fe</b>	55.8	0.035	11.35	2.56	1.39	351	0.19	0.205	7.540
<b>Cr</b>	52.0	0.038	3.38	3.1	1.6	0	0	0	11.578
<b>Li</b>	6.9	0.264	0.95	70.5	0	548	21.1	9.6	86.731
<b>Cl</b>	35.5	0.055	15.8	33.5	13.7	-	-	-	16.980
<b>B</b>	10.8	0.174	4.27	767	1722	527	62.3	19.2	55.680
<b>Sm</b>	150.4	0.013	38	9640	1400	-	-	-	4.004
<b>Gd</b>	157.3	0.013	172	41560	390	-	-	-	3.828
<b>U</b>	238	-	-	-	-	-	-	-	2.529
<b>Th</b>	158.9	-	-	-	-	-	-	-	2.594

In order to calculate the production of a nuclide from the neutron flux, it is necessary to divide the neutrons into the thermal and epithermal energy components. The neutrons that form from  $\alpha$ -decay reactions generally start at about 0.5 to 3 MeV, although they can range up to 10 MeV (FABRYKA-MARTIN, 1988). These energetic neutrons can be thermalized or captured by the non-target nuclei present in the sample. The

probability that a neutron will reach thermal energy levels without being captured is called the resonance escape probability ( $p(E_{th})$ ). This is described in Fabryka-Martin (1988) and is calculated from other references in that work. The equation is shown below:

**Equation 36**

$$p(E_{th}) = \exp \left[ \frac{-I_{eff}}{\sum_i \xi_i N_i (\sigma_{sc})_i} \right]$$

Where:

$\sigma_{sc}$  - cross-section of element  $i$  for scattering of neutrons [ $\text{cm}^2$ ]

$\xi_i$  - average log decrement of energy per collision

$N_i$  - atomic concentration of element  $i$  [atoms/gram]

**Equation 37**

$$I_{eff} = \sum_i N_i (I_a)_i$$

Where:

$I_{eff}$  - effective resonance integral of rock for absorption of neutrons in epithermal region [ $\text{cm}^2/\text{g}$ ]

$I_a$  - dilute resonance integral

The total neutron flux is the combination of the thermal and epithermal neutron fluxes. The thermal neutron flux is described by Equation 38 while the epithermal neutron flux is described in Equation 39 (FABRYKA-MARTIN, 1988):

**Equation 38**

$$\phi_n(E_{th}) = \frac{p(E_{th})P_n}{\sigma_m} \quad [\text{neutrons} * \text{cm}^{-2} * \text{yr}^{-1}]$$

**Equation 39**

$$\phi_n(E_{eth}) = \frac{(1-p(E_{th}))P_n}{I_{eff}} \quad [\text{neutrons} * \text{cm}^{-2} * \text{yr}^{-1}]$$

**Equation 40**

$$\sigma_m = \sum_i N_i (\sigma_a)_i$$

Where:

$\sigma_m$  - total or macroscopic thermal neutron absorption cross-section of the rock matrix [cm<sup>2</sup>]

$\sigma_a$  - total absorption cross-section of element i for thermal neutrons [cm<sup>2</sup>]

The production of the desired nuclide can be calculated using the fluxes. Once the total production of the nuclide from the alpha decay of U and Th is known, it can be subtracted from the total sample inventory. The remaining nuclide is assumed to originate entirely from cosmogenic production.

**Equation 41**

$$P_i = N_{tg} \sigma_{tg} \Phi_n (E_{th}) + N_{tg} (I_R)_{tg} \Phi_n (E_{eth})$$

Where:

$P_i$  - production of the nuclide from radiogenic productions [nuclei/g/year]

$N_{tg}$  - Atomic concentration of target element [at/g]

$\sigma_{tg}$  - reaction cross-section of target element for thermal neutrons [cm<sup>2</sup>]

$(I_R)_{tg}$  - dilute resonance integral [cm<sup>2</sup>]

**2.1.5.4 Changes in Position**

An obvious change in position is the rolling of a boulder or the movement of a slab of rock (ZREDA, 1994). This can be caused by trees rolling a boulder (CERLING and CRAIG, 1994b), earthquakes (BULL, 1996), or by simple slope instability. This type of change is not always evident during sampling. The best way to avoid the problems caused by position change is to sample only stable areas, avoiding samples on the sides of

slopes, and to take numerous samples so that it is evident if one sample returns an anomalous age (ZREDA, 1994).

Changes in position vertically, i.e. changes in elevation, can affect the production rates of a nuclide within a sample over time. This elevation change can happen through tectonics or isostatic rebound depending on the geology of the area. Isostatic rebound is common in areas that have undergone glaciation (DETHIER et al., 1995; SWANSON and CAFFEE, 2001), sea level changes (ZREDA, 1994), or have had other masses of water removed rapidly. For example, Lake Bonneville was a large lake around 18,000 years ago, which has since then shrunk to the current Great Salt Lake of Utah due to a catastrophic flood and climate changes (OVIATT et al., 1992). A large weight was rapidly removed from the earth's crust at this location, causing it to undergo isostatic rebound, or rise slowly over time due to the release of pressure (OVIATT et al., 1992). Tectonics can also move samples significantly over the exposure history of a sample. In Lal (1991), the method of calculating the exposure age after changes in elevation is explained. In general, the effect of this type of uplift must be determined on a case-by-case basis. For the chlorine-36 samples in this study, the effects of isostatic rebound were estimated to be much less than 5% (LIFTON, 2005) and were not included in the production rate corrections applied to the samples.

### **2.1.5.5 Chemical Weathering**

Finally, chemical weathering of a sample can cause the incorporation or loss of chlorine-36. The addition of non-cosmogenic chlorine-36 due to the precipitation of secondary minerals or the release of cosmogenic chlorine-36 through weathering can cause the overall inventory of chlorine-36 to be altered (CERLING and CRAIG, 1994b).

This is impossible to calculate due to infinite possibilities and individual variation of sample characteristics. The best policy is to avoid sampling heavily weathered samples (ZREDA, 1994).

### **2.1.6 Uncertainties**

Age uncertainties (both systematic and random) associated with accuracy of chlorine-36 dating are typically on the order of 5-15%, although it can be more or less depending on the individual sample and the constraints on the surrounding geological history (PHILLIPS et al., 1996; PHILLIPS et al., 1997). The random uncertainty contributed by AMS (Accelerator Mass Spectrometry) analysis of the  $^{36}\text{Cl}/^{35}\text{Cl}$  ratio is usually in the range of 2-5%. Other quantified uncertainties include the random uncertainty in the elemental concentration of each sample and the random uncertainty associated with other measured quantities, such as sample mass and spike mass. Typically, the AMS uncertainty has been the only uncertainty propagated into the chlorine-36 ages (ZREDA et al., 1991) because the other uncertainties and biases associated with the technique are difficult to quantify. These unquantified uncertainties include laboratory error, processing uncertainties, and the scaling issues discussed above that may contribute up to 20% in sample systematic and random uncertainty and make it difficult to report total uncertainties in age results (ZREDA and PHILLIPS, 1994). If chlorine-36 ages are going to be quantitatively compared to other isotopes, it would be necessary to report the total uncertainties (including laboratory uncertainties and not just AMS uncertainties) because the uncertainties and biases will not be the same between the different nuclide methods (ZREDA and PHILLIPS, 2000). At this time, these additional uncertainties are not adequately quantified and this is an area of active research in the CRONUS-Earth project.

## **2.2 Production Rate Discrepancies**

To date, geological calibrations have been used to determine the commonly used production rates of most cosmogenic nuclides (CERLING and CRAIG, 1994a; EVANS, 2001; HANDWERGER et al., 1999; NISHIZUMI et al., 1989; PHILLIPS et al., 1996). Geological calibration uses independently constrained ages of carefully selected geologic sites to calculate the production rate for *in situ* cosmogenic nuclides. However, geological calibrations for chlorine-36 have yielded varying production rate parameters (EVANS, 2001; EVANS et al., 1997; PHILLIPS et al., 2001; STONE et al., 1996; STONE et al., 1998; SWANSON and CAFFEE, 2001). There are several possible explanations for the discrepancies among research groups, including technology, independent age constraints, scaling, production mechanisms, and preparation technique. Note that the chlorine-36 production rates discussed here are more appropriately termed production parameters due to their use in a model dependent on other parameters, such as scaling factors. However, these parameters represent the production rate of chlorine-36 in each pathway for the particular model used here and will be referred to as production rates or sets of production rates in this study.

### **2.2.1 Possible Sources of Discrepancy**

The technology for analyzing the samples has improved over the last decade, since several of the earlier calibrations were performed (EVANS et al., 1997; PHILLIPS et al., 1996; STONE et al., 1996). The carbon-14 techniques and the chronology have also been updated since many of these studies have been performed (STUIVER et al., 2005). Accelerator mass spectrometry has also improved since cosmogenic isotopes were originally measured (ELMORE and PHILLIPS, 1987). AMS detection limits have

improved in the last decade and the determination of chlorine contents in rocks has been improved through the use of isotope dilution mass spectrometry during AMS analysis (DESILETS et al., 2006a; ZREDA and PHILLIPS, 2000; ZREDA et al., 1991). Perhaps better instrumental results will yield more compatible production rates. These differences in procedures and techniques may have contributed to the different controversial rates now prevalent in the literature.

Although every group attempted to use a well-constrained surface, it is possible that the independent constraints for the surfaces were incorrect, which in turn yielded erroneous chlorine-36 production rates. In fact, the availability of pristine sites with adequate age constraints is the most limiting factor for obtaining reliable nuclide calibrations (PHILLIPS et al., 1996). Phillips et al. (1996) acknowledged that their calibration dataset was not ideal due to lack of reliability in the independent chronology of the sites. In Swanson's production rate study, many assumptions were made about the carbon reservoir for the shells used to radiocarbon date the sample as well as the deglaciation history of the area (SWANSON and CAFFEE, 2005; SWANSON and CAFFEE, 2001). Although he justified all assumptions, it is possible that using a single age for the entire deglaciation of a large area and applying a single carbon-14 reservoir correction to the entire area were not good assumptions and this causes doubt as to the true independent age of the surface (EASTERBROOK, 2003).

At some point, each research group was forced to scale the site-specific production rate to a general reference point of sea level and high latitude (GOSSE and PHILLIPS, 2001) in order to compare the results to other research groups' production rates. As discussed in detail above, the scaling is not trivial and there is currently no consensus about the best

method to use. In all three cases, the research groups used Lal (1991) scaling to adjust the results. However, it is well-known that Lal scaling does not incorporate important effects such as atmospheric anomalies, geomagnetic field changes, or other temporal effects on production rates. Due to this, the Lal scaling may be more appropriate for some samples, such as those at high latitudes and lower elevations, than for other samples, such as the higher elevation samples (EVANS et al., 1997) and those in equatorial regions. The general assumption that the samples will all be affected in a consistent manner may not be true due to effects not included in Lal scaling that may affect samples in the calibration dataset differently (SWANSON and CAFFEE, 2001).

As detailed above, chlorine-36 is produced by many mechanisms, not all of which are as well quantified as others. Other cosmogenic nuclides, such as beryllium-10, are produced by a limited number of pathways. For beryllium-10, the main production pathway is spallation in quartz (NISHIZUMI et al., 1989). Due to the uniform composition of quartz, beryllium-10 production is consistent from sample to sample. Spallation production is relatively simple to calculate because the production within a sample follows an exponential trend. Chlorine-36 is produced through spallation, similarly to beryllium, as well as other pathways such as thermal neutron absorption and negative muon capture. It is important to note that chlorine-36 is produced by two different spallation pathways from two target elements, K and Ca. Unfortunately, due to the diffusive nature of low-energy neutrons, the total production within a sample does not follow a simple exponential pattern and is more complicated to calculate (PHILLIPS et al., 2001). Muons are similarly complex, requiring individual treatment as well (STONE et al., 1998). Because there are so many complicated pathways, it is possible that each

group may have calculated these pathways in a slightly different manner. For this reason, the multiple mechanisms of chlorine-36 production may have contributed to the difference in published production rates.

Finally, the processing techniques used for chlorine-36 preparation vary depending on laboratory and investigator, and generally can be classified as either whole rock or mineral separate procedures. Some laboratories, such as Phillips and Swanson (ZREDA, 1994; ZREDA et al., 1991), work mainly with whole rock samples, while others, such as Stone (STONE et al., 1996), separate out particular mineral phases for analysis. In order to address the production rate of a particular chlorine-36 pathway, mineral separates can provide a means to physically separate one pathway from others within the rock. However, whole-rock samples are calibrated based on the chemical composition of the rock. Whole rock analyses, by definition, include production by all pathways within a single sample and they have the advantage of being simpler to perform. Mineral separates isolate a single production pathway, although not all pathways are examined within a single sample. The discrepancies between the two techniques may also include other minor laboratory technicalities and these procedures will be examined closely during an upcoming interlaboratory comparison to determine if the technique differences are the source of the discrepancy.

### **2.2.2 Production Rates in the Literature**

The current production rates for the three main chlorine-36 pathways come from three main research groups and are referred to as the Phillips, Stone, and Swanson production rates even though there are many authors and coauthors. The actual production rates and sources are shown below in Table 4. The chlorine-36 production

rates vary significantly from author to author. In each case, the research group collected samples from a location of known age, processed the samples, and calibrated the rates based on the results.

There were distinct methods used to calculate the production rates for each research group. Phillips used chi-squared minimization based on solving simultaneous equations (PHILLIPS et al., 2001). Stone used mineral separates and calibrated each pathway separately using mineral phases of a particular composition (EVANS et al., 1997; STONE et al., 1996). Finally, Swanson made calculations based on the mean production of groups of samples separated into target element groups to distinguish between pathways (SWANSON and CAFFEE, 2001).

A brief overview of the calibration by each author is listed Table 4 to illustrate the differences among the locations, methods, and results. In the case of the Swanson production rates, those of calcium and potassium were modified to reflect only the portion from spallation. This adjustment was performed by calculating the percentage of production from muons at the particular calibration site using CHLOE (PHILLIPS and PLUMMER, 1996) and then subtracting this amount from the total reported production. The uncertainties were propagated according to Bevington and Robinson (1992), although the errors did not change significantly given the number of significant figures.

Study/Source	Location(s)	Type of sample	Altitude (m)	Latitude	Age (cal ka )	Type of Calibration	Production rates
Phillips (PHILLIPS et al., 2001)	Utah	Basalt flow	1445	39°N	16.5	Whole rock	Ca: 66.8±6.8 K: 137±60 P <sub>f</sub> (0): 626±43
	Idaho	Basalt flow	1367-1798	43-44°N	2.1-13.7		
	New Mexico	Glacial erratic boulder	2058-2578	35°N	3-18.2		
	Wales	Boulder on beach	375	52°N	11.8		
	Ellesmere Island	Glacial polished bedrock	80-100	80°N	9		
	Northwest Territories	bedrock	20	68°N	14.8		
Arizona	Meteor Crater ejecta	1730	35°N	49			
Stone (EVANS et al., 1997)	Sierra Nevada	Glacial bedrock	3000-3600	38°N	13.1	Mineral separate	K: 170±25 K: 241±9
	Scotland	Glacial bedrock	520	58°N	11.6		
	Antarctica	Bedrock	2000-2200	70°S	Steady State		
Stone (STONE et al., 1996)	Tabernacle Hill, Utah	Basalt flow	1445	39°N	17.3	Mineral separate	Ca: 48.8±4.8
Stone/Evans (EVANS, 2001)	Scotland	Glacial bedrock	520	58°N	11.6	Mineral separate	P <sub>f</sub> (0): 740±63
Swanson (SWANSON and CAFFEE, 2001)	Puget Lowland, Washington	Moraine boulders and glacial bedrock	10-140	47.5-48.4°N	15.5	Whole rock	Ca: *83.8±5 K: *211±18 P <sub>f</sub> (0): 762±28

**Table 4-Production rates from various research groups for chlorine-36 (EVANS et al., 1997; PHILLIPS et al., 2001; STONE et al., 1996; STONE et al., 1998; SWANSON and CAFFEE, 2001). The values for Ca and K include are spallation values only. Units for production rates are Ca: [atoms <sup>36</sup>Cl (g Ca)<sup>-1</sup>yr<sup>-1</sup>], K: [atoms <sup>36</sup>Cl (g K)<sup>-1</sup>yr<sup>-1</sup>], secondary neutron production (P<sub>f</sub>(0)): [neutron <sup>36</sup>Cl (g air)<sup>-1</sup>yr<sup>-1</sup>]. \*These values originally reported as total production values for muon and spallation production. Original values for total production from Ca: 91±5, K: 228±18.**

In order to discuss the discrepancy among the production rate parameters, a comprehensive test of all three sets of production rate parameters on a single independently-dated site would be very useful. Prior to this study, all three production rates had not been simultaneously compared on a single surface. For this study, the Lake Bonneville shoreline in Utah was chosen as the test site due to its well-constrained lake-level history that includes more than 80 radiocarbon dates (OVIATT et al., 1992). Once the ages resulting from the use of each of the production rate parameters were compared, the main differences among the rates were easier to assess. Ages calculated with each of the sets of production rate parameters yielded either reasonable or unreasonable ages based on the carbon-14 constraints of the site. Understanding which production rates yielded the closest ages allowed us to focus on which possible causes of the discrepancy were the most important.

Using the Bonneville site, a new set of production rate parameters was also calculated using the newly processed data and compared to the originally published values. These new preliminary rates, although not a final set of production parameters, allowed for a determination of whether the community is headed in the correct direction to resolve this debate. These new parameters were based solely on the new data collected during this project, using only the best technology to obtain the results, which allows for an examination of the technological aspect of the discrepancy. During the continuation of this study, more sites will be added to the calculations in order to constrain the latitude, elevation, and temporal changes in the production rates. Eventually, the goal will be to obtain a final set of production rate

parameters based on the most recent datasets from all three laboratories and agreed upon by the chlorine-36 community.

## 3 METHODS

The geological calibration portion of the CRONUS-Earth project involves the work of many collaborating scientists. In this case, the sample sites were agreed upon by the entire group, while the individual samples at a specific location were determined by the smaller group of researchers who physically collected the samples. In both cases, the highest standards were used to select the sites. These samples were then processed in the laboratory and interpreted. The methods for each one of these steps is discussed below.

### ***3.1 Cosmogenic Nuclide Calibration Site Requirements***

The primary selection site criterion for the calibration sites was that it needed to be well-dated by independent methods. In order to perform a geologic calibration, independent confirmation of the age of the site is necessary. The uncertainty in the ages must also be very small in order to produce an accurate production rate. In this case, the duration of the event that created the surface must be very small in order to reduce the possible uncertainty in the final production rate (LIFTON, 2005).

In order to calibrate all the different nuclides at a single location, it is necessary to have appropriate lithologies. Not all nuclides can be processed from a

single lithology. For example, chlorine-36 analysis can be performed on practically any lithology, while beryllium-10 analysis requires significant amounts of quartz. Ideally, lithologies would be present for analysis of cosmogenic beryllium-10, aluminum-26, neon-21, chlorine-36, helium-3, and carbon-14.

In a practical sense, it is difficult to meet all these requirements precisely at a single geological location. The goal of this geological calibration is to use the best possible surface to calibrate all the nuclides simultaneously. Part of the discrepancy in the chlorine-36 production rates might be attributed to the selection of the calibration sites. Perhaps having the different investigators process samples from the same surface, even the same samples, will resolve some parts of the problem.

### ***3.2 Individual Sample Requirements***

Individual samples representing the desired surface must be collected with care. In many cases of cosmogenic dating, corrections can be made for shielding or other geometrical concerns. However, for calibration studies, it is desirable to have as few corrections as possible because any uncertainties will be carried through into the final production rate calculations at the end of the study.

The individual sample sites were chosen based on desirable characteristics decided upon by the CRONUS-Earth committee. These characteristics include high relative topographic location to avoid shielding from ash, soil, or nearby objects, original surface texture to avoid eroded samples, and a sample location which is not near edges or cracks to avoid edge effects. The high relative topography is important to make sure that there are no shielding corrections for either topography, such as nearby tumuli or slopes, or cover by other material, such as pyroclastic material from

eruption or soil (GOSSE and PHILLIPS, 2001). The covering material is usually blown off of topographic highs and accumulates in the depressions in the landscape (ZREDA, 1994). While sampling, it is generally possible to avoid obvious depressions where accumulation might be a problem. Ideally, only samples with zero erosion would be collected. The closest we can get to this ideal situation is to sample only those areas that have original surface texture. If the original surface texture, such as pahoehoe ropes or wave polish, is preserved, it is clear that little erosion (< 1 cm) has occurred at that particular location (CERLING and CRAIG, 1994b). Finally, in order to get samples that are not near edges (GOSSE and PHILLIPS, 2001), a rock saw can be used to take samples from the center of boulders or tumuli. If there are cracks, chisels can also be used, but can be unfeasible if there are no natural crevices. Also, a rock saw provides a more consistent depth, which helps to reduce uncertainty in the final calculations.

### **3.3 Lake Bonneville Chronology**

Lake Bonneville was a large closed-basin lake during the late Pleistocene in the basin that is now occupied by the Great Salt Lake (Figure 8). Gilbert originally named Lake Bonneville as well as the several stages (labeled in Figure 9) that left lasting marks on the landscape (GILBERT, 1890). However, a detailed chronology of the fluctuations of the lake level between 30 C-14 ka and 12 C-14 ka was developed by Oviatt et al. (1992) using more than 80 radiocarbon dates (Figure 9).

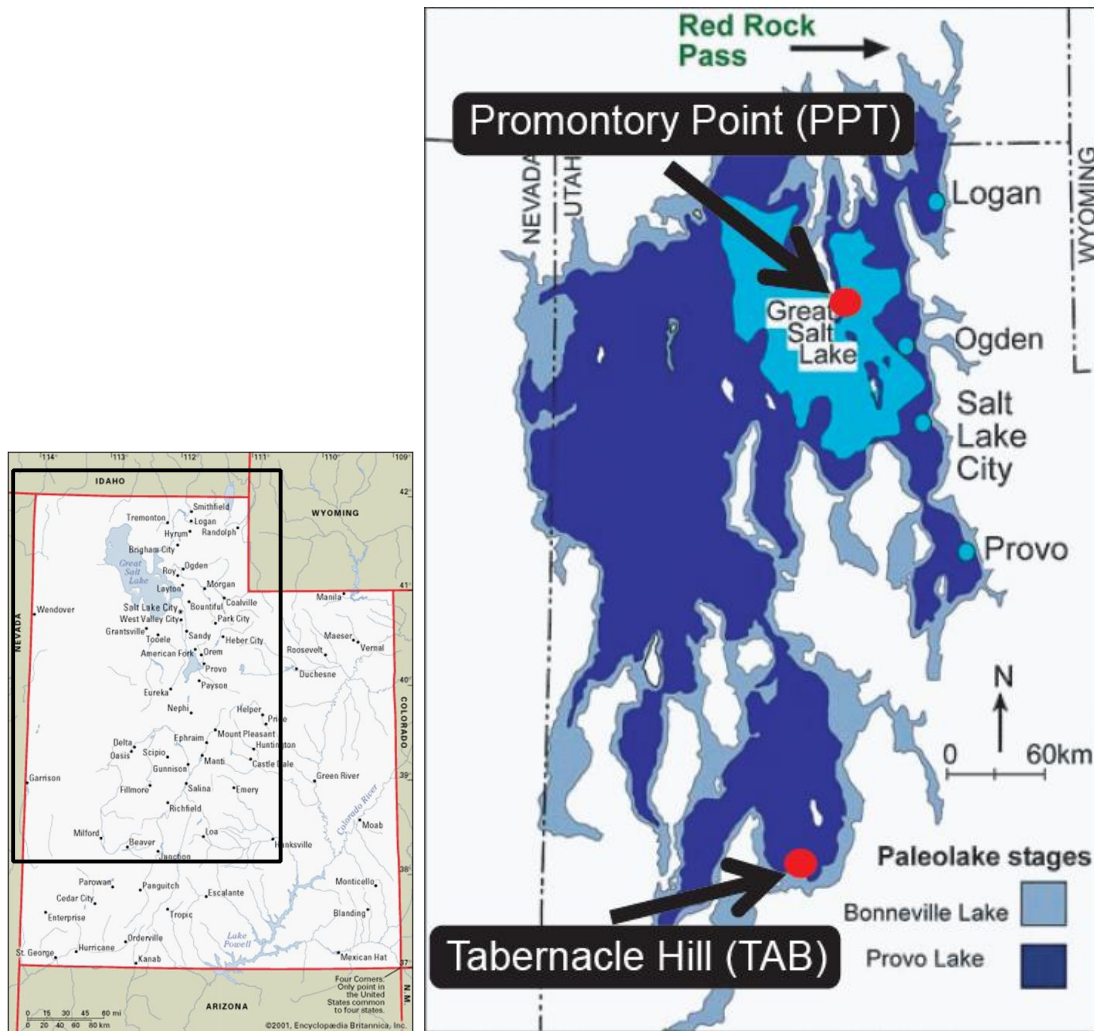


**Figure 8-(left)** A map of Utah with a box showing where the more detailed study area map is located (MERRIAM-WEBSTER, 2001). **(right)** Map of the current Great Salt Lake showing Bonneville extent. Modified from Digital Geology of Idaho, Idaho State University (IDAHO STATE UNIVERSITY, 2006). The two sample locations are shown by red circles and arrows.

Two sample sites were selected within the Bonneville basin: Promontory Point and Tabernacle Hill (Figure 8). The merits of each site will be discussed individually in a later section. These two sample sites are found on the Bonneville shoreline and the Provo shoreline, respectively, so the focus of this study is on the Bonneville and Provo stages of the lake history (between ~19-14 C-14 ka).

The first transgression events in the most recent lake chronology, between approximately 30-22 <sup>14</sup>C ka, have very little chronology information compared to the other phases of the lake history (OVIATT et al., 1992). After a period of relatively shallow occupation, the lake levels rose relatively quickly from a very low level (probably at or below the modern lake levels) to a mid-range lake level around 26.5 <sup>14</sup>C ka. The lake level oscillated over a vertical distance of about 45 m between 22-20 <sup>14</sup>C ka. The Stansbury shoreline was formed during these oscillations, also known as the Stansbury oscillation (see Figure 9).

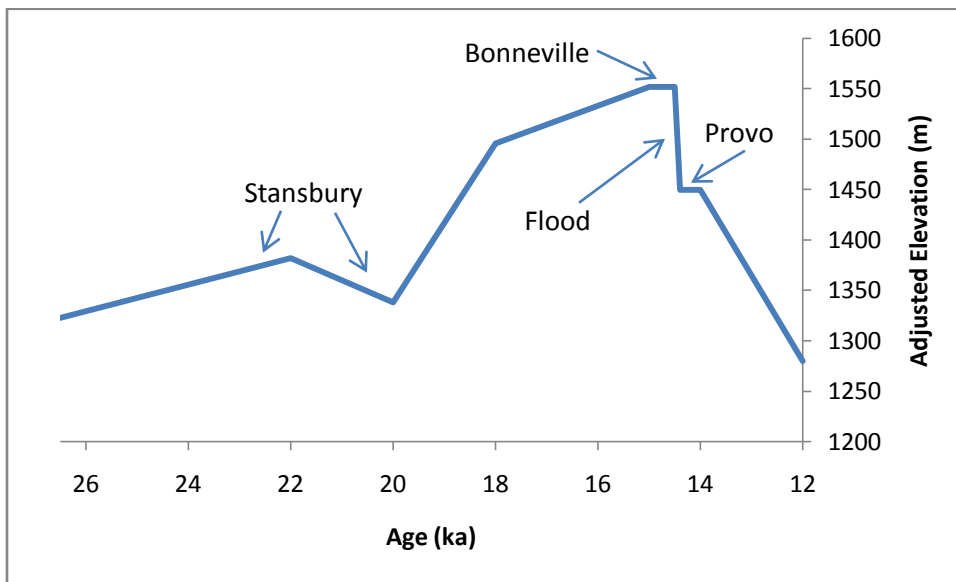


**Figure 9-Shoreline curve for Lake Bonneville (modified from OVIATT et al., 1992). The ages given here do not correspond to the ages provided in the table due to the use of carbon-14 ages here and the use of cal years in the table. This curve is designed to show the relative shoreline curve for the history of the lake. The labels represent the named shorelines and the major flood event.**

The final transgression leading to the Bonneville stage began around 20 C-14 ka (OVIATT et al., 1992). Based on lake cores, there were several smaller-scale (30-50 m) fluctuations in lake level during the transgression. However, none of these smaller fluctuations are evident at the large-scale shoreline level (OVIATT, 1997). At the end of this transgression, the lake reached its highest elevation at 1552 m. The

highest shoreline, the Bonneville shoreline, formed at this elevation when the lake level stabilized (OVIATT et al., 1992). At this point, the lake was very large, with an area of more than 52,000 km<sup>2</sup> (32,000 sq. miles) (DEGREY et al., 2008) and a depth of over 330 m (1000 feet) (UTAH GEOLOGICAL SURVEY, 2008). The lake was large enough that waves with sufficient energy to erode bedrock were created along the fetch of the lake. The large waves allowed the lake to cut deeply into the surrounding bedrock through wave action despite the relatively short (< 1.7 kyr) occupation of the shoreline at this elevation (OVIATT and MILLER, 2005).

A period of intermittent overflow at Red Rock pass was initiated no earlier than 15.3 <sup>14</sup>C ka based on radiocarbon data (OVIATT et al., 1992). This type of overflow may have continued for up to 500 years before the threshold at Red Rock Pass (Figure 8), an alluvial fan dam, failed and the catastrophic Lake Bonneville flood engulfed the Snake River plain to the north of the lake (OVIATT et al., 1992). During this flood event, the lake level dropped approximately 100 m very rapidly releasing almost 5000 cubic km of water (DEGREY et al., 2008). Afterwards, the lake level stabilized at the elevation of the bedrock sill at Red Rock pass and the Provo level shoreline formed. During the stabilization period, the intermittent overflow probably continued (OVIATT et al., 1992).

Sometime shortly after the flood, but during the Provo shoreline occupation, the Tabernacle Hill basalt erupted into the Provo stand of the lake. It is clear from pillow basalts around the margin of the flow and other geologic evidence, that the basalt erupted into a lake approximately at the level of the Provo shoreline (OVIATT and NASH, 1989). However, there is no evidence on the top of the basalt to indicate

that it was ever completely covered by the lake, indicating that the eruption occurred after the Bonneville flood event. This unique geological situation provides an excellent calibration site.

After the establishment of the Provo shoreline, the basin closed and a rapid shoreline regression began. There are alternative opinions that the Provo shoreline was occupied during both transgressive and regressive phases (SACK, 1999) or that the Provo level was occupied for a much longer period than originally thought (GODSEY et al., 2005). However, the exposure history of the Tabernacle Hill basalt is unaffected by these alternative opinions because the eruption occurred very early in the Provo shoreline history and an eruption during the transgressive phase would have shown evidence of eventual cover by water from the Bonneville shoreline occupation. Although the chronology is not completely constrained, it is clear that the lake dropped to very low levels, possibly lower than the modern Great Salt Lake, by approximately 12 <sup>14</sup>C ka (OVIATT et al., 1992).

### **3.3.1 Radiocarbon constraints on the Bonneville and Provo Shorelines**

The chronology presented above is considered to be one of the most reliable in the world for a Pleistocene lake (OVIATT et al., 1992). Although there are numerous radiocarbon ages providing constraints on the different lake level stages, there are a few very important dates that delimit the particular events of interest. These important ages are discussed here in detail.

Very little is known about the beginning of the occupation of the Bonneville shoreline. There is a single <sup>14</sup>C date on the charcoal of a pre-Bonneville soil (#19 in Table 5) which limits the beginning of occupation to no earlier than 18.9 cal ka

(OVIATT et al., 1992; OVIATT and MILLER, 2005). This piece of charcoal was from a pre-Bonneville soil and was located under a barrier spit near Kanosh, UT and was approximately 6 m below the crest of the spit. There are other radiocarbon ages from Bonneville shoreline tufa and fossils that are close to 18.5 cal ka (see #11-13 in Table 5) that support occupation by this time (GODSEY et al., 2005; OVIATT et al., 1992). Based on this information, the oldest conservative limit for the initial occupation of the Bonneville shoreline is 18.9 cal ka, although the occupation may have begun slightly later.

The  $^{14}\text{C}$  ages constraining the exposure age at Promontory point, which is the end of the wavecutting event and the abandonment of the shoreline, are based on the age of the Bonneville flood itself. Although there are overlapping dates for the end of the Bonneville shoreline and the beginning of the Provo shoreline (OVIATT and MILLER, 2005), estimates of the flood age between these shoreline stages can be made statistically based on the surrounding radiocarbon dates. The age of the Bonneville flood was calculated by Borchers (personal communication, 2005) using a maximum likelihood estimate based on 19 radiocarbon ages. Based on the location of the radiocarbon material, it is known that 10 of the ages postdate the flood while 9 of the ages predate the flood. The pertinent radiocarbon ages, calendar ages, locations, and other relevant information is listed in Table 5. For this analysis, ages 1-10 are after the flood event at age  $t$ , and ages 11-19 are before the flood event at age  $t$ . The probability distribution for each one of the radiocarbon ages is based on the calibrated output of Calib 5.0 (STUIVER et al., 2005) and is shown in Figure 10. The equation for the maximum likelihood ( $L$ ) that the flood occurred at time ( $t$ ) before present is

shown in Equation 42. This equation assumes that each radiocarbon age is independent.

**Equation 42**

$$L(t) = P(\text{age 1 after } t) * \dots * P(\text{age 10 after } t) * P(\text{age 11 before } t) * \dots * P(\text{age 19 before } t)$$

Each of the results from the likelihood equation (Equation 42) was plotted and the results were normalized. The normalized plot is shown in Figure 11. The most probable date of the flood was 17.4 cal ka. The uncertainty on the age,  $t$ , was found by determining the 68% confidence interval based on the normalized probability, which gives the age range 17,179 to 17,607 cal yr within the 68% (or 1 sigma) confidence interval.

A very similar result for the Bonneville flood age was obtained by Balco (personal communication, 2005) using a Monte Carlo analysis of the same 19 ages. The 68% confidence interval results were 17,180-17,605 cal yr, or less than 1% different from the maximum likelihood calculation. Based on the essentially identical age result from two independent methods, I take the age of the Lake Bonneville flood event, and thus the exposure age of the Promontory Point site, to be  $17.4 \pm 0.2$  cal ka. This result also limits the total occupation of the Bonneville shoreline at Promontory Point to less than 1.5 kyr.

**Table 5-Radiocarbon information for ages used in Bonneville flood calculations (modified from OVIATT and MILLER, 2005).**

#	Lab ID	C-14 age	C-14 Error	Cal year Min	Cal year Max	Lake Level	Material	Elevation (m)	Stratigraphic Interpretation	Reference
1	1 B-15316	13110	50	15198	15847	at	Gastropods	1420	backshore muddy sandy gravel	(GODSEY et al., 2005)
2	AA-19045	13290	115	15313	16240	up	<i>Fluminicola</i>	1426	sandy spit just below Provo shoreline	Light, 1996
3	B-159810	13580	40	15807	16563	up	Gastropods	1436	14m below Provo shoreline	(GODSEY et al., 2005)
4	B-153158	13660	50	15919	16675	at	<i>Stagnicola</i>	1435	1.5m below Provo shoreline	(GODSEY et al., 2005)
5	WW4147	13705	40	15985	16713	up	<i>Stagnicola</i>	1412	sandy marl 30 m below Provo shoreline	*Miller & Oviatt, unpublished
6	AA-19040	13850	115	16065	16949	up	<i>Stagnicola</i>	1427	Bear River delta graded to Provo shoreline	Light, 1996
7	W-899	13900	400	15456	17891	up	mollusk shells	1426	Bear River delta graded to Provo shoreline	(*BRIGHT, 1963; *RUBIN and BERTHOLD, 1961)
8	WW4148	14090	40	16397	17138	up	<i>Stagnicola</i>	1412	sandy marl 30 m below Provo shoreline	*Miller & Oviatt, unpublished
9	AA-19059	14290	125	16559	17672	up	<i>Stagnicola</i>	1439	sand just below Provo shoreline	Light, 1996
10	B-23803	14320	90	16640	17605	at	Tufa	1436	Provo shorezone	(OVIATT and NASH, 1989)
11	B-50770	14420	370	16334	18557	up	<i>Stagnicola</i>	1535	5m below Bonneville B1 shoreline	(GODSEY et al., 2005)
12	B-146004	14730	140	17215	18516	up	<i>Stagnicola</i>	1532	30m below Bonneville shoreline	(GODSEY et al., 2005)
13	SI-4227C	14730	100	17263	18481	at	tufa, innermost 18%	1552	Bonneville shoreline	(*CURREY et al., 1983; *Stuckenrath, R. pers comm. 1979)
14	B-39294	14830	160	17382	18619	up	<i>Stagnicola</i>	1525	sand 30 m below Bonneville shoreline	Oviatt et al.1994 (in press)
15	B-169099	15060	50	18098	18632	up	<i>Stagnicola</i>	1540	6m below Bonneville shoreline	(GODSEY et al., 2005)
16	B-156852	15080	90	18067	18673	up	<i>Stagnicola</i>	1530	just below Bonneville shoreline	(GODSEY et al., 2005)
17	B-151451	15080	90	18067	18673	up	<i>Stagnicola</i>	1527	20m below Bonneville shoreline	(GODSEY et al., 2005)
18	W-5261	15100	140	18018	18742	down	Wood	1538	transgressive lagoon/bar complex	(*SCOTT, 1988)
19	B-23174; ETH-3518	15250	160	18088	18861	down	Charcoal	1545	pre-Bonneville soil	(*OVIATT, 1991)

\*Indicates reference cited in Oviatt et al. (1992)

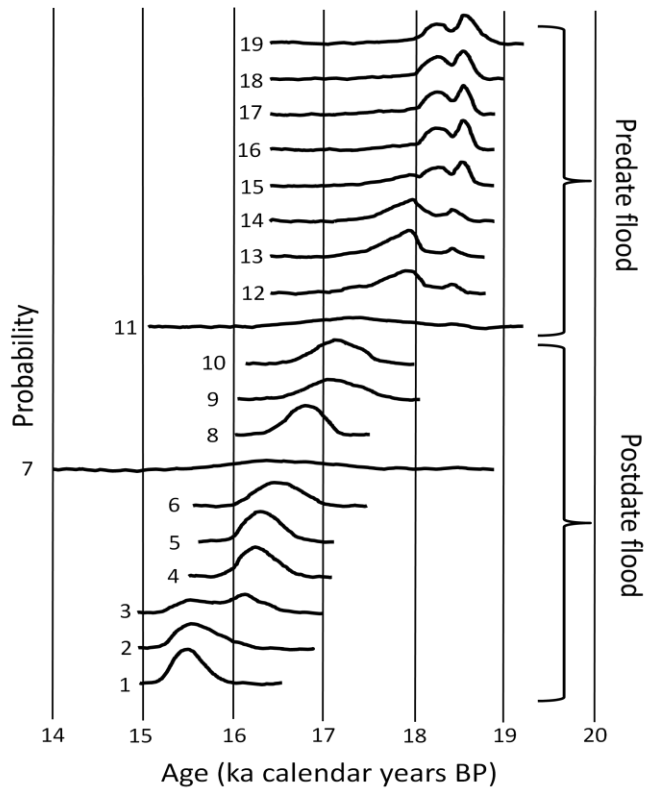


Figure 10-Calendar year probability distributions for the radiocarbon ages used in the Bonneville flood age analysis (Balco, pers. comm., 2005). The numbers correspond to the radiocarbon dates in Table 5. The probability density functions were created using Calib 5.0 (STUIVER et al., 2005). The y-axis is probability and the x-axis is calendar age BP. Sample numbers 1-10 postdate the flood and sample numbers 11-19 predate the flood event.

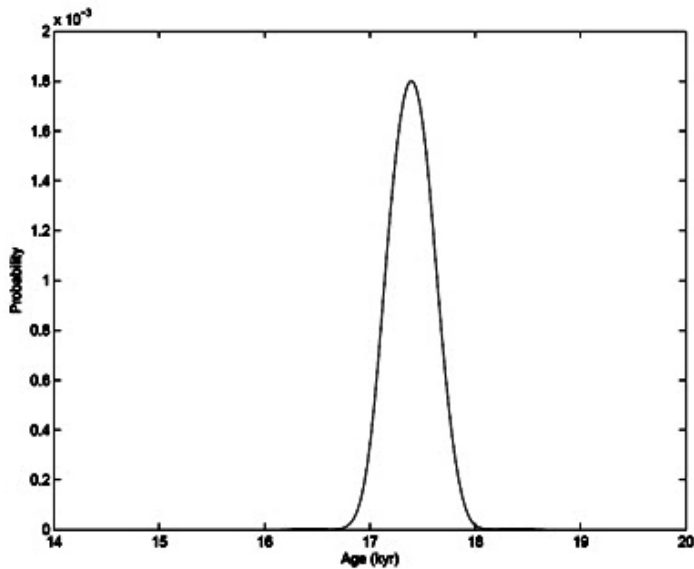
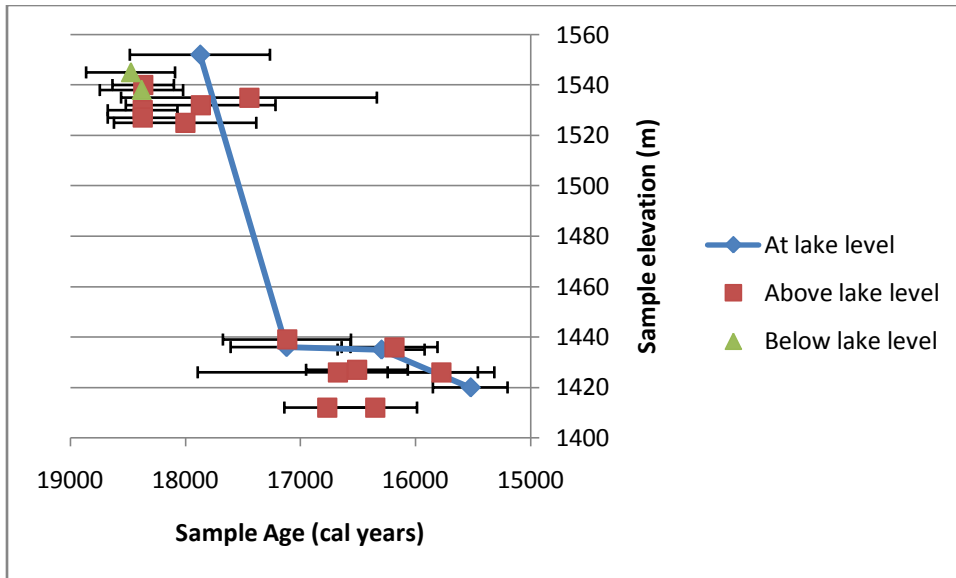


Figure 11-Probability density for the maximum likelihood function for the Bonneville flood age (Borchers, personal communication, 2005).



**Figure 12-Carbon-14 chronology for the Lake Bonneville shoreline using the 19 data points shown in Table 5. The Blue line connects the samples that are at the lake level. The ages correspond to the calendar year ages shown in Table 5.**

The age constraints on the Tabernacle Hill basalt flow are also well known. The Tabernacle Hill basalt erupted shortly after the retreat of Lake Bonneville to the Provo stage but before the establishment of the Provo stage features such as tufa (OVIATT and NASH, 1989). The Lake Bonneville flood, with an age of  $17.4 \pm 0.2$  cal ka as discussed above, provides the oldest limiting age on the Tabernacle Hill basalt.

Before considering the remaining Tabernacle Hill radiocarbon constraints, it is important to consider that not all radiocarbon dated materials provide the same level of confidence. Oviatt et al. (1992) provides a list of the datable materials in order of their reliability. In order of most to least reliable, the datable materials from the Bonneville area are wood, charcoal, dispersed organic matter, gastropod shells, ostracode valves, tufa, and other carbonates. However, each of these materials has both positive and negative aspects. For example, while wood and charcoal are preferred to carbonate

material, the interpretation of the exact depositional scenario is often considerably more difficult, introducing other possible uncertainties (OVIATT et al., 1992).

Radiocarbon dates on carbonates are advantageous, especially for tufas, because the exact depositional scenario is known. In these cases, no assumptions need to be made about when a tree died, for example, in order to complete the chronology. However, carbonates have other distinct disadvantages. The potential uncertainties include the hard-water effect, the inclusion of dead carbon in detrital grains, fractionation, and contamination by post-depositional contribution of young carbon (OVIATT et al., 1992). These problems can typically be avoided by careful collection and processing as well as a  $\delta^{13}\text{C}$  adjustment to account for fractionation (OVIATT et al., 1992). For the purposes of this study, only tufas that have undergone rigorous collection and cleaning are considered.

In general, tufas form as a result of both physico-chemical reactions and biologic activity at ambient temperatures (FORD and PEDLEY, 1996). While earlier ideas about tufa focused entirely on degassing of  $\text{CO}_2$  from the waters causing precipitation, it has since been shown that tufas commonly contain the remnants of bacteria and other biologic organisms (FORD and PEDLEY, 1996). Within the Bonneville lake basin, Provo shoreline tufa forms at approximately 1460 m elevation and occurs in three general forms: capping tufa, beachrock, or capping tufa over beachrock (FELTON et al., 2006). The tufa generally formed within the uppermost 10 m of the mean shoreline elevation and was typically found in areas of largest fetch of the lake (FELTON et al., 2006).

The tufa encrustations on the Tabernacle Hill basalt provide a radiocarbon constraint on the youngest possible age of the basalt. The tufa sample yielded an age of

14,320 ± 90 radiocarbon years B. P. (Beta-23803, OVIATT and NASH, 1989) or 16.6 to 17.6 cal ka (#10 in Table 5). This means the youngest possible age of exposure is 16.6 cal ka. Tufa ages can be problematic due to recrystallization issues so these samples were carefully collected and prepared as described by Oviatt et al. (1992). Essentially, the original tufa sample was collected from underneath an overhang, crushed to coarse sand size, and the outer 50% dissolved to remove any possible younger precipitates. Because the tufa formed on a basalt, which contains no carbon, the possibility of contamination from detrital carbon is also low (OVIATT et al., 1992). The flood age of 17.4 ± 0.2 cal ka and the tufa sample on the basalt with an age of 16.6 to 17.6 cal ka constrain the age of the basalt flow to 17.1 ± 0.5 cal ka.

This younger limiting age was reconfirmed using two tufa samples collected during the CRONUS-Earth sampling trip. The tufa samples were prepared using a similar method and sampling only the densest part of the tufa sample (Lifton, personal communication, Nov. 2, 2008). The results from the new samples have two sigma ranges of 13415-13697 cal years BP and 15372-16125 cal years BP (Lifton, personal communication, Nov. 2, 2008; STUIVER and REIMER, 1993; STUIVER et al., 2005). Although these samples do not further constrain the previously determined window of first exposure, the samples do support the published tufa information. These samples also appear to support Godsey's interpretation of extended Provo shoreline occupation after the Bonneville flood (GODSEY et al., 2005).

### **3.4 Promontory Point Site Description**

Promontory point is at the tip of a ridge feature on the north side of the current Great Salt Lake. The Bonneville shoreline cut very deep benches into the rocks in this

area leaving large cliffs after the abandonment of the shoreline (see Figure 13 and Figure 14). Based on the height of the remaining cliffs, erosion removed large amounts of material, on the scale of tens of meters, from this area during the Bonneville shoreline occupation (LIFTON et al., 2001). Joints within the quartzite facilitated the erosion (LIFTON et al., 2001). The two formations present on this bench are the late Precambrian Mutual Formation and the early Cambrian Tintic Quartzite Formation (LIFTON et al., 2001).



**Figure 13-Foreground shows the wavecut bench where samples were taken. Background shows other wavecut benches (Photo by Nishiizumi, 2005).**

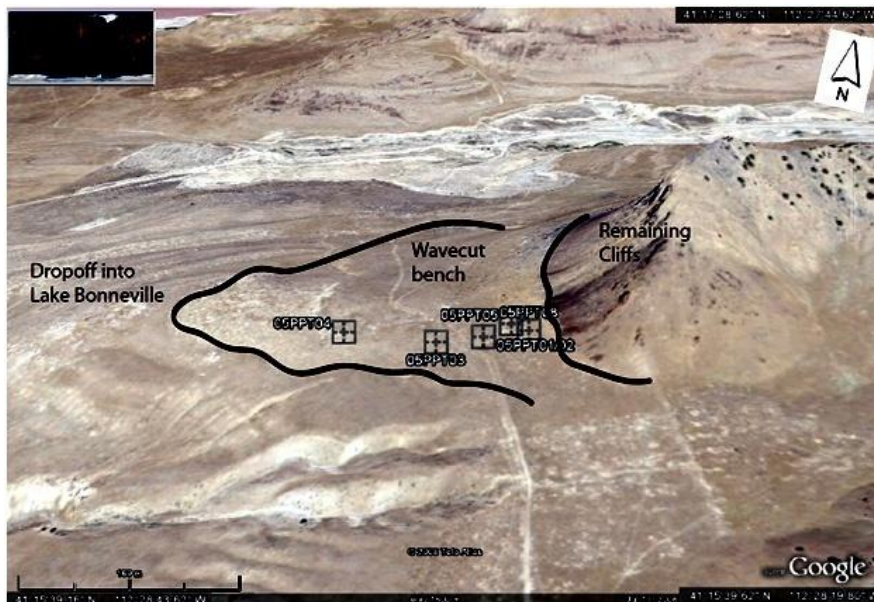


**Figure 14-Promontory Point map showing the approximate outline of the remaining cliff (the base of which is shown in black on the far right), the approximate lake edge of the wavecut bench (shown in blue on the far left), and the approximate transect along which samples were collected to make sure that the samples were not being influenced by inheritance or other factors dependent on position in relation to the cliffs. Samples plotted using Google Earth (GOOGLE, 2008).**

In order to quantify the characteristics of the site, the existing cliffs were used to estimate the amount of material removed and water depths during the shoreline occupation. These calculations are important because both of these factors could affect the inheritance at the site, primarily from muons. The penetration of muons through the rock was calculated based on the previous amount of material that was assumed to have covered the site. This is calculated to be >40-50 m of overburden (LIFTON, 2005). Although Lifton (2005) performed this calculation for the muogenic production of beryllium-10, the muon penetration is independent of the nuclide so the percentage differences should be directly applicable to chlorine-36. At 40 m of overburden, with an assumed pre-exposure time of  $1 \times 10^7$  years and a low erosion rate of 0.1 mm/kyr, the percentage difference between  $^{10}\text{Be}$  production from both pre-exposure and 18 kyr of exposure after erosion compared to only the production from 18 kyr exposure is about 6.5%. This is a maximum value only and a more realistic value is probably a difference of 3% or less. These uncertainties have been neglected in these calculations until a more rigorous computation can be performed for chlorine-36 based on the actual sample locations instead of a generic location, as was done for these calculations.

A similar issue exists for the depth of water above the samples after the bench was cut. Water above the sample locations would reduce the production of the samples due to absorption of the cosmic rays by the water. The water depth is estimated to range from an average value of about 10 m to a maximum value of 17 m based on the fine-grained deposits in locations above the wavecut benches (LIFTON, 2005). Unfortunately, it is more difficult to constrain the duration of the water cover, although a reasonable estimate of 500-2000 years can be made based on the carbon-14 dates in the area

(LIFTON, 2005). Using these values, Lifton (2005) calculated the difference in production due to the presence of water to range between 2.7% to a maximum of 11%. The most realistic values are probably less than 5%. Once again, this uncertainty will be addressed in the future using a more rigorous model, although the overall uncertainty is expected to be small. The erosion of the cliff also presents a problem with the exact time of exposure because bedrock further from the cliff may have been exposed earlier than the samples closer to the cliff face. In order to collect samples with the fewest possible problems, bedrock closest to the cliff was more desirable because this minimizes the possibility of inheritance. In this case, the shielding corrections necessary due to this sampling procedure introduce less uncertainty to the overall age calculation than the possible inheritance issues present at greater distances from the cliff face.

Based on the considerations above, it is clear that there is less possibility for inheritance at the most recently eroded areas, i.e. the areas closest to the cliff. These areas should have been eroded last and exposed to fewer cosmic rays due to a shorter exposure time and more initial rock cover. Ideally, the sampling of the bench would have been restricted to bedrock areas near the cliff because bedrock is subject to less variation in exposure history than boulders. Unfortunately, there was a lack of bedrock close to the cliff so some wave-polished boulders of similar lithology to the cliff were sampled as well in the hopes that they were eroded out close to the end of the Bonneville shoreline occupancy. 05PPT08 is an example of one of these boulders. Ultimately, samples along a transect from the cliff base to the farthest point on the bench were analyzed to determine if there is an issue with the inheritance due to different exposure ages from

erosion. This general sample transect is shown in Figure 15 and sample positions relative to each other are shown in Figure 16.

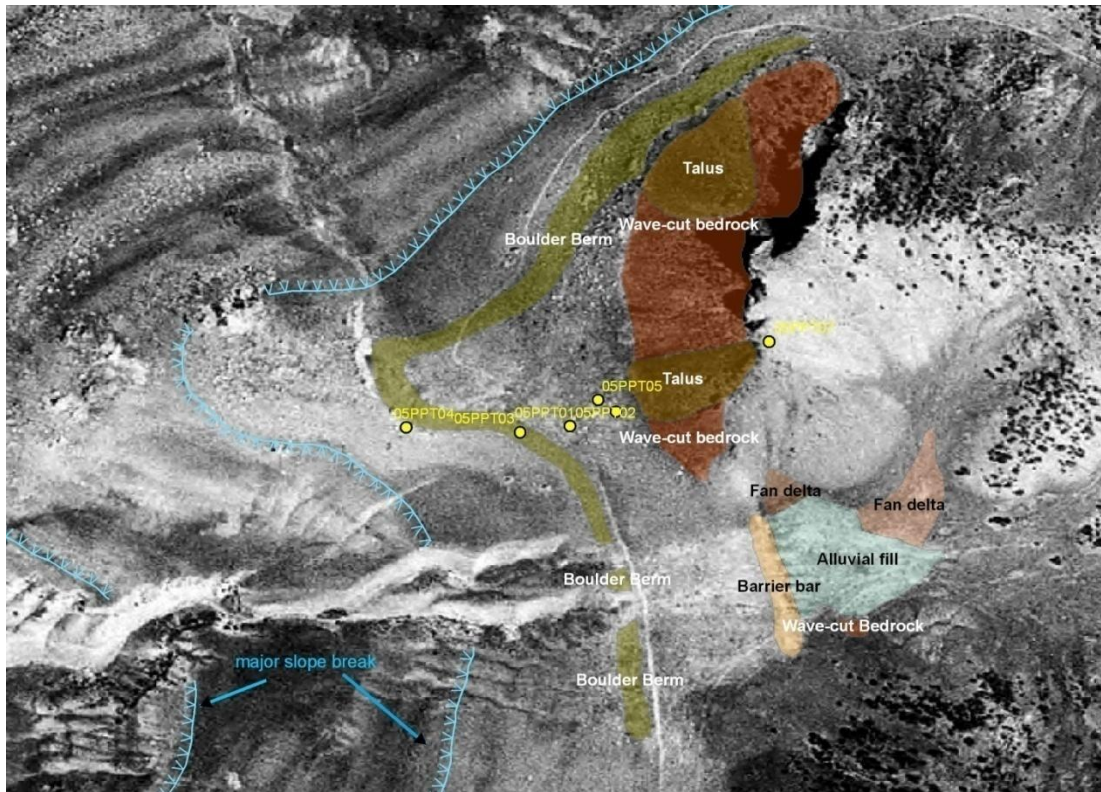


Figure 15-Promontory Point sample locations (yellow dots) shown on a geomorphic surface map (Mapping by F. M. Phillips, 2005).



Figure 16-Photo showing Promontory Point sample positions relative to each other (Photo by Nishiizumi, 2005).

Promontory Point sample locations were chosen based on sample characteristics as described above. Although much of the bedrock had very little topography (the sampled surface was sometimes less than 0.5 m above the surrounding topography), all attempts were made to sample only those bedrock outcrops that were topographic highs of the landscape. Figure 17 shows an example of a sampled outcrop. Once again, samples on or near edges or large cracks were avoided to reduce any geometric issues or edge effects. Finally, the original surface texture, in this case indicated by a wave-polished patina on the sample, was sought out to reduce effects associated with erosion. The wave-polish only survives as long as there is essentially no erosion of the surface.



**Figure 17-Marc Caffee Sampling Promontory Point quartzite bedrock outcrop (Photo by F. M. Phillips, 2008). Note: person sampling is standing on wave-polished surface.**

Descriptions for each sample, including photographs, coordinates, composition, and other pertinent sample information have been included in the appendix in sections 8.1 and 9.2. Sample 05PPT04 is a large bedrock exposure at the lake end of the wave-cut bench. Sample 05PPT05 is one of the light-colored quartzites closest to the talus slope.

For the calibration exercise, Promontory Point provides a unique opportunity to examine chlorine-36 calibration rates. One sample collected from the site had very low potassium and calcium concentrations, which isolates the thermal neutron production pathway. In general, the Promontory Point quartzite is very low in calcium, which allows for calibration of the production from potassium and thermal neutron absorption pathways. The constraints on the production pathways will help with the identification of problems with the current production rates as reported in the literature and discussed in section 2.2.

### ***3.5 Tabernacle Hill Site Description***

The Tabernacle Hill basalt flow, southwest of Salt Lake City and the current Great Salt Lake, is a basalt flow erupted shortly after the retreat of Lake Bonneville to the Provo stage. The flow, originally described by Gilbert (1890), is an approximately circular basalt flow (see Figure 18) with a central crater and surrounded by an asymmetrical tuff cone and smaller cinder cones (OVIATT and NASH, 1989). The basalt flow covers approximately 17 km<sup>2</sup> (6.5 mi<sup>2</sup>).

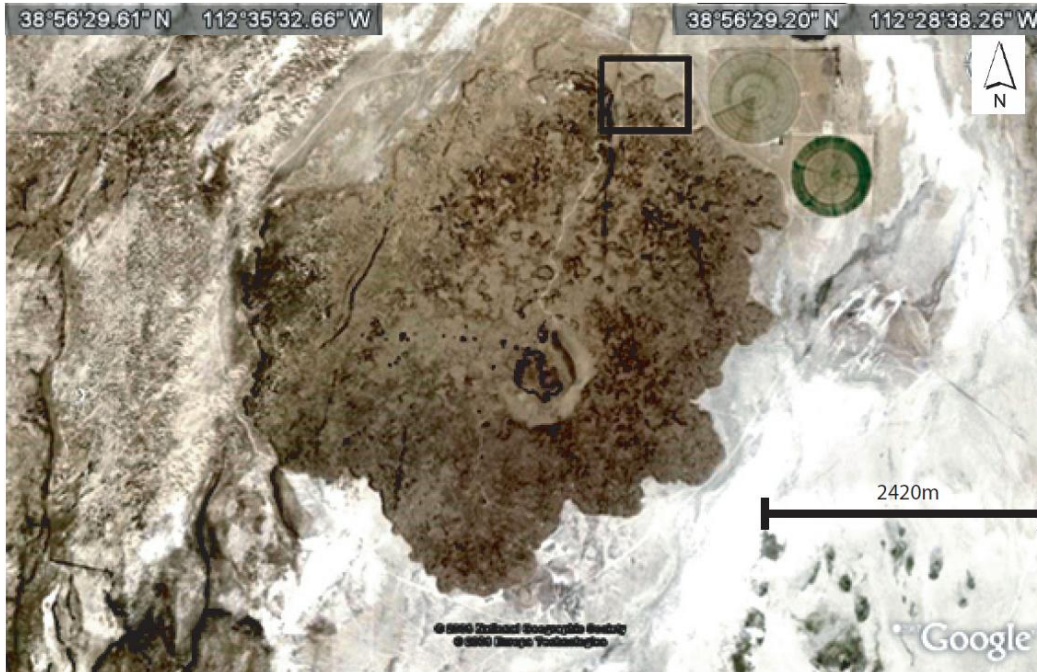


**Figure 18-Tabernacle Hill basalt flow (satellite image from Google Earth) (GOOGLE, 2008). The sample area is indicated by a box and details are shown in Figure 20. Coordinates shown across the top represent the approximate location of the top corners.**

Several faults, typically trending NNE, cut the basalt (see Figure 19). One of the larger faults cuts the basalt flow in the northern area and appears to have facilitated the opening of a vent (see Figure 19 and Figure 20). Pyroclastic debris spewed from the primary vent at the center cone and covered a significant local area based on the areal extent of the deposits found in the Lake Bonneville lacustrine deposits (OVIATT and NASH, 1989). The smaller vent in the north also has basaltic tuff and probably covered a more localized area with pyroclastic material.

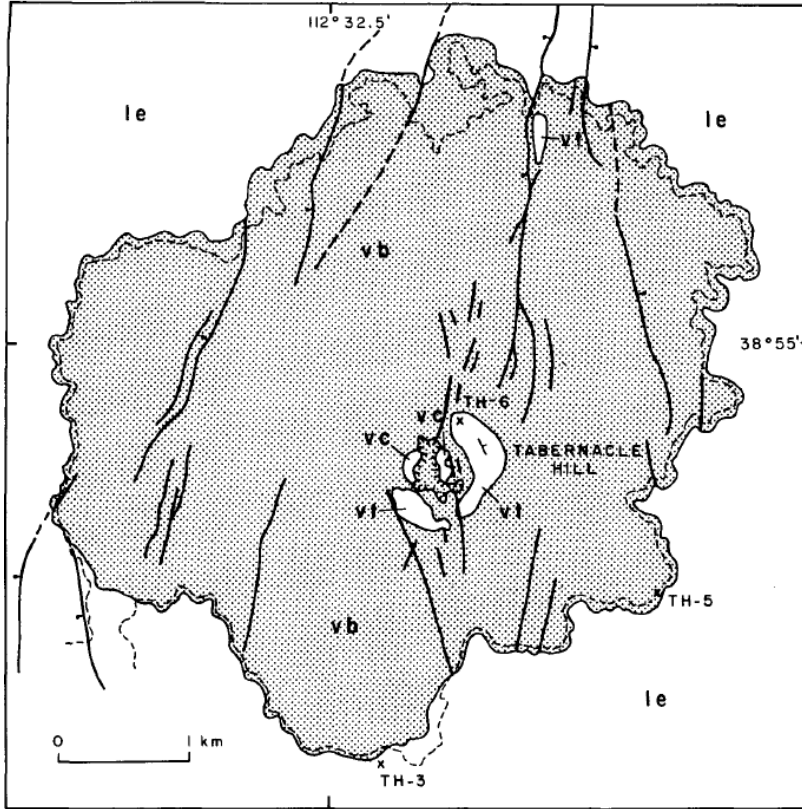


Figure 19-Geologic map of Tabernacle Hill basalt flow showing faults, basaltic tuffs (vt), basalt (vb), and lacustrine/eolian deposits (le), and scoriaceous cinders (vc) (OVIATT and NASH, 1989). The dashed line is the 1445 m contour line.

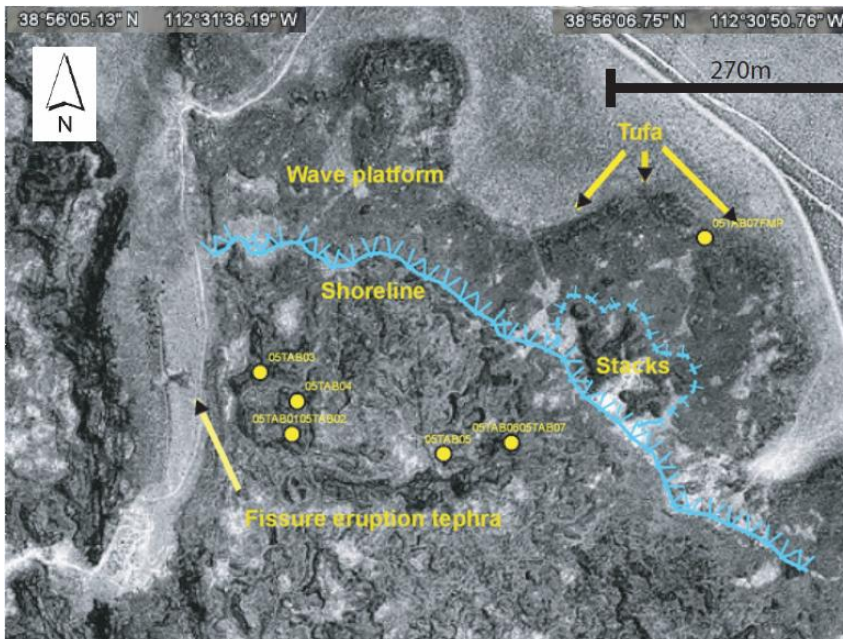


Figure 20-Locations of samples on the basalt flow. Other important features, such as tufa and the wave platform, are labeled. The area that looks stippled is the basalt while the surrounding, uniform terrain is the surrounding plains (Mapping by F. M. Phillips, 2005).

According to the description by Oviatt and Nash (1989), there are several features that indicate that this basalt flow was erupted into water including rounded pillows with glassy external texture and coarser internal texture, wave-rounded cobbles and boulders, and the uniform altitude of the outer edge. The best evidence for eruption into water is the pillow basalts, which traditionally have a distinct fast-cooled outer portion with a glassy texture and a slower-cooled internal crystalline structure (PRESS and SIEVER, 2001) as seen at Tabernacle Hill. The altitude of the outer edge is 1445 m, which is approximately 3 m lower than the known Provo shoreline nearby, although this difference could be due to incomplete isostatic rebound or magma chamber subsidence (OVIATT and NASH, 1989). Because there is no evidence of eruption into water on the top of the flow, it is clear that this eruption occurred after the flood that lowered the lake level from the Bonneville to the Provo stage.

The classification of the Tabernacle Hill central cone as a tuff cone is further evidence for the presence of a lake closet to the base level of the vent when it erupted. A tuff cone must erupt into a shallow body of water in order for the distinctive identifying features to form (CAS and WRIGHT, 1988). A tuff cone has a typical sequence of deposits as well as a particular geometry (CAS and WRIGHT, 1988). This sequence typically includes volcanic breccias, followed by surge deposits intermixed with minor air-fall deposits, subsequently covered by massive air fall tuff or lapilli deposits, with the sequence capped by surge deposits. The typical geometry of the tuff cone includes steep inner and outer slopes, a small cone diameter, and a crater floor that is above the surrounding terrain. In this case, according to Oviatt and Nash (OVIATT and NASH, 1989), the Tabernacle Hill fissure eruption displays characteristics that are consistent

with classification as a tuff cone, and therefore it was probably erupted into, or on the margin of, shallow water. In addition to the classification as a tuff cone, Condie and Barsky (1972) note the partially to completely cemented tuff-breccia of the outer cone indicating probable eruption into water.

During the Provo shoreline occupation, the margins of the basalt flow were bombarded by waves causing the erosion of the edges and resulting in the presence of rounded cobbles at the wave margins (OVIATT and NASH, 1989). The constant-elevation margin is at the Provo shoreline elevation, clearly indicating the water level. The occupation of the Provo shoreline over the years also allowed for the formation of tufa on the outside edges of the basalt flow. Tufa forms only near the surface of a lake due to the turbidity necessary to help precipitate the carbonate. In the Lake Bonneville area, the tufa encrustations typically form in areas undergoing erosion and areas that have little sediment input (FELTON et al., 2002; FELTON et al., 2006). This bolsters the other evidence for the shoreline at the Provo level.



**Figure 21-Tufa encrustation on Tabernacle Hill basalt flow (Photo by F. M. Phillips, 2005).**

Samples were collected from the north side of the volcanic cone to the east of the fissure-eruption tephra. The samples were collected within 500 m of each other in an attempt to obtain samples that would be uniform in composition and exposure history. Samples were collected from areas at the tops of the tumuli (see Figure 22) in order to eliminate the need for a significant shielding factor and the possibility of cover by soil or pyroclastic material. Previous work by Stone (STONE et al., 1996) showed little evidence of tephra cover based on his measurements. Eolian cover is a known problem for the western part of the flow, so this area was also avoided (LIFTON, 2005). The samples were also taken well away from any edges or cracks in order to reduce edge effects or other geometrical considerations. A rock saw was commonly used to collect samples from the middle of the tumulus (see Figure 22). Finally, the original surface texture of pahoehoe ropes (see photos in appendix 9.1) was used to distinguish samples that had undergone

very little erosion. Seven basalt samples were collected along with one tufa sample. These samples are labeled 05TAB01, 05TAB02, etc. Individual sample information, including photos, GPS coordinates, and shielding information, is included in the appendix in 8.2 and 9.1.



**Figure 22-(left) Tabernacle Hill basalt tumulus and (right) using a rock saw to collect a sample.**

### **3.6 Chemical Processing**

The original rock samples were taken to the PRIME Lab in Indiana where the samples were photographed in detail and weighed. Density determinations were also performed on the samples in the laboratory. Part of the sample was crushed to the fine sand size and homogenized using a commercial sample splitter according to the procedure outlined in the appendix in 10.1. The rest of the sample was archived as whole rock for future tests or other unforeseen needs. The homogeneous aliquots were mailed to the participating laboratories.

Using the homogenous aliquot in the lab, a sample was split out using a cone-and-quarter technique (described in section 10.4.4) to obtain a representative sample for analysis (referred to as “trial 1” throughout this study). When a duplicate sample needed to be run, the cone-and-quarter technique was used on the remaining original aliquot to

obtain the second sample (referred to as “trial 2”). The samples were chemically prepared in the laboratory in Socorro, New Mexico, using the procedure outlined below. This procedure was modified from Zreda (1994). The entire process is described in detail in the appendix in section 10.

The samples were leached with dilute nitric acid to remove meteoric chloride (STONE et al., 1996). Using the cone-and-quarter technique, a small fraction of the leached sample was split, powdered, and sent to other laboratories to determine the bulk rock composition. Analyses performed by other laboratories include XRF (X-Ray Fluorescence) analysis for total elements, XRF analysis for uranium and thorium concentrations, and NAA (Neutron Activation Analysis) for boron and gadolinium concentrations. No XRF aliquot was run for trial 2 samples because the samples were assumed to be homogeneous (see section 4.1 for detailed discussion).

Some of the leached and powdered sample was also used to measure the chloride concentration in each sample. The chloride concentration is used to estimate the amount of sample to dissolve and the amount of chlorine-35 spike to add. The chlorine-35 spike is an NaCl solution with the chlorine component being 99.6%  $^{35}\text{Cl}$ . The addition of this spike to the sample allows a very accurate measurement of the total chloride within the sample by employing the principle of isotope dilution mass spectrometry (IDMS) (DESILETS et al., 2006a). The in-house measured chloride concentration is used only to provide a basis for estimating the masses of rock and spike to use in the dissolution and the more accurate IDMS results are used in the final age calculations. The in-house chlorine measurement employs an ion-specific electrode to measure the Cl concentration in a two-ring diffusion cell (ARUSCAVAGE and CAMPBELL, 1983; ELSHEIMER, 1987).

The measured chloride concentrations were used in conjunction with two computer programs to calculate the amount of sample to dissolve and the amount of chlorine-35 spike to be added. CHLOE (PHILLIPS and PLUMMER, 1996), a surface exposure age calculator, was used to estimate the  $^{35}\text{Cl}/(\text{total Cl})$  ratio using the inputs of estimated age and erosion rate. Then an in-house program called LabCalcs was used to estimate the rock and spike amounts to dissolve based on the estimated  $^{35}\text{Cl}/\text{total Cl}$  ratio and the total Cl concentration. This calculation is necessary to ensure that the final sample ratios will be within the optimum measurement capabilities of the AMS facility.

The sample was weighed out using the cone-and-quarter technique and then the spike was weighed and added to the sample. The sample was then dissolved using nitric and hydrofluoric acids to release the Cl from the rock. After dissolution, silver chloride (AgCl) was precipitated out of the dissolved sample and purified through successive dissolutions and reprecipitations. Sulfur, an interfering isobar of  $^{36}\text{Cl}$  during AMS analysis, was removed through precipitation of barium sulfate during the purification steps. Finally, the silver chloride samples were rinsed, dried, packaged, and sent to the AMS laboratory for analysis.

### **3.7 Interpretation of the AMS results – CHLOE**

The measurements made at the AMS (Accelerator Mass Spectrometry) facility include the R/S ( $^{36}\text{Cl}/\text{total Cl}$ ), S/S (the stable/stable ratio which is the  $^{35}\text{Cl}/^{37}\text{Cl}$  ratio), and the measurement uncertainty associated with each of these values for each sample. Once AMS results were received, they were interpreted using the program CHLOE (PHILLIPS and PLUMMER, 1996). CHLOE is an Excel program that includes the coded cosmogenic nuclide production equations from Gosse and Phillips (2001) and has a

simple user interface for surface-exposure age calculations. Because several production rate sets were being compared, the chlorine-36 production rate parameters were not constant in the program. The production rate parameters used in CHLOE to calculate the ages for each set of production rates are shown in Table 6. The appropriate AMS information about the sample was entered into the spreadsheet and then the desired chlorine-36 production rate parameter set was selected on the parameter page. No other CHLOE parameters were modified for the production-rate comparisons.

**Table 6-Production rate parameters varied in CHLOE for each production rate scheme. The research group references are as follows: Phillips (PHILLIPS et al., 2001), Stone (EVANS, 2001; EVANS et al., 1997; STONE et al., 1996; STONE et al., 1998), and Swanson (SWANSON and CAFFEE, 2001).**

Production Rate	Ca [a/(gCa*yr)]	K [a/(gK*yr)]	P <sub>f</sub> (0) [neutrons/(g*yr)]
Phillips	66.8 ± 6.8	137 ± 60	626 ± 43
Stone	48.8 ± 3.4	170 ± 25	740 ± 63
Swanson	83.8 ± 5.0	211 ± 18	762 ± 28

The output of this program was the age of the sample in relation to erosion rate. Based on geological data, such as original wave-polished texture, there was a basis to assume very low erosion rates for all the samples (discussed further in sections 4.2 and 4.3). Using this information, the final result was the age of the sample for each of three production rate schemes. These ages were compared to determine which set of production rates yielded the closest agreement with the independent age data from the site.

The weighted-mean ages were calculated using the following formula (BEVINGTON and ROBINSON, 1992):

**Equation 43**

$$\mu = \frac{\sum \frac{x}{\sigma^2}}{\sum 1/\sigma^2} \text{ where } \mu = \text{uncertainty weighted mean, } x = \text{sample age, and}$$

$\sigma$  = one standard deviation sample uncertainty.

The uncertainty for the weighted mean was calculated using this formula (BEVINGTON and ROBINSON, 1992):

**Equation 44**

$$\sigma_{\mu}^2 = \frac{1}{\sum \left( \frac{1}{\sigma^2} \right)}$$

The weighted means were compared to the bounding carbon-14 ages to evaluate the different chlorine-36 production rate schemes.

**3.8 Calculations of New Production Rates**

The new production rates were calculated using a Matlab code written by Borchers (personal communication, 2007) and based on the equations in Gosse and Phillips (2001). The code was used to fit the production rate parameters for calcium, potassium, and thermal neutron production to the reproducible data using chi-squared minimization (see section 4.1 for a definition of “reproducible” as used in this study). An example of the type of equation is shown below for spallation production (based on LIU et al., 1994):

**Equation 45**

$$P_i(Z) = S_T(P_i)_0 \exp\left(\frac{-Z}{\Lambda_{f,e}}\right)$$

Where:

$P_i(Z)$  - Production within the sample at depth Z [atoms/ (g \* yr)]

$(P_i)_0$  – Normalized surface production rate [atoms/ (g \* yr)]

$S_T$  – Scaling factor [unitless]

$\Lambda_{f,e}$  - Effective fast neutron attenuation length [ $\text{g}/\text{cm}^2$ ]

The normalized surface production rate,  $(P_i)_0$ , on the right-hand side of the equation was changed while the actual production on the left-hand side of the equation was compared to the actual measured concentration within the samples. The differences between the calculated and measured concentrations were minimized to arrive at the new production rates.

The uncertainties in this method arise in several places. It is already known that the AMS uncertainties are not the only uncertainties in the cosmogenic method, although they are typically the only ones reported. There are not enough replicates in order to constrain the variability in the sample processing. A conservative value of 10% was used for the sample processing uncertainty. The probability distributions shown in Figure 10 were used to quantify the uncertainties in the carbon-14 ages. For this study, the age of the Tabernacle Hill basalt was taken to be 17.1 cal ka while the age for the exposure of the Promontory Point quartzite was taken to be 17.4 cal ka.

### **3.9 Reduced Chi-Squared Calculation**

In order to calculate the goodness of fit of the data to the independent age constraints, the reduced chi-squared metric was calculated. This metric is calculated based on the expected age (E) and the observed/calculated age (O). The chi-squared uses the uncertainty for each sample ( $\sigma$ ) to weight the sum of the sample results. The chi-squared ( $\chi^2$ ) is calculated using the following formula (BEVINGTON and ROBINSON, 1992):

**Equation 46**

$$\chi^2 = \sum \frac{(O-E)^2}{\sigma^2}$$

The reduced chi-squared ( $\chi_v^2$ ) value is calculated by dividing the original chi-squared value by the number of samples, minus the number of parameters that are being determined. The number of fitted parameters in this case is three because all three production rate parameters are being determined from the data. Ideally, the reduced chi-squared values should be around 1 if the data are close to the expected values (BEVINGTON and ROBINSON, 1992). Mathematically, this is represented below:

**Equation 47**

$$\chi_v^2 = \frac{\chi^2}{v} \quad \text{where } v = n-3$$

**3.10 Blank Correction**

A small blank correction was applied to all the sample results discussed in this study. This calculation corrects for  $^{36}\text{Cl}$  and stable chloride added to the sample during processing. The magnitude of the blank correction was calculated based on the amount of chlorine-35 spike and the quantities of reagents (such as hydrofluoric and nitric acids) added to the samples. Although the blank-subtraction calculations for this study used average values from blanks run in the laboratory, blanks were run for each batch of samples and the results for these blanks can be found in the appendix in chapter 12. A blank sample consists of a small sample of Week's Island halite, which contains very low amounts of chlorine-36, prepared in the same manner as the other samples. This blank sample is dissolved with similar quantities of reagents and spike as other samples. The blank corrections applied to the samples analyzed for this study were calculated based on the results of a systematic study of the chlorine-36 samples by isotope dilution mass

spectroscopy (IDMS). In the systematic study, Week's Island halite (see appendix in section 12) was analyzed in triplicate as sample blanks with spike and reagents, sample blanks without spike but with reagents, blanks with spike but without reagents, and blanks without spike or reagents (see THOMAS, 2005 for details). Based on this systematic analysis, it was possible to calculate the mass of chlorine as well as the atoms of chlorine-36 added to the sample from the reagents as well as that added from the spike. These calculations are explained in detail below.

To calculate the additional amount of chloride added to the sample as a function of the volume of reagents ( $Cl_r$ ), the known amount of chloride in the original blank solution ( $Cl^b$ ) was subtracted from the final amount measured in the blank sample after processing ( $Cl^a$ ). This value was then averaged and divided by the total volume of reagents used to prepare the sample ( $V_r$ ). The value obtained was  $1.6 \times 10^{-3}$  mg Cl added per milliliter of reagent used. The equation used to find this value is shown below in Equation 48.

**Equation 48**

$$Cl_r = \frac{(Cl^b - Cl^a)}{V_r}$$

Where units are:  $Cl_r$  – [mg Cl added/mL reagent used],  $Cl^b$  – [mg Cl],  $Cl^a$  – [mg Cl],  $V_r$  – [mL reagent].

To calculate the amount of  $^{36}\text{Cl}$  added by the processing and addition of the spike ( $Cl_{36s}$ ), the samples that had identical treatment except for the addition or lack of spike were compared. The total atoms of chlorine-36 in the sample were calculated for each sample. For the sample that had reagents but no spike added, an average value ( $Cl_{36o}$ ) for the samples was  $4.6 \times 10^5$  atoms of chlorine-36. This value is indistinguishable from

the samples that had no spike or reagents added and therefore represents the atoms of chlorine-36 added through the general processing of the sample in the lab and should be subtracted from each sample. The second part of the chlorine-36 correction pertains to the spike contribution. The average  $^{36}\text{Cl}$  value ( $\text{Cl}36_0$ ) was subtracted from the individual spiked sample chlorine-36 inventory ( $\text{Cl}36_{\text{spike}}$ ). This additional contribution is directly from the addition of the chlorine-35 spike. These values were divided by the individual mass of spike added ( $M_s$ ) and then averaged. This average value was  $1.3 \times 10^5$  atoms of  $^{36}\text{Cl}$  added/mg spike (as NaCl). The equation is shown below in Equation 49.

**Equation 49**

$$\text{Cl}36_s = \left( \frac{\text{Cl}36_{\text{spike}} - \text{Cl}36_0}{M_s} \right)$$

Where units are:  $\text{Cl}36_s$  – [atoms  $^{36}\text{Cl}$  added/mg spike (as NaCl)],  $\text{Cl}36_{\text{spike}}$  – [atoms  $^{36}\text{Cl}$ ],  $\text{Cl}36_0$  – [atoms  $^{36}\text{Cl}$ ],  $M_s$  – [mg spike (as NaCl)].

Using these values, the appropriate amount of chlorine or chlorine-36 was subtracted from each sample based on the amount of spike and processing acids used in the individual sample. In general, the hydrofluoric acid is added at a ratio of 2.5:1 (hydrofluoric acid (mL): sample mass (g)) while nitric acid is added at a ratio of 1:2 (nitric acid (mL): sample mass (g)). The amount of spike added to each sample varied based on the chemical composition of the sample, but it was typically between 1-5 mg.

The calculated chlorine concentration is actually the total chlorine concentration, which is defined here as the sum of rock and total processing chlorine. After converting the total chlorine concentration to a total mass in the sample ( $\text{Cl}_t$ ), the chlorine from the blank (processing chloride multiplied out for the volume of reagents used) was subtracted

from the total chloride, leaving only the rock chloride ( $Cl_{rock}$ ), as shown below in Equation 50.

**Equation 50**

$$Cl_t - (Cl_r * V_r) = Cl_{rock}$$

In order to return to the concentration of rock chloride instead of the mass of rock chloride, the rock chloride mass ( $Cl_{rock}$ ) was divided by the total sample mass ( $M_{rock}$ ) to yield the chloride concentration in the rock ( $Cl_{calc}$ ), as shown below in Equation 51.

**Equation 51**

$$\frac{Cl_{rock}}{M_{rock}} = Cl_{calc}$$

The R/S ratio returned from the AMS facility is defined as the ratio of chlorine-36 to total chloride for the spiked sample. This ratio is converted to units of atoms  $^{36}Cl$  from both the sample rock and the processing as shown in Equation 52.

**Equation 52**

$$R/S \times 10^{15} * Cl_t * \frac{1g}{1000mg} * \frac{1}{MW} * N_A = Cl36_{tot}$$

Where:

MW – Molecular weight [35.968 g/mol],  $N_A$  – Avagadro’s number [6.02 x10<sup>23</sup> atoms/mol],  $Cl_t$  – total chloride [mg], R/S – ratio of chlorine-36 to total Cl [unitless],  $Cl36_{tot}$  – total atoms of  $^{36}Cl$

The atoms of chlorine-36 added in the sample processing ( $Cl36_s * M_s + Cl36_0$ ) was subtracted from the total  $^{36}Cl$  to yield the total atoms of  $^{36}Cl$  from the original rock sample ( $Cl36_{rock}$ ):

**Equation 53**

$$Cl36_{tot} - (Cl36_s * M_s + Cl36_0) = Cl36_{rock}$$

To return to the R/S ratio of the rock, also referred to as  $R_m$ , the atoms of  $^{36}\text{Cl}$  were divided by the total chlorine in the sample (after some conversion) as shown in Equation 54. Note that the factor of  $10^{15}$  is used because ratios (which are usually on the order of  $10^{-14}$  or  $10^{-13}$ ) are reported as numbers times  $10^{-15}$  by the cosmogenic community.

**Equation 54**

$$R_m = \frac{Cl36_{rock}}{\left( Cl_{rock} * M_{rock} * \frac{1 \text{ g}}{1000 \text{ g}} * \frac{1}{MW} * N_A \right) x 10^{15}}$$

## 4 RESULTS

The chlorine-36 results from the CRONUS-Earth Lake Bonneville geological calibration site are presented here. The results from this study are composed of seven samples from the Tabernacle Hill site and six samples from the Promontory Point site, along with duplicates for each. For each sample, the age was calculated using the Phillips production rate (PHILLIPS et al., 2001) and a reasonable erosion rate based on geologic data in the field, which was less than 1 mm/kyr. These ages were used to calculate weighted mean overall site age. An overview table of results is presented in Table 7.

**Table 7-Results table showing all results from (a) Tabernacle Hill and (b) Promontory Point. The chloride concentration (ppm), the R/S ratio ( $^{36}\text{Cl}/\text{tot Cl} \times 10^{-15}$ ), and the atoms of  $^{36}\text{Cl}$  in the sample all refer to the values for the rock and not the spiked sample. The unit of ppm is used in lieu of mg/kg due to its use as the conventional unit in cosmogenic nuclide research.**

<i>a</i>	Cl conc (ppm)	R/S ratio	atoms $^{36}\text{Cl}$	<i>b</i>	Cl conc (ppm)	36/35 ratio	36 atoms
<b>05TAB01</b>	79	316	416471.8	<b>05PPT01</b>	62	231	210405.6
<b>05TAB01B</b>	86	290	415492.8	<b>05PPT01B</b>	46	298	210232.3
<b>05TAB02</b>	84	284	392389.4	<b>05PPT02</b>	38	365	218812.3
<b>05TAB02B</b>	92	283	427880	<b>05PPT02B</b>	50	280	210972.5
<b>05TAB03</b>	105	238	405144.1	<b>05PPT03</b>	41	278	173707.9
<b>05TAB03B</b>	109	244	432791.7	<b>05PPT03B</b>	57	148	114201.8
<b>05TAB04</b>	71	339	400265.6	<b>05PPT04</b>	41	221	132824.4
<b>05TAB04B</b>	75	326	405450.6	<b>05PPT04B</b>	43	213	134332
<b>05TAB05</b>	183	153	425056.5	<b>05PPT05</b>	44	323	215193.9
<b>05TAB05B</b>	68	335	370642.4	<b>05PPT05B</b>	40	271	162751.5
<b>05TAB06</b>	83	374	504908.2	<b>05PPT08</b>	115	153	230920.7
<b>05TAB06B</b>	88	260	366844.5	<b>05PPT08B</b>	114	150	222687.2
<b>05TAB07</b>	149	183	453824				
<b>05TAB07B</b>	120	219	436718.3				

#### **4.1 Discussion of Reproducibility**

Although these samples were processed with the utmost care, there were some fundamental problems with reproducibility of AMS results, and therefore calculated ages, from duplicate samples. The problem of reproducibility is serious. In Figure 23, the sample ages are plotted to show variations between duplicate samples. These duplicate samples were run in separate batches that were analyzed in fall 2005 for Tabernacle Hill trial 1, winter 2007 for Tabernacle Hill trial 2, spring 2007 for Promontory Point trial 1, and fall 2007 for Promontory Point trial 2. Ideally, all samples would plot along the 1:1 line shown on the graph. It is clear that this is not the case. There are several possible reasons for this including the investigator's inexperience with the laboratory technique, heterogeneity of samples, and the use of the blank. All these problems are discussed in

detail below, along with details of the new laboratory procedure that is now in place to resolve these issues and improve the reproducibility. It is expected that the new techniques recently implemented in the laboratory, such as the use of a splitter, will help to reduce laboratory errors and increase the reproducibility of the samples.

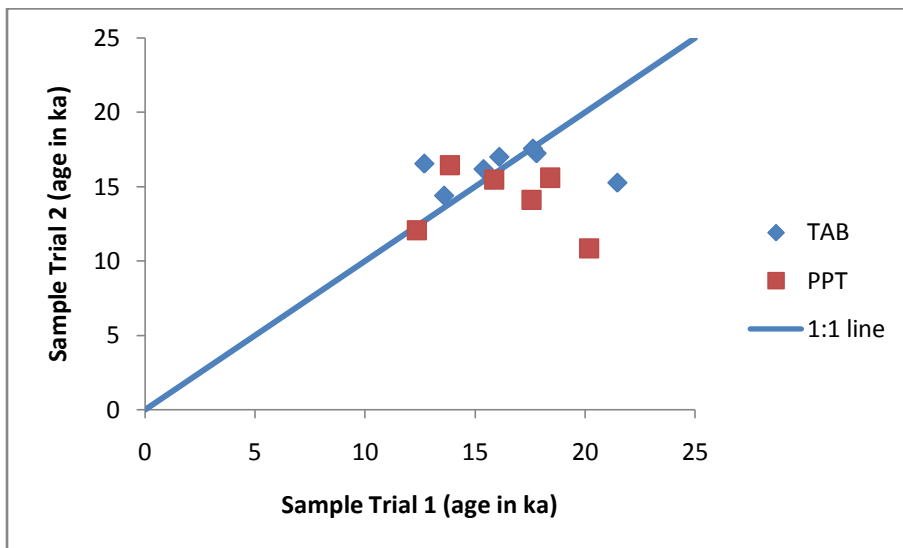


**Figure 23-Reproducibility of TAB and PPT samples using the Phillips production rate. A 1:1 line is plotted for reference.**

There were significant problems with reproducibility in both sets of samples. The first reason was inexperience in processing samples. Because these were among the first samples run through the laboratory after my arrival at New Mexico Tech, I had not perfected the technique needed to consistently process samples. By the time the second set of samples was processed, more batches had been run and the processing was more consistent between samples and batches. There was general improvement in the second batch of Tabernacle Hill sample ages (see Figure 25), most likely due to increased familiarity with the processing procedures.

Another key reason for the discrepancy is that the samples were not split using a splitter and therefore may not have been homogenous, as was assumed. Only one XRF

measurement was performed for the two samples because they were all assumed to be homogenous. Even though care was taken to split the samples and take a representative sample for XRF through the cone and quarter technique (see appendix section 10.4.4), the samples were most likely not as homogenous as originally assumed.

Another possible contribution to the reproducibility problem could be the use of glass beakers for all the samples in this study. The method has now been updated to use small plastic beakers for several reasons. First of all, because glass is much heavier than plastic, the uncertainty in the spike measurements using plastic beakers should be smaller. The plastic beakers weigh about the same or less than the samples being measured, instead of glass beakers where the beaker weighed several times the weight of the spike being measured. Second, because there are numerous plastic beakers, they can all be washed and dried prior to weighing out batches of samples and spike. This way, the spike added to each sample can be weighed in a separate beaker. Using the current methods, one glass beaker is used for all the samples in a batch. Only the first sample has a dry beaker and all the samples after that have a possibility residual spike, despite numerous rinses. A final unexpected advantage to the plastic beakers is that, whereas the glass beaker is hydrophilic, the plastic beaker is hydrophobic and the spike beads up and is almost quantitatively added to the sample in the first pour, even without the additional rinsing. The spike usually wetted the surface of the glass beakers and it was difficult to determine if the spike was quantitatively added or not. The plastic beakers should provide a more accurate and consistent measurement of the spike added to each sample.

Finally, the blank samples will be systematically rotated through each of our sample bottles and other equipment. This ensures that there will be no significant

contribution from a specific piece of labware. The blank is currently being subtracted out of samples as part of our new effort to control the reproducibility of samples in the laboratory. Blanks will be run more often, increasing from one every few batches to one processed with every batch. This should help to identify if there are any problems in the laboratory or with the AMS results for our samples.

Since the original processing, analytical procedures have been established in the laboratory to increase the analytical reproducibility including new treatments of the blanks, new ways to measure the spike, using a splitter, and always testing each aliquot for XRF, as well as other techniques. Mineral separates will also help to improve the accuracy of the Tabernacle Hill data by providing data for an isolated production pathway in a particular sample. However, mineral separates were not in the scope of this work and will be performed later. All of the Tabernacle Hill samples are scheduled to be reprocessed using the new procedures to ensure that the highest quality data will be used in the geological calibration studies in CRONUS-Earth.

Although these new procedures are in place, they were not in place during the processing of these samples and the results must be reinterpreted in light of this knowledge. Because there were issues with the ability to duplicate results, only those samples with reproducible results were used in the calculations of mean age, uncertainty, or production rates. Reproducible samples are defined here as duplicate samples yielding values within AMS uncertainty of each other. Using only reproducible samples should eliminate those samples that had significant contribution from any of the lab problems discussed above. The sample numbers of reproducible samples are listed in the individual results sections.

Another concern is that occasional reproducible results fall far from the carbon-14 bounds. In these cases, the weighted means will be reported for both the reproducible samples as well as the reproducible samples close to the bounds, eliminating reproducible samples that are far from the bounds. However, because this study also includes production rate calibration studies, it is important to note that these reproducible samples away from the bounds will still be used in the production-rate calculations. The distance from the carbon-14 bounds are ultimately controlled by the production rates. As discussed before, the production rates are not robust, especially for low energy neutron absorption, which could lead to a significant error in the apparent age of the sample (i.e. looking young compared to the carbon-14 bounds) if production is dominated by this pathway. For the production-rate calibration study, we have considered all reproducible samples, regardless of their relation to the carbon-14 bounds, to be appropriate for this reason.

The chlorine-36 results shown here should be considered preliminary results only. Due to the reasons described above, many of the samples are scheduled to be reprocessed using the updated techniques. When those samples are completed, the results will hopefully provide more robust results. Until then, these results are being presented and only the most reliable results are being used for the understanding of the production rates or the calculation of new preliminary production rates.

## **4.2 *Tabernacle Hill Results***

The results from Tabernacle Hill depend on the erosion rate at the site. It is necessary to constrain the erosion rates since the results do depend so heavily on the chosen erosion rate. The age-erosion rate relationship at Tabernacle Hill is graphed in

Figure 24 below. Based on the geological evidence, primarily the surface texture of the sample, it was possible to assess reasonable range of erosion rates for the site. In the samples, clear pahoehoe ropes are seen. In order for the surface pahoehoe ropes to remain distinct, as they were for all collected samples (see photos of each sample in the appendix in section 9.1), there cannot have been large amounts of erosion. Cerling and Craig (1994b) estimate not more than 1 cm of total erosion (a rate of 0.58 mm/kyr for Tabernacle Hill) for ropes to remain distinct, while Dunbar (1999; 2004) estimates a significantly higher erosion rate for basalts with Pahoehoe ropes equal to ~8.5 cm of total erosion at Tabernacle Hill (a rate of 5 mm/kyr). It is also possible that higher erosion rates are appropriate for younger samples while the outer very friable layer is removed progressively, with erosion rates slowing significantly after the denser inner material is reached (DUNBAR and PHILLIPS, 2004). It is most likely that the actual erosion rate of the Tabernacle Hill basalt is between these two estimates. Based on the fact that a 5,000 year old flow in New Mexico had already lost its shiny outer layer (DUNBAR, 1999), the higher erosion rate is probably only appropriate for the first 5,000 years or less, with a lower erosion rate being appropriate for the remaining 12,000 years of the exposure time. An appropriate integrated rate for this sample should be closer to the lower bounding erosion rate than the upper. Although the sample age does change based on erosion rate, it is a fairly small percentage overall. For a sample with an erosion rate of up to 2 mm/kyr, there is only a 5% change in the sample age compared to a sample with no erosion. Based on all of this information, an erosion rate of 0.9 mm/kyr was chosen for this site. All the graphs from this point on will show Tabernacle Hill sample results for

this erosion rate, however, the mean ages are shown for the entire range of erosion rates for comparison.

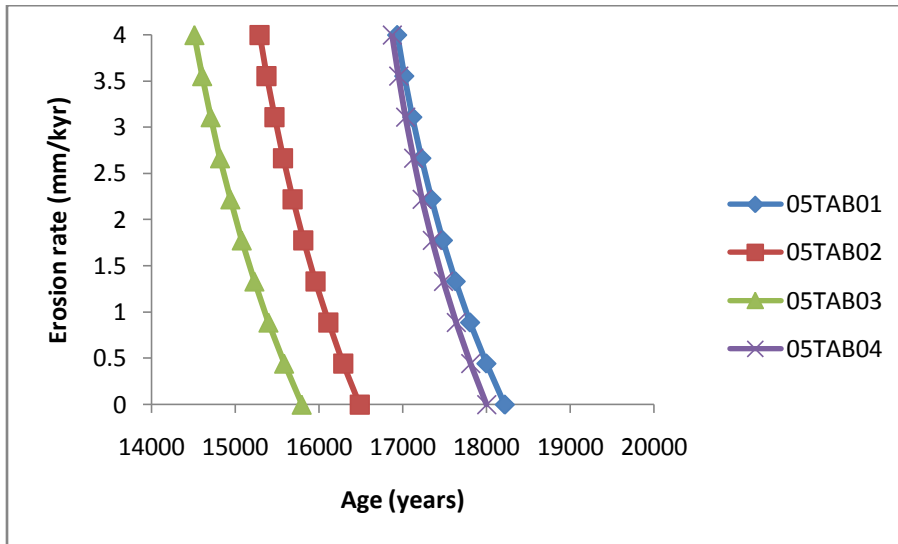


**Figure 24-Varying age with different erosion rates for the best reproducible samples for Tabernacle Hill.**

The Tabernacle Hill results from both trials calculated using the Phillips production rates are graphed in Figure 25. The weighted mean values for the samples are shown in Table 8 for several erosion rates. It is clear that the Tabernacle Hill samples are not consistent between runs. There are at least two samples that were not reproducible, 05TAB05 and 05TAB06. These two samples were therefore excluded from all the interpretations of the data.

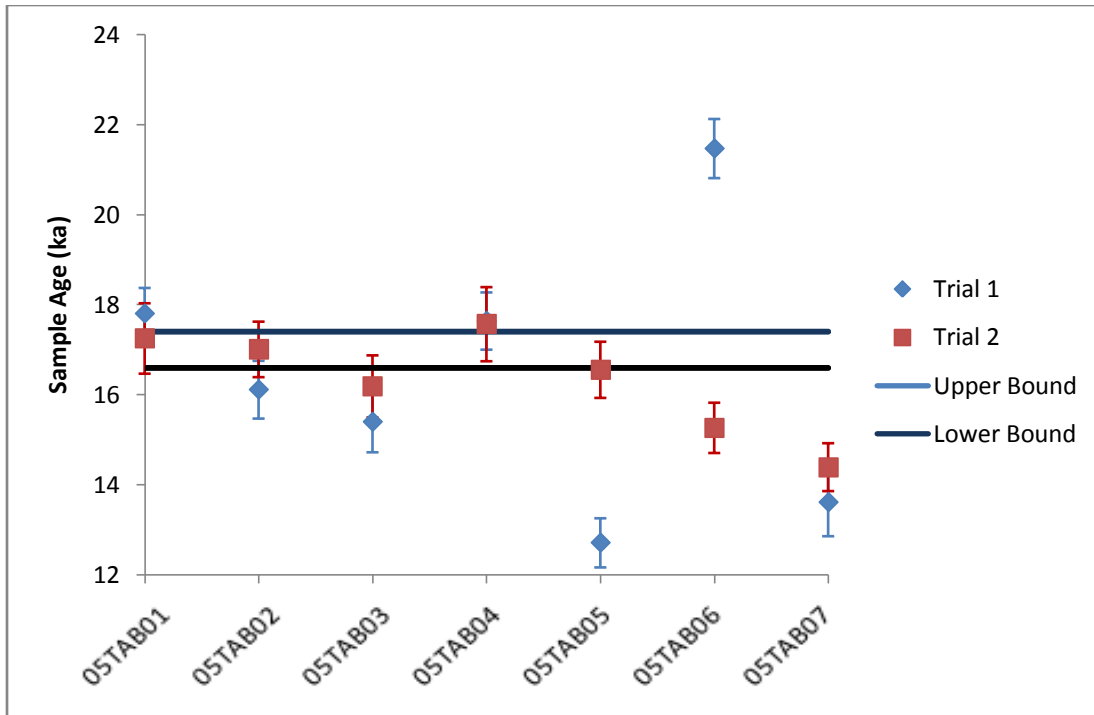


Figure 25-Tabernacle Hill sample results using the Phillips production rate (PHILLIPS et al., 2001) and 0.9mm/kyr erosion rate. Trial one and trial two are the duplicates of the same set of samples. The upper bound (Bonneville flood age of 17.4 cal ka ) and lower bound (carbon-14 date on tufa at 16.6 cal ka ) are also shown for comparison with the results. Duplicate samples of 05TAB04 plot on top of each other. Y-axis error bars represent the 1 sigma errors calculated from the original PRIME Lab reported errors. The reproducible samples are 05TAB01 through 05TAB04 and 05TAB07.

Table 8-Calculated age for Tabernacle Hill using Phillips chlorine-36 production rates with varying erosion. The reproducible samples are 05TAB01-04, and 05TAB07. The best samples, those reproducible samples closest to the C-14 bounds, are 05TAB01-04 only.

Erosion (mm/kyr)	Reproducible samples (ka)	Best samples (ka)
0.0	16.7 ± 0.2	17.3 ± 0.2
0.4	16.4 ± 0.2	17.1 ± 0.2
0.9	16.3 ± 0.2	16.9 ± 0.2
1.8	16.6 ± 0.2	15.9 ± 0.2
3.1	16.2 ± 0.2	15.6 ± 0.2
4.0	16.0 ± 0.2	15.4 ± 0.2

From the graph, it is also evident that the samples do not consistently fall within the independently established age bounds for the surface. The first four samples and their duplicates fall within uncertainty of at least one of the bounding ages. However, the remaining three samples do not plot close to these bounds. Sample 05TAB07

consistently plots very young. Possible reasons for the consistently young age is a geological problem with the surface, such as excess erosion that was not apparent in the field, a problem with the current production rates used to calculate the sample age, or laboratory error. However, because the sample is reproducible, laboratory error is unlikely. Sample 05TAB07 was considered reproducible but is not considered in the “best” samples, or those that plotted close to the carbon-14 bounds.

### **4.3 Promontory Point Results**

Erosion must be considered at Promontory Point due to the sensitive sample chemistry. For this site, the age-erosion rate relationship is demonstrated in Figure 26. For an erosion rate of 1.1 mm/kyr, there is a difference of about 5% from the age calculated with zero erosion. This illustrates that, although these samples are made out of a more resistant material (quartzite) than the Tabernacle Hill samples, the Promontory Point sample ages are more dependent on erosion due to the chemical composition of the samples. However, based on the wave polish still visible on the sampled bedrock and boulders, it is clear that little or no erosion has taken place. A reasonable erosion rate adopted for these samples is a zero erosion rate because any measurable erosion would have removed the wave polish. All plots of Promontory Point results will be shown for a zero erosion rate. Weighted mean ages will still be shown for several erosion rates to illustrate the general trend of the sample ages in relation to erosion.

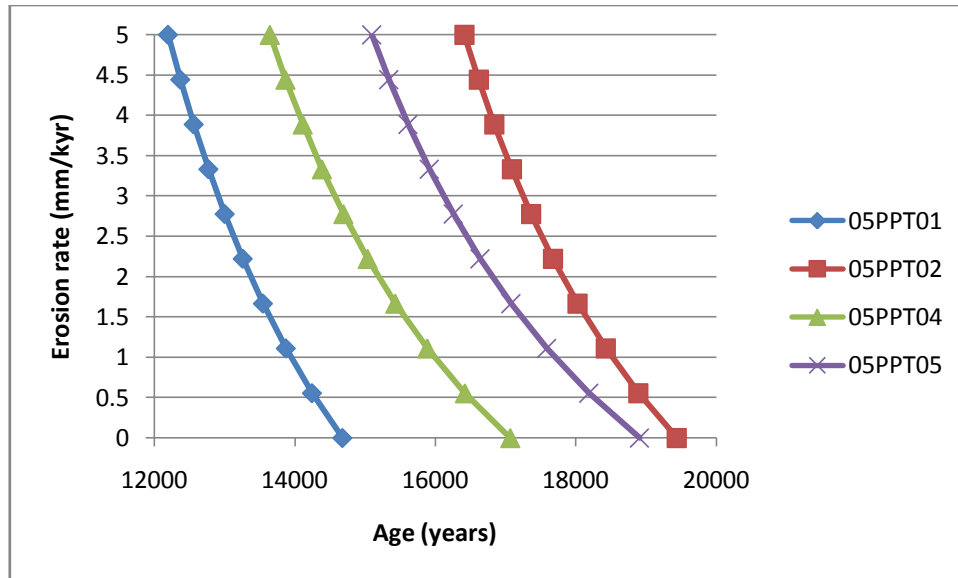


**Figure 26-Varying age due to different erosion rates for the best reproducible samples from Promontory Point. These results are calculated using the Phillips production rate.**

The Promontory Point results are plotted in Figure 27 while the weighted mean ages are shown in Table 9. From the graph, it is clear that sample 05PPT03 exhibited very poor reproducibility and is therefore considered an outlier. The majority of the samples are duplicated relatively well, although only samples 05PPT04 and 05PPT08 are duplicated within uncertainty of each other. For the purposes of this study, I considered samples with duplicates slightly outside of uncertainty ranges, like sample 05PPT01, to be reproducible.

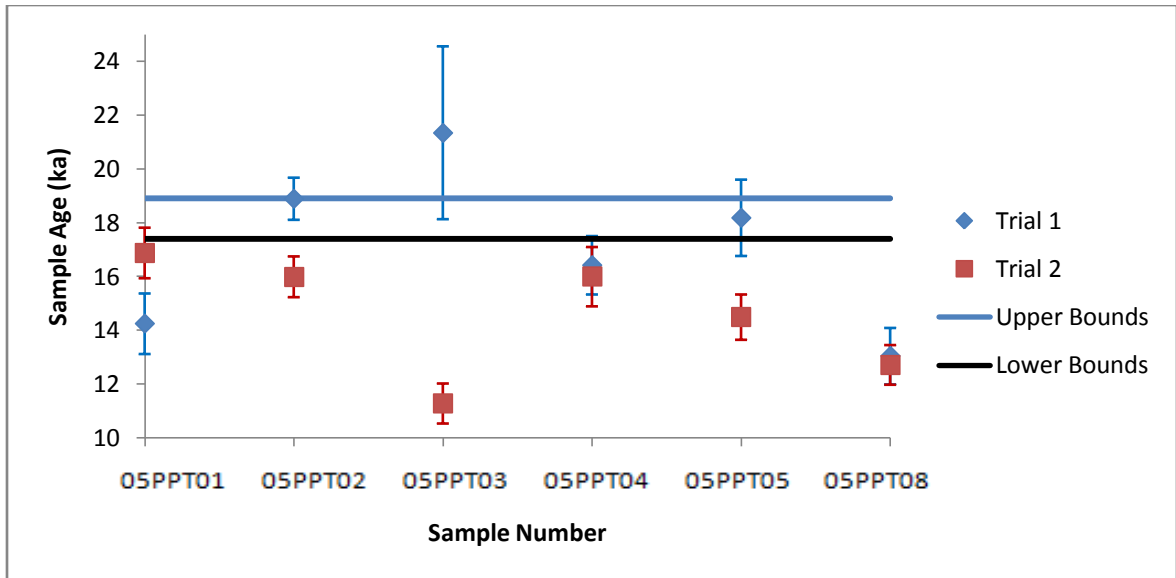


**Figure 27 - Promontory Point data calculated using the Phillips production rate (PHILLIPS et al., 2001) and with an erosion rate of 0.56 mm/kyr. Trial one and trial two are the duplicates of the same set of samples. The upper (carbon-14 date of 18.9 cal ka ) and lower (Bonneville flood age of 17.4 cal ka ) carbon-14 bounds are also shown for comparison with the results. Duplicate samples of 05PPT04 and 05PPT08 plot on top of each other. Y-axis error bars represent the 1 sigma errors calculated from the original PRIME Lab-reported errors. The reproducible samples are all samples except 05PPT03.**

Even though the samples are reproduced fairly well, the samples do not consistently fall within the predetermined carbon-14 bounds of the surface. All the samples are either within carbon-14 bounds or too young except 05PPT03, which has already been considered an outlier. Even considering a zero erosion rate (see Table 9), which is the oldest possible age, the best samples are barely within the lowest C-14 bound.

**Table 9-Weighted mean ages for Promontory Point samples calculated using the Phillips production rates and varying erosion rates. The reproducible samples are all those except 05PPT03. The best samples, those closest to the carbon-14 bounds, are all the samples except 05PPT03 and 05PPT08.**

Erosion (mm/kyr)	Reproducible samples (ka)	Best samples (ka)
0	16.6 ± 0.3	17.4 ± 0.4
0.56	15.8 ± 0.3	16.8 ± 0.3
1.11	15.3 ± 0.3	16.3 ± 0.3

## 5 DISCUSSION

The chlorine-36 results from the Lake Bonneville geological calibration site provide some insight into the production rate discrepancy. However, combined with the data from other laboratories, including other nuclides, this information can be even more useful. This section will discuss how the results relate to the production rates in the literature as well as compare this data to results from other laboratories. Finally, a preliminary production rate will be presented and compared to the published chlorine-36 production rates. All of this information will be examined in the context of the production rate discrepancy.

### ***5.1 Tabernacle Hill***

#### **5.1.1 Chlorine-36 Interlaboratory Comparison**

The Tabernacle Hill samples are being run by several different laboratories for chlorine-36. To date, only two laboratories have analyzed the Tabernacle Hill samples for chlorine-36: Zreda (personal communication, 2006) and this study. The interlaboratory comparison of results is shown in Figure 28 as ages calculated from the results, with the original data available in the appendix in chapter 11. Having a second set of chlorine-36 data allows for a check on the reproducibility of the samples between laboratories as well as a comparison of different techniques.

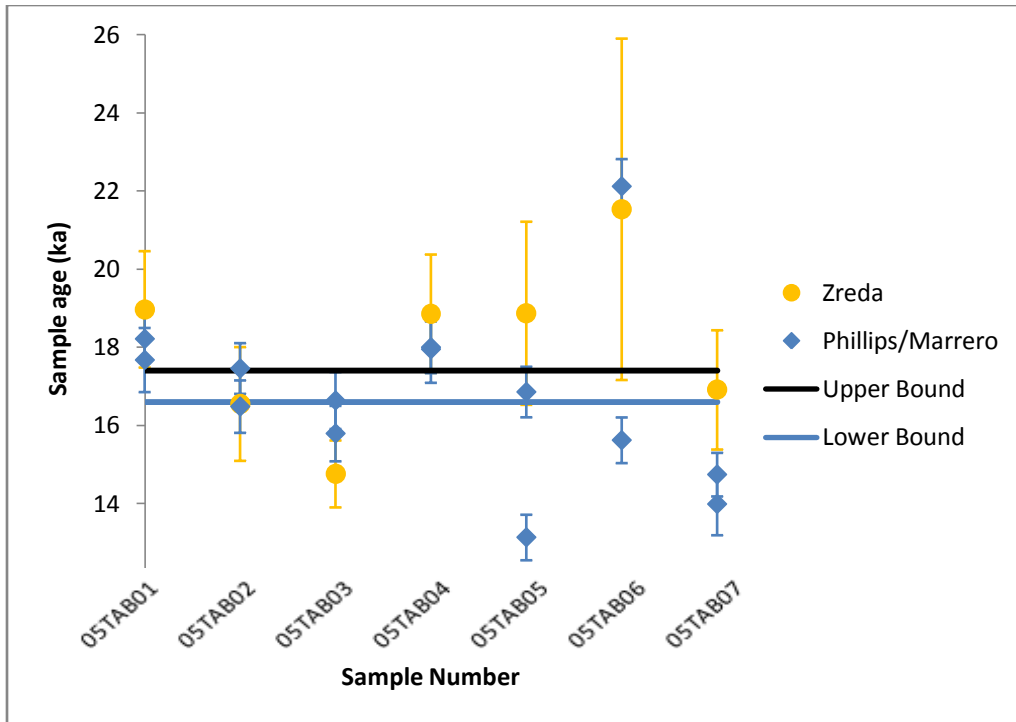


**Figure 28-Comparison of chlorine-36 Tabernacle Hill results from Zreda (personal communication, 2006) and Phillips/Marrero. The Phillips/Marrero results assume an erosion rate of 0.9mm/kyr. Y-direction error bars represent the 1-sigma errors calculated from the original PRIME Lab-reported errors. All ages calculated using the Phillips production rates.**

Both data sets show significantly more scatter than expected originally, with samples ranging from much too young to much too old. It is interesting to note that Zreda's results fall within uncertainty of at least one of the Phillips/Marrero results for all samples except 05TAB07, where the error bars are very close. However, this agreement does not line up with the carbon-14 age bounds, or even with both trials. An interesting example of this is point 05TAB06. This point is not reproducible in my data set, with the first trial giving an age greater than 20 ka. This seemed inappropriate based on the carbon-14 bounds and was originally discounted based on probable laboratory error. When I reran the sample in trial 2, the age was much more reasonable based on the bounding ages. However, the sample is also anomalously high in Zreda's dataset (>20 ka) indicating that there may be a geological problem with this sample and that the first

trial may not have appeared too old due to laboratory error. However, this would require that there was a problem with the second trial age for this sample instead. In one set of field notes, this sample was described as a particularly good sample site (Kurz, personal communication, 2005), showing no indication of any obvious misgivings about the geology of this sample site. There are also no indications that this sample was different during the laboratory processing. It is also important to note that the uncertainty is very high on Zreda's sample as well. Sample 05TAB06 has been excluded from all calculations until this dilemma is resolved.

The results for samples 05TAB01, 02, and 04 are very similar, both to each and other and between datasets. Sample 05TAB03 is also within uncertainty of both the other data and the carbon-14 bounds. It is clear from this agreement that these four samples are the most reliable samples in the dataset. The large uncertainties on Zreda's dataset and lack of agreement between samples 05TAB05-07 confirms the decision to calculate the mean age and other statistics based solely on the first four samples of the dataset.

### 5.1.2 Helium-3 Comparison

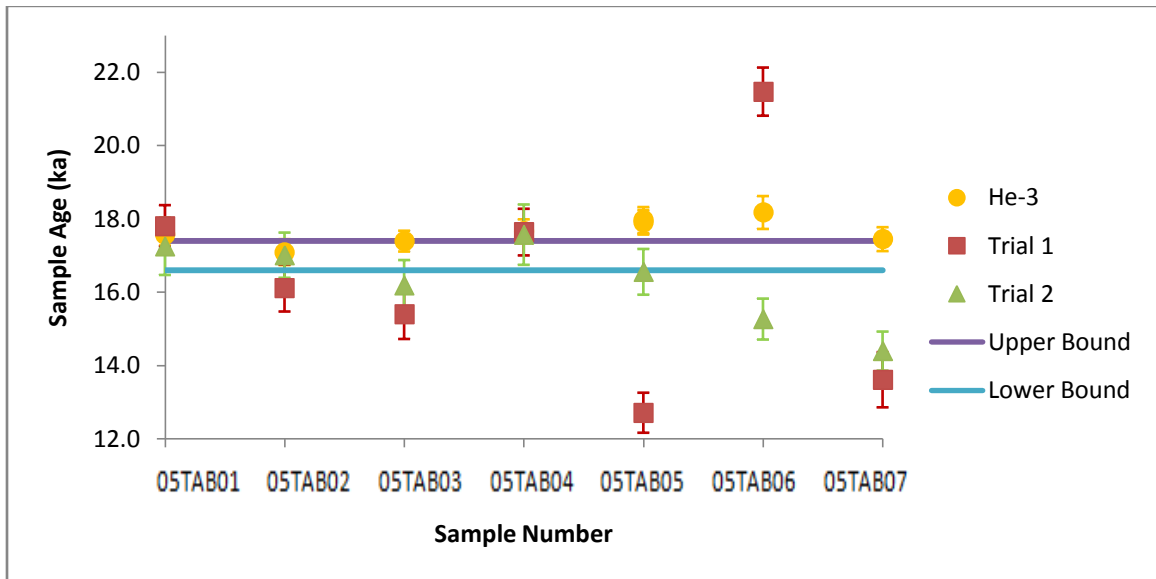


**Figure 29-Tabernacle Hill data from our laboratory (chlorine-36, trial 1 &2) compared to Helium-3 results from the Isotope Geochemistry Facility at WHOI, under the supervision of Mark Kurz (personal communication, 2006). Y-direction error bars on the chlorine-36 samples represent the 1 sigma errors calculated from the original PRIME Lab reported errors. Kurz' ages and error bars are shown as he reported them.**

The only nuclide other than chlorine-36 that has been analyzed on Tabernacle Hill is helium-3 (Kurz, personal communication, 2006). The original helium-3 data can be found in the appendix in chapter 11. The helium-3 ages were consistent for all of the samples (Figure 29). The helium-3 results from Kurz and chlorine-36 results from my laboratory are within uncertainty for samples 05TAB01 through 04TAB04. The sample results diverge after this point. Based on this, our choice of 05TAB01 through 04 as reliable samples is further confirmed. The weighted mean age using helium-3 is  $17.6 \pm 0.1$  ka, with the mean using only samples 05TAB01-04 is  $17.4 \pm 0.2$  ka.

The Tabernacle Hill results are enigmatic, primarily due to the conflicting results of duplicate samples as well as the confirmation of the anomalous result of 22 ka by both our laboratory and Zreda for 05TAB06. These samples are being reanalyzed with our new sample procedures, but because some of the problems have been duplicated in other

laboratories, it is necessary to continue to look for another cause outside of laboratory problems.

## **5.2 Promontory Point**

For Promontory Point, there have been several analyses of beryllium-10 performed at other laboratories in addition to the chlorine-36 analysis performed in our laboratory. The original beryllium-10 data can be found in the appendix in section 11. The Promontory Point data from both chlorine-36 and beryllium-10 show relatively consistent results. Most samples are within uncertainty; however, samples 05PPT03 and 05PPT08 show significant discrepancies between the different cosmogenic nuclide results. In general, the beryllium ages are much more consistent than the chlorine-36 ages. This comparison highlights that the two nuclides are not in complete agreement as well as the importance of better chlorine-36 processing techniques. In the future, comparing a production rate calculated from the beryllium data to the current beryllium production rate could also be useful to test the production rates of the different nuclides performed on splits of the same sample.

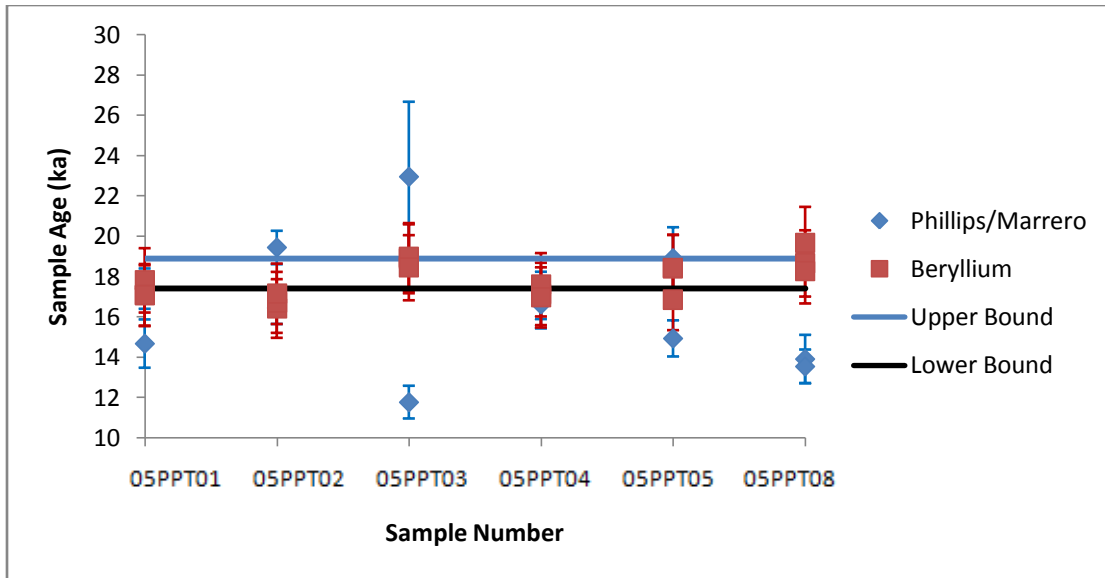


**Figure 30-Promontory Point results showing both the chlorine-36 analysis performed in our laboratory and the beryllium-10 results from three different laboratories reported anonymously to CRONUS-Earth. The ages for the Be-10 data were calculated using the Be-10 web calculator (BALCO, 2007). The scaling scheme for the Be-10 is Lal/Stone (time-dependent)(LAL, 1991; STONE, 2000), while the scaling scheme for the  $^{36}\text{Cl}$  data is Lal (LAL, 1991). Y-direction error bars on the chlorine-36 data represent the 1 sigma errors calculated from the AMS-reported errors. Upper and lower bounds refer to carbon-14 bounding ages.**

Sample 05PPT08 is a unique sample. Beryllium-10 results that are within the carbon-14 bounds generally indicate that there were not geological problems with the samples. However, the chlorine-36 sample ages were consistently younger than the bounds, indicating that there must be another reason for the discrepancy between the beryllium-10 and chlorine-36 results. The sample results are very similar for the two  $^{36}\text{Cl}$  trials so this does not support laboratory error as the reason for the discrepancy. One possible explanation is the use of an incorrect production rate for the thermal neutron absorption pathway. This pathway is one of the least calibrated pathways and the most complicated. For this particular sample, it is extremely important due to the low concentrations of both potassium and calcium in the sample (see appendix in section 8.1 for sample composition). If the production rate for the thermal neutron pathway was too high, it would result in a younger apparent sample age. I hypothesize that this sample

indicates that the Phillips et al. (2001) production rate for chlorine-36 through the thermal neutron absorption pathway is possibly too high.

Based on the problems with this dataset, it is clear that work on the geological calibration and laboratory processing technique needs to be continued. The ages on a well-dated surface should be straightforward and comparable between laboratories. The differences in mean age using the three different chlorine-36 production rates also causes concern because all three are used by scientists working with chlorine-36.

### ***5.3 Production rate comparison***

There are three primary chlorine-36 production rates cited in the literature, Phillips (PHILLIPS et al., 2001), Stone (EVANS, 2001; EVANS et al., 1997; STONE et al., 1998), and Swanson (SWANSON and CAFFEE, 2001). These three rates do not agree and provide different ages for a given set of samples. Using the samples from the Lake Bonneville geological calibration site, these production rates were compared and the best fitting rate for this site was chosen. The three production rate results were compared side-by-side at each sample site, looking at the calculated ages for the best samples selected for Tabernacle Hill and Promontory Point.

### 5.3.1 Tabernacle Hill Production Rate Comparison

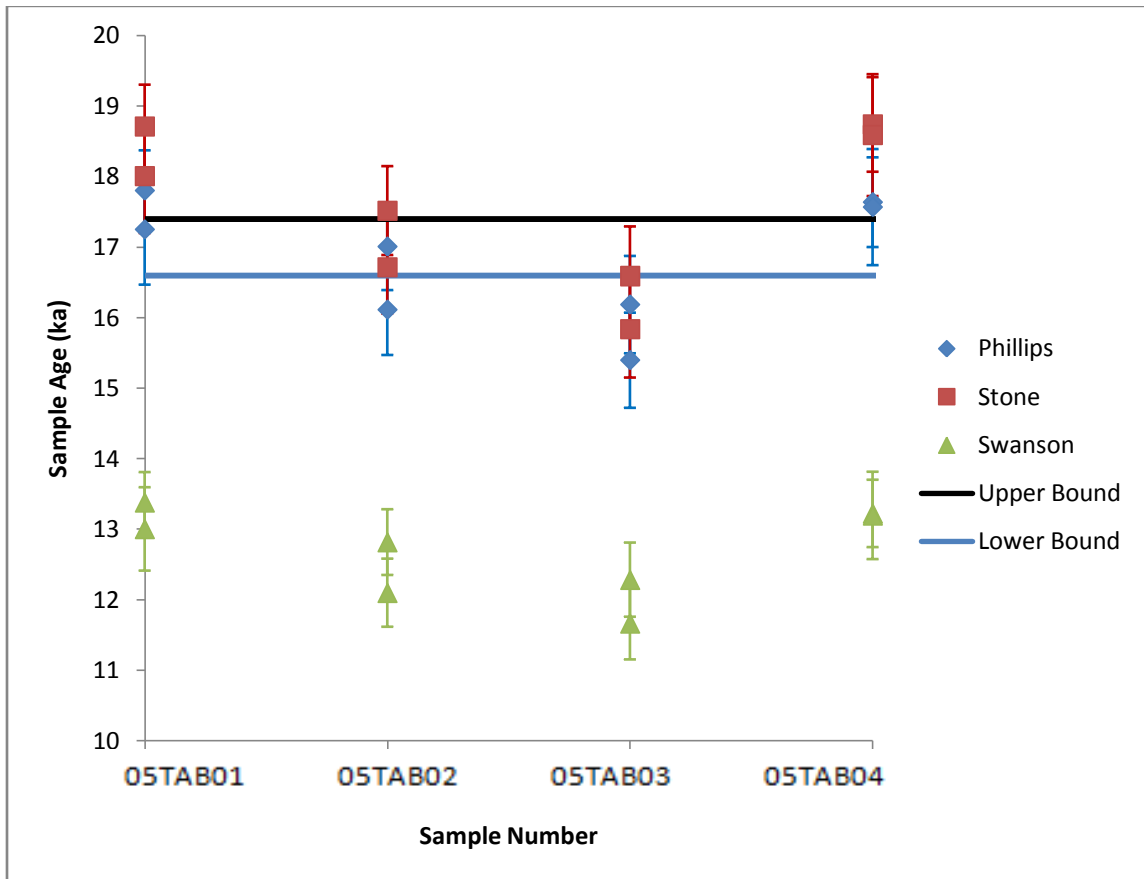


Figure 31-TAB results comparing production rates of Phillips (PHILLIPS et al., 2001), Stone (EVANS et al., 1997), and Swanson (SWANSON and CAFFEE, 2001) at 0.9mm/kyr erosion. The graph shows only the first four samples because these are the reproducible samples with the best results. Y-direction error bars represent the 1 sigma errors from the AMS measurement.

The three production rates give three different mean ages for the samples (Figure 31). These are numerically compared in Table 10. The Phillips and Stone ages are typically within uncertainty of each other, while the Swanson ages are significantly lower. The Phillips and Stone rates yield sample ages that cluster around the independently determined bounding ages. The Stone results are higher than the Phillips ages by about 5%, which pushes the sample average, 17.6 ka, just above the carbon-14 limiting date of 17.4 ka. The reduced chi-squared values are shown in parentheses next to the ages and these values demonstrate the goodness of fit of the data to the independent carbon-14 bounds. Although the Phillips age is technically the best fit age, the Stone age

is close and should be considered as a reasonable production rate at this site as well. The Swanson rate does not produce ages that are close to any carbon-14 bounds and does not appear to provide anything close to the correct age, being lower than the lowest bounding age by more than 20%. It is clear that the Swanson production rate does not provide reasonable ages at this location.

**Table 10-Weighted mean ages using Phillips, Stone, and Swanson chlorine-36 production rates for the Tabernacle Hill samples. Only samples 05TAB01-04 have been used in these calculations for reasons discussed previously. This is calculated for different erosion rates. The most reasonable erosion rate is 0.9 mm/kyr. The carbon-14 bounds are 16.6 ka – 17.4 ka. Reduced chi-squared values are shown in parentheses next to the age.**

Erosion Rate	Phillips	Stone	Swanson
0 mm/kyr	17.3 ± 0.2 ka (3.0)	18.2 ± 0.3 ka (4.5)	12.9 ± 0.2 ka (6.0)
0.9 mm/kyr	16.9 ± 0.2 ka (3.4)	17.6 ± 0.2 ka (5.1)	12.7 ± 0.2 ka (6.8)

### 5.3.2 Promontory Point Production Rate Comparison

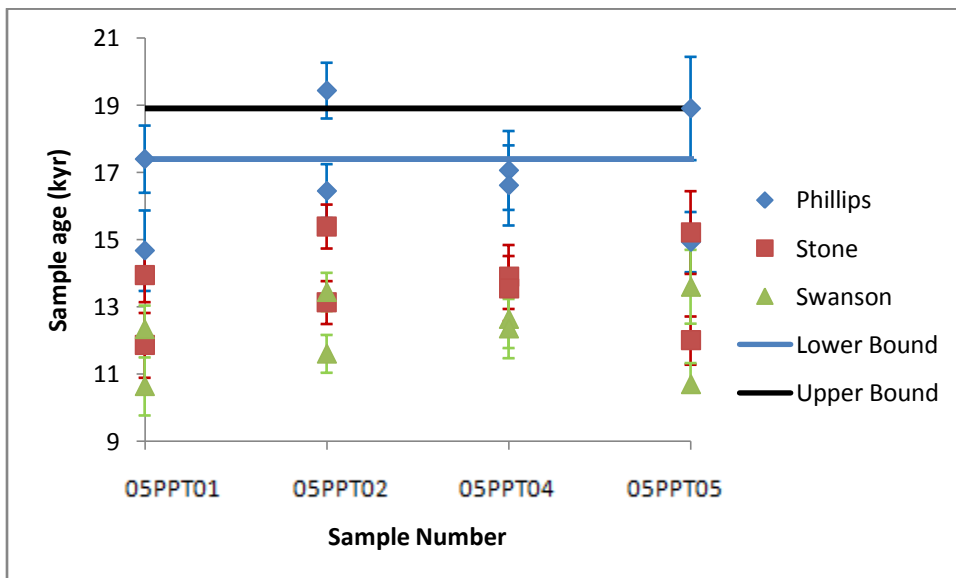


**Figure 32-Ages calculated using all three production rates (Phillips, Stone, and Swanson) for Promontory Point samples. Only the best samples, 05PPT01, 05PPT02, 05PPT04, and 05PPT05, were used in this calculation. These ages are calculated for zero erosion.**

A similar exercise can be performed on the Promontory Point dataset. In this case, the best samples are 05PPT01, 02, 04, 05 due to their reproducibility and closeness to the independent age. This eliminates samples 05PPT03 and 05PPT08 from the dataset.

The graph (see Figure 32) shows the results for the ages calculated with no erosion rate. This is the oldest possible age using each production rate. Even assuming zero erosion, only the Phillips production rate is within uncertainty of the lowest bound. The weighted means are shown in Table 11 along with the reduced chi-squared values to demonstrate the goodness of fit for each set of data. Due to the chemical composition of these samples, the Stone age is actually lower by about 20% than the Phillips age (Table 11). Because the 05PPT samples have very little Ca, the higher Stone rates for both K and neutron absorption pathways compared to Phillips' rates (Table 12) leads to a lower age of the samples in this case. Again, the Swanson rate yields the youngest samples of all, which are younger than the expected surface age by about 30%. It is clear from the reduced chi-squared metric that the Phillips rate provides the best match to the independent age constraints. In this case, both the Stone and Swanson production rates yield ages that appear geologically unreasonable at this particular site.

**Table 11-Comparison of production rates at Promontory Point using only samples 05PPT01-02 and 05PPT04-05. These ages are shown for varying erosion rates. The carbon-14 bounds are 17.4 ka for the lower bound and 18.9 ka for the upper bound.**

<b>Erosion Rate</b>	<b>Phillips</b>	<b>Stone</b>	<b>Swanson</b>
0 mm/kyr	17.4 ± 0.4 ka (10.2)	13.6 ± 0.3 ka (15.2)	12.1 ± 0.3 ka (20.3)
0.56 mm/kyr	16.8 ± 0.3 ka (9.7)	13.3 ± 0.3 ka (14.6)	11.9 ± 0.2 ka (19.5)
1.11 mm/kyr	16.3 ± 0.3 ka (9.4)	13.0 ± 0.3 ka (14.2)	11.7 ± 0.2 ka (18.9)

**Table 12-Production rates for chlorine-36 pathways listed by research group. Swanson rates have been adjusted to show only spallation pathways in order to be comparable to the other rates.**

<b>Production Rate</b>	<b>Ca</b> [a/(gCa*yr)]	<b>K</b> [a/(gK*yr)]	<b>P<sub>f</sub>(0)</b> [neutrons/(g*yr)]
Phillips	66.8 ± 6.8	137 ± 60	626 ± 43
Stone	48.8 ± 3.4	170 ± 25	740 ± 63
Swanson	83.8 ± 5.0	211 ± 18	762 ± 28

### 5.3.3 Insights from Other Nuclides

The helium-3 ages, discussed in section 5.1.2, also provide a comparison among the different proposed chlorine-36 production rates. As shown in Figure 33, the helium-3 ages also overlap within uncertainty of the ages calculated using the production rates of both Phillips and Stone. Although the helium-3 results could include systematic biases common among all cosmogenic nuclides, the ages also fall within uncertainty of the carbon-14 bounding ages indicating that any systematic biases are likely insignificant. The helium-3 data provide the second line of evidence (the first being carbon-14 ages) that the ages calculated with the Phillips and Stone rates are in better agreement with the independent age than the ages calculated using the Swanson production rates. The Swanson production rates are not appropriate for this location.

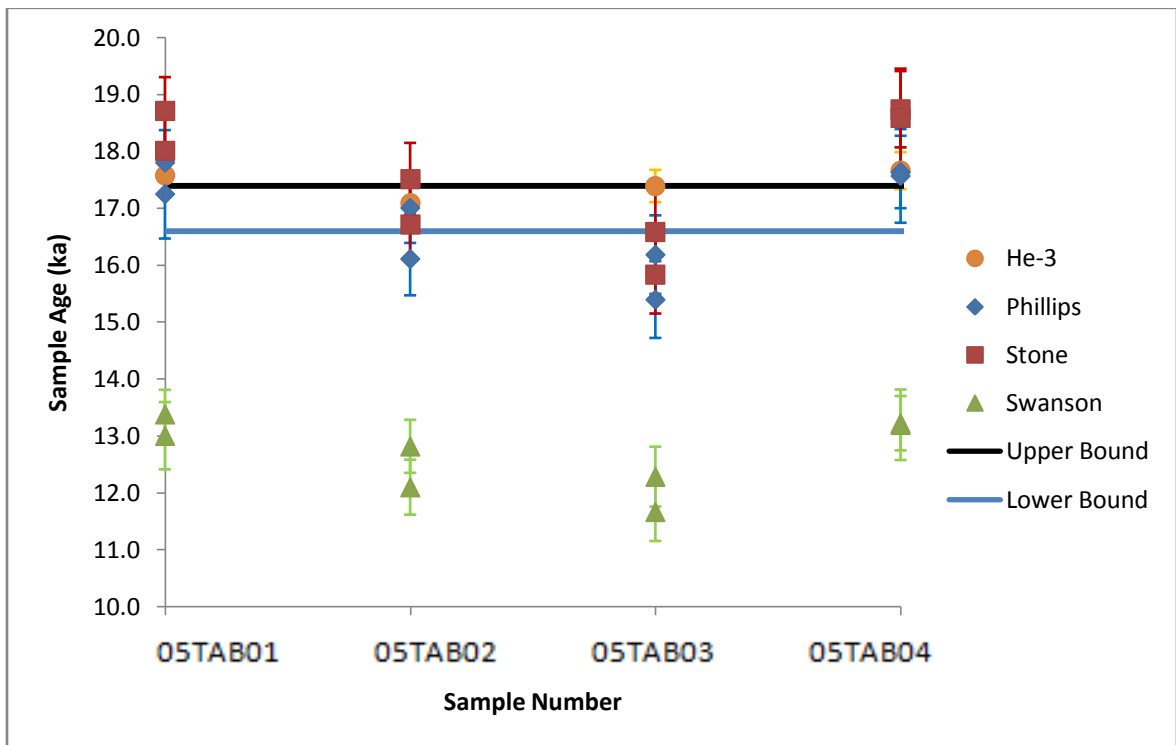
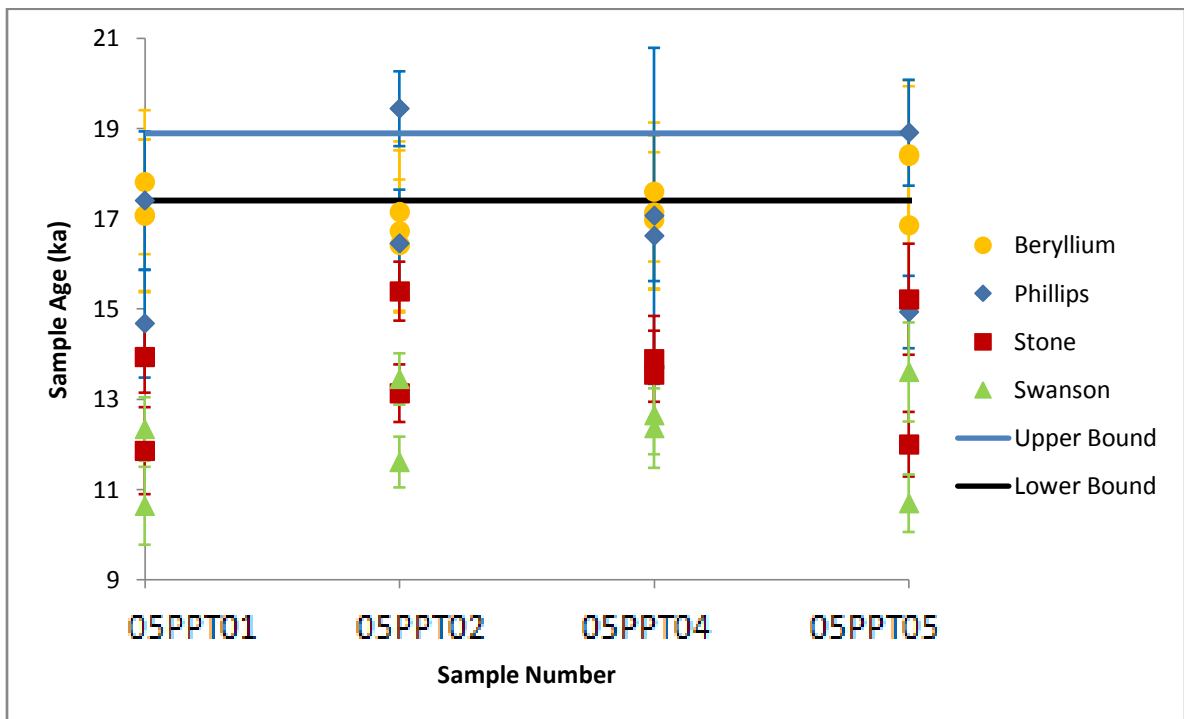


Figure 33-Comparison of all the production rates for Chlorine-36 with the Helium-3 data for Tabernacle Hill reproducible samples close to the C-14 bounds. 0.9 mm/kyr erosion rate.

Similarly to the helium-3 data, the beryllium-10 data can also provide another check on the chlorine-36 production rates. In this case, both the Stone and Swanson rates disagree with the beryllium-10 data (see Figure 34). Again, there may be systematic biases common to all cosmogenic nuclides, but the agreement of the Phillips calculated ages, the beryllium-10 data, and the carbon-14 bounds indicates that the systematic biases must be small. The Phillips rates produce ages that are well within the uncertainties of the beryllium-10 results. This supports the conclusion that the Phillips rates are the most appropriate at this location.



**Figure 34-Comparison of results from Be-10 and Chlorine-36 production rates for Promontory Point samples. These results are calculated for zero erosion.**

Although there are some problems with the samples, they do illustrate that the method, either mineral separates or whole rock, used to determine the production rates do not inherently lead to different production rate calculations. The Swanson rate uses a whole rock method and differs drastically from the other rates. However, the Phillips

rates, using whole rock methods, and Stone rates, using mineral separates, give closely matching results in some cases, so it is clear that this may have a second order effect on the rates, although not a primary effect. This is a factor that should be addressed in detail in the future, but other reasons should be examined for the production rate discrepancy.

#### **5.4 Preliminary Production Rates**

The production rate sets of all three commonly cited research groups, Phillips (PHILLIPS et al., 2001), Stone (EVANS, 2001; EVANS et al., 1997; STONE et al., 1996; STONE et al., 1998), and Swanson (SWANSON and CAFFEE, 2001), do not always seem to work in both cases of these well dated Bonneville shoreline sites. The Swanson age is consistently too low, while Phillips and Stone are both closer to the expected age. However, neither of these parameter sets is ideal either. Another way to test the schemes is to calculate a new set of production rate parameters based on our data. Assuming the independent age constraints are correct and the incorrect ages we calculated are due to incorrect production rates, these new rates can indicate in which direction the production parameters must move in order to reconcile the difference.

The new production rate parameters calculated here are not intended to be used in lieu of published production rates. These numbers are provided simply to determine how the production rate discrepancy might be resolved in the future. These new production rate parameters were determined using a Matlab code to calculate the production rate of a set of samples when given the constraining ages and the chlorine-36 concentrations (Borchers, personal communication, 2007). Only the reproducible samples of the dataset were used in the production rate calculation.

The samples from Promontory Point were critical in this part of the study due to their low calcium concentrations. One sample from this set also had low potassium, allowing the production rate of the remaining production pathway, the absorption of low-energy neutrons by chlorine-35, to be precisely determined. The rest of the Promontory point samples, with a combination of production from potassium and neutron absorption, allowed for the calibration of potassium production rates. Finally, the Tabernacle Hill samples, which contained appropriate minerals for all three production pathways, allowed for the calculation of the production rate for calcium. This unique set of sample chemistries allowed for a complementary production rate calculation.

The production rate calculation resulted in a calcium rate of  $67.1 \pm 2.3$  atoms  $^{36}\text{Cl}$  (gram Ca\* yr) $^{-1}$ , a potassium rate of  $158 \pm 11$  atoms  $^{36}\text{Cl}$  (gram K\* yr) $^{-1}$ , and a neutron absorption rate of  $638 \pm 27$  neutrons (gram\*yr) $^{-1}$ . In Table 13, the comparison of this calculation to the previously published production rates shows the differences between the rates. The calculated rates are all lower than those proposed by Swanson, which is in accordance with the abnormally young Swanson ages for the Bonneville sites. With the new lower rates, the calculated age of the shoreline increases. The potassium rate falls in between the Stone and Phillips production rate schemes. Finally, the calcium and thermal neutron absorption rates are both very similar to the Phillips rate.

**Table 13-Preliminary production rates calculated from the reproducible samples in the Tabernacle Hill and Promontory Point datasets. These are preliminary numbers only and are not intended to be used in lieu of published rates at this point in time. The rates highlighted in dark blue are lower than the rates calculated here, while rates highlighted in light pink are higher than those calculated here.**

	Ca [a/(gCa*yr)]	K [a/(gK*yr)]	P <sub>f</sub> (0) [neutrons/(g*yr)]
Phillips	66.8 ± 6.8	137 ± 60	626 ± 43
Stone	48.8 ± 3.4	170 ± 25	740 ± 63
Swanson	83.8 ± 5.0	211 ± 18	762 ± 28
This study	67.1 ± 2.3	158 ± 11	638 ± 27

In order to quantitatively assess the new production rates, they were used to calculate ages for both the Tabernacle Hill and Promontory Point sites, shown in Figure 35 and Figure 36, respectively. The reduced chi-squared metric was calculated based on the chlorine-36 inventories and compared to the predicted inventories calculated using the other published production rates. The results are shown in Table 14. The new production rate has the lowest reduced chi-squared value for both sites as well as the combined value. Based on the reduced chi-squared metric, the new production rate appears to be significantly better at the Promontory Point site than any of the published values. The reduced chi-squared metric clearly shows the Phillips parameters provide the least-biased calculated ages for this set of samples. It is logical that the preliminary production parameters are very similar to the Phillips parameters. The Stone parameters are also close for at least one site while the Swanson parameters are obviously not a reasonable choice at either site.

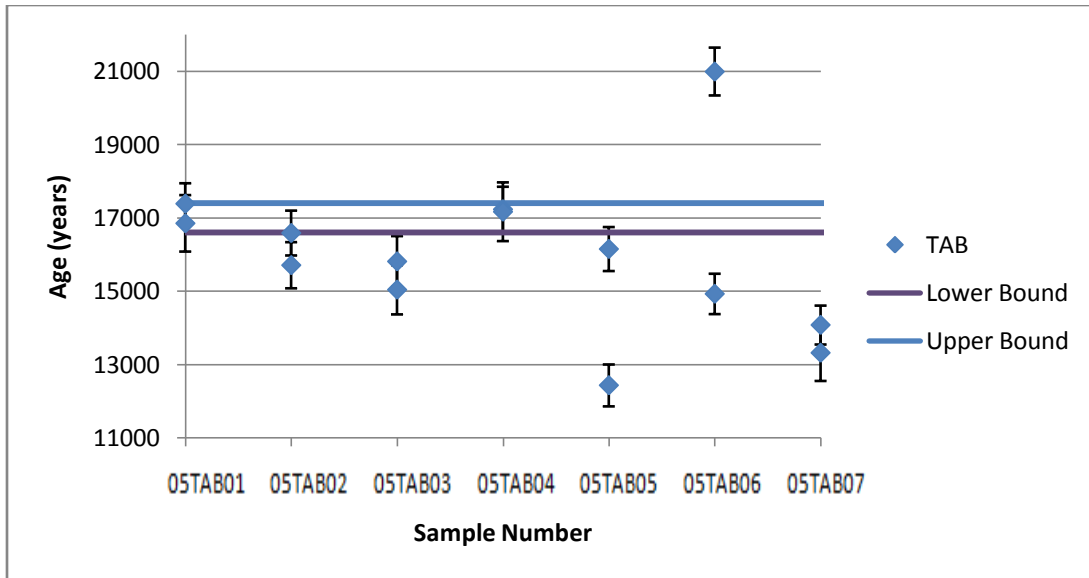


Figure 35-Tabernacle Hill results using the new production rates.

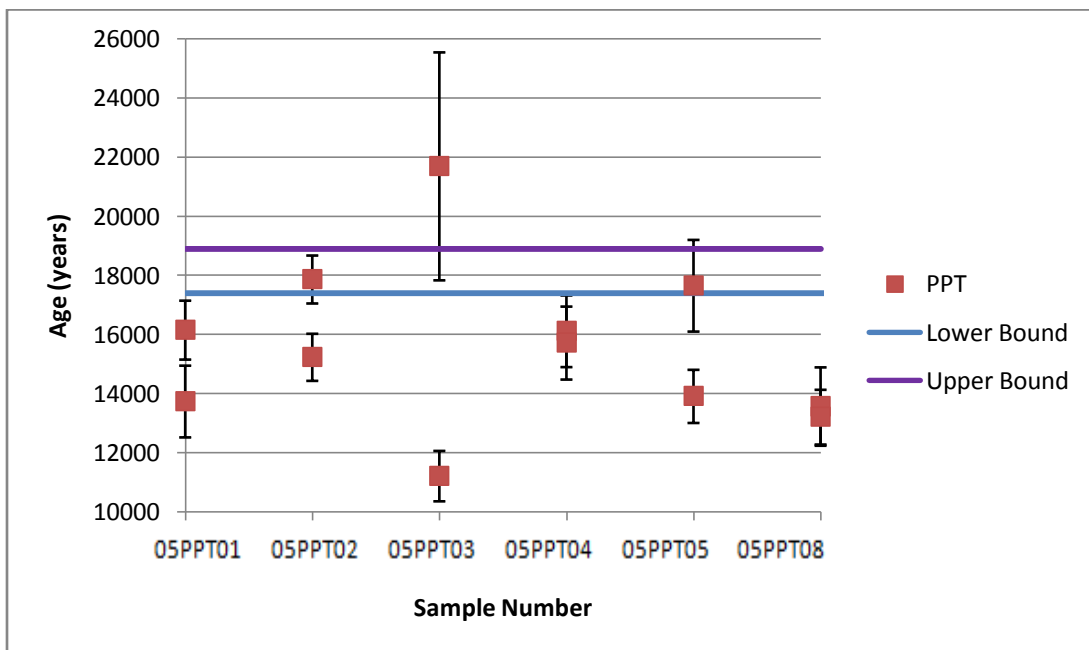


Figure 36-Promontory Point ages calculated using the new production rates.

Table 14-Reduced chi-squared for each of the production rate sets, including the new production rate calculated in this study. The number in parentheses next to the site name is the preferred erosion rate at that site in mm/kyr.

	New Prod Rate	Phillips	Stone	Swanson
TAB (0.9)	1.7	3.4	5.1	6.8
PPT (0)	5.1	10.2	15.2	20.3
<b>Overall</b>	<b>2.9</b>	<b>5.9</b>	<b>8.8</b>	<b>11.7</b>

#### **5.4.1 Sensitivity Analysis for Preliminary Production Rates**

The new production rates were calculated for surface samples from the sites used in this study with erosion rates as discussed above. However, some parameters in the calibration are particularly sensitive to factors such as erosion and exposure age, both of which do have some inherent uncertainty. In order to look at these preliminary production rates more quantitatively, it is important to understand how they might vary based on the uncertainties of the erosion and exposure age parameters.

Due to the lack of numerous carbon-14 dates to limit the exposure age of Tabernacle Hill, a sensitivity study was performed to look at how the different possible exposure ages might affect the calibrated production rates. Also, the erosion rate of Tabernacle Hill was addressed during this sensitivity study. For Promontory Point, the erosion rate is clearly close to 0 based on the visible wave polish. However, due to the extreme sensitivity of the calibrated rates to the erosion at Promontory Point, a sensitivity analysis was performed to look at how the rates would change with erosion at the site. The variations in production rate are shown in Figure 37 for  $P_f(0)$ , Figure 38 for potassium, and Figure 39 for calcium.

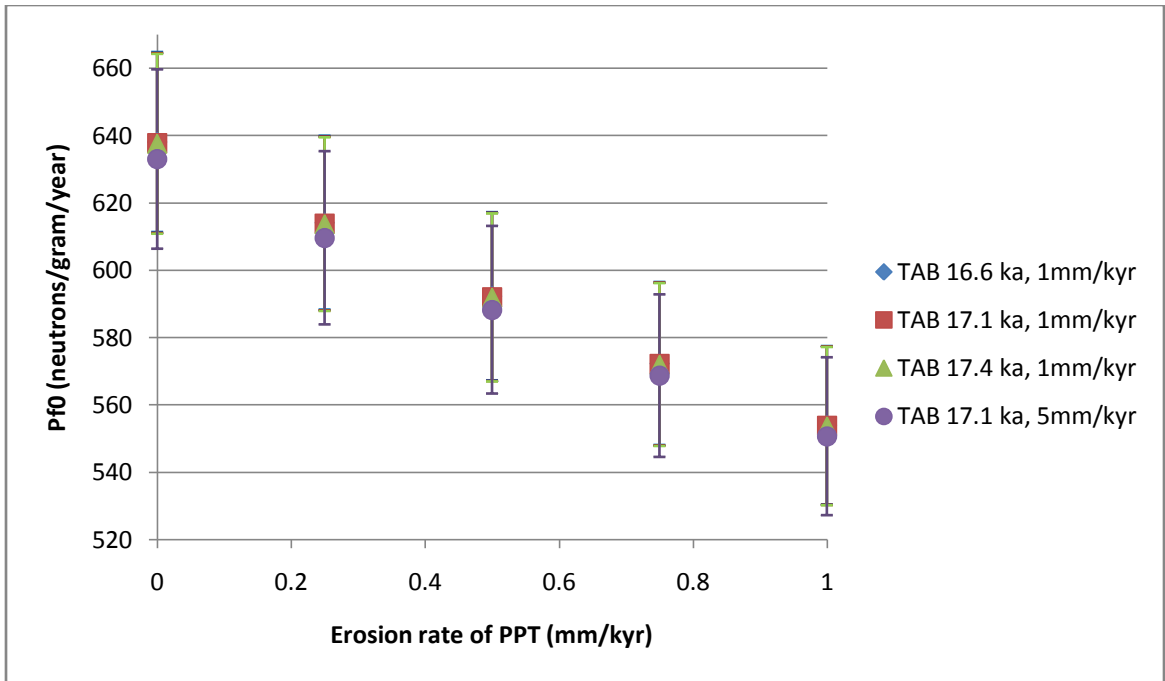


Figure 37-  $P_f(0)$  production rate sensitivity study looking at PPT erosion rate, TAB erosion rate, and TAB exposure age.

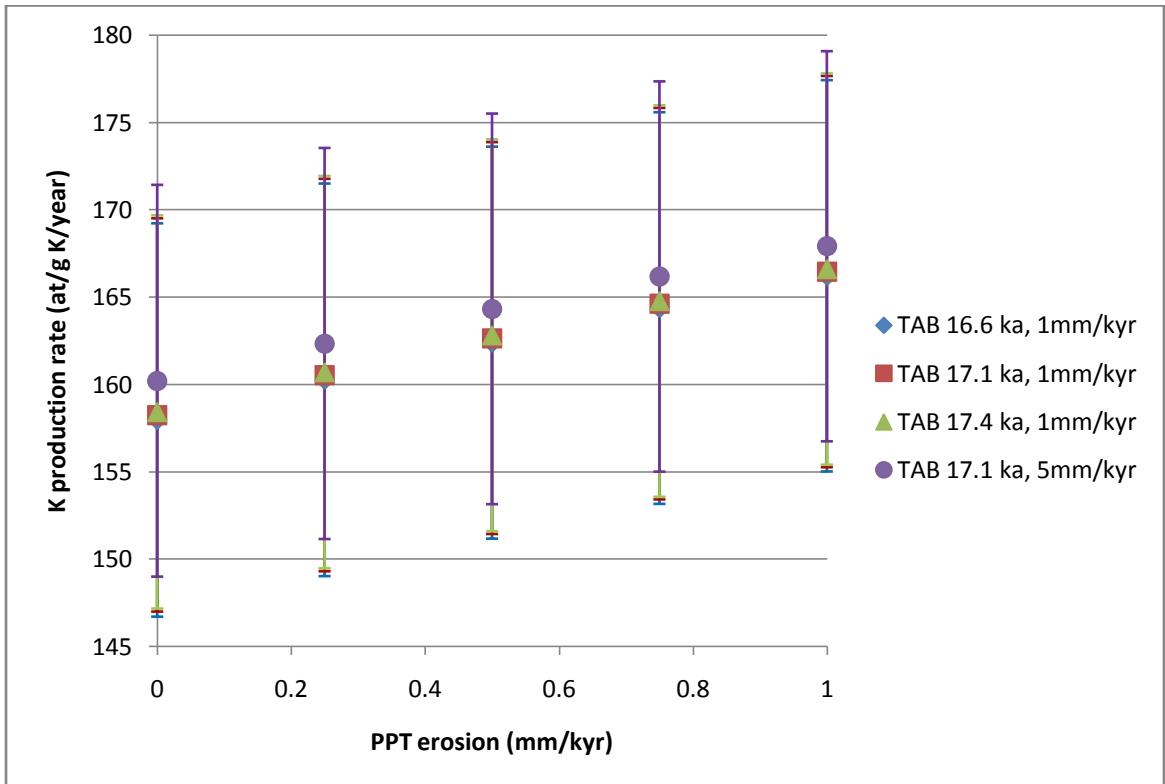
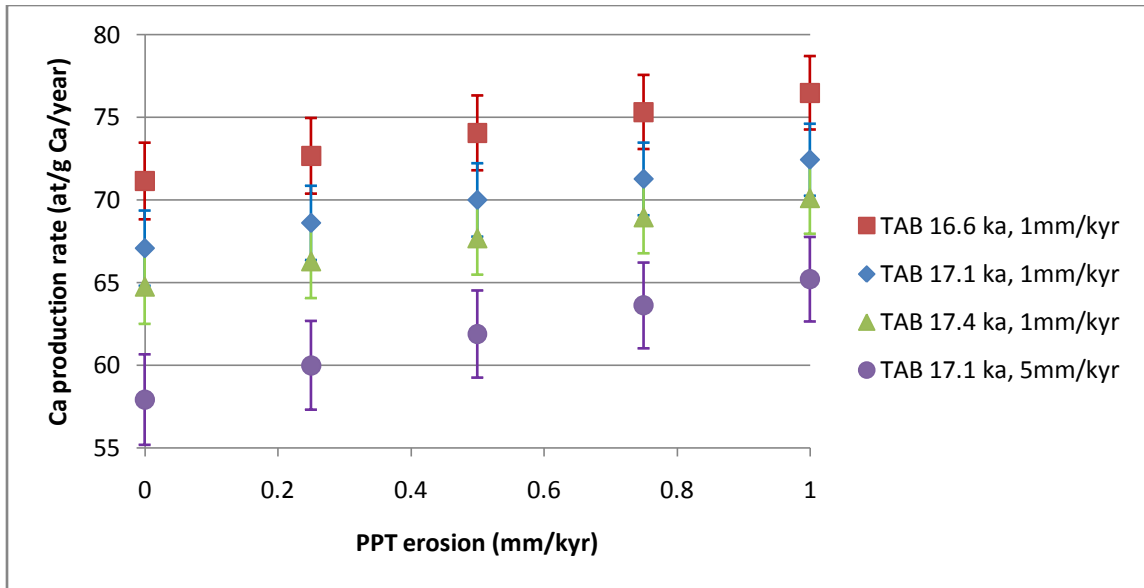


Figure 38- Potassium production rate sensitivity study looking at PPT erosion rate, TAB erosion rate, and TAB exposure age.



**Figure 39-Calcium production rate sensitivity study looking at PPT erosion rate, TAB erosion rate, and TAB exposure age.**

For  $P_f(0)$ , the most significant effect is the erosion of Promontory Point, which causes production rates to decrease significantly with increased erosion. The Tabernacle Hill erosion rate causes a small change in the calibrated rate while the exposure age of Tabernacle Hill appears not to affect the results for  $P_f(0)$ . This is logical because the Promontory Point samples are the primary control on the calibration of the  $P_f(0)$  parameter.

For potassium production rates, the most significant effect appears to be the erosion rate of Promontory Point as well. Once again, this follows logically because the Promontory Point samples have the largest influence on the outcome of the potassium production rate. The erosion rate and exposure age of Tabernacle Hill both exert a minor effect on the production rate.

The calcium production pathway is controlled primarily by the samples from Tabernacle Hill. The sensitivity results support this by showing the most significant

effect from the Tabernacle Hill erosion rate, with some effect from the Tabernacle Hill exposure age and a minor change from the Promontory Point erosion rate.

Based on the wave polish visible on the rocks, it seems clear that the Promontory Point erosion rate is relatively close to 0 mm/kyr. Also, the carbon-14 age constraints on the Tabernacle Hill exposure age limit the uncertainty in production parameters due to this geologic uncertainty. Although there is little variation due to the differences in exposure age despite the uncertainty. This leaves only one uncertainty that cannot be well constrained: the Tabernacle Hill erosion rate. The Tabernacle Hill erosion rate causes the most significant changes in the calcium production rate in the calibration studies. For this reason, the calcium production rate is the least certain of the three calibrated pathways.

Another factor to examine is the use of surface samples versus samples at depth for calibrating the thermal neutron absorption pathway. Shown below (Figure 40) is a graph of the effects of erosion on the chlorine-36 concentration depth profile. The best depth to use for calibration of the Promontory Point site is approximately 40 g/cm<sup>2</sup> (about 15 cm) due to the mechanics of thermal neutron absorption. At this depth, the concentration is practically invariant to erosion rate. The ideal depth decreases for Tabernacle Hill samples (see Figure 41) because the main production mechanism within the sample is spallation from calcium and potassium. The best calibration depth for Tabernacle Hill is approximately 20-25 g/cm<sup>2</sup> (about 7-8 cm). For both Promontory Point and Tabernacle Hill samples, these depths are significantly below the depth of the collected samples, which was typically around 4 cm.

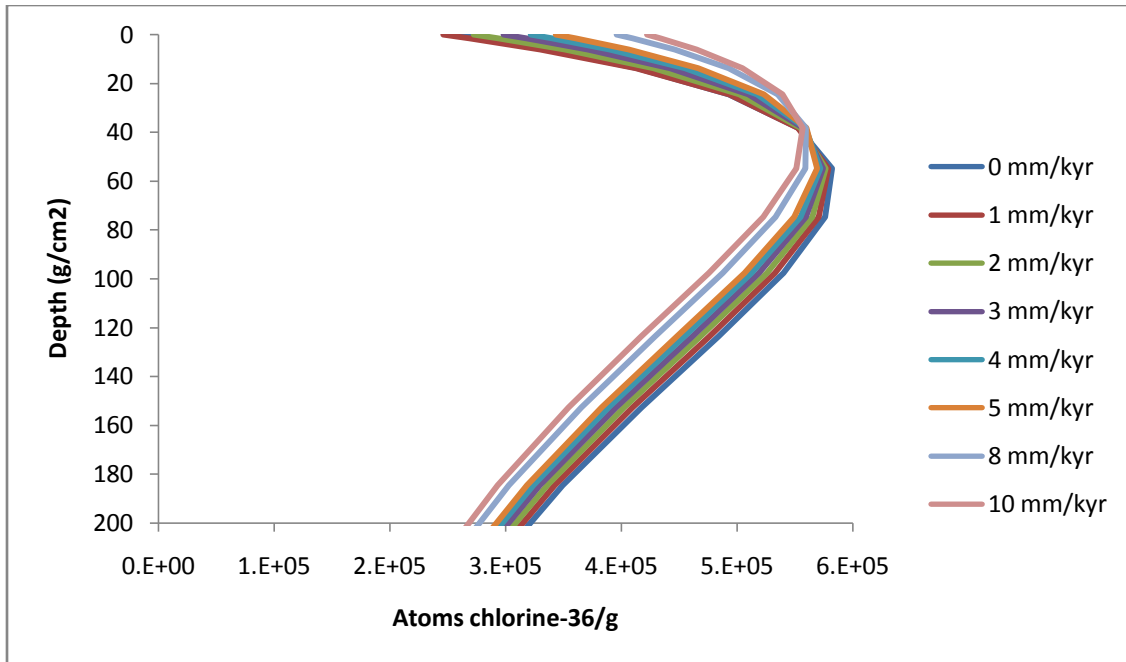


Figure 40-Depth profiles for sample 05PPT08 for varying erosion rates.

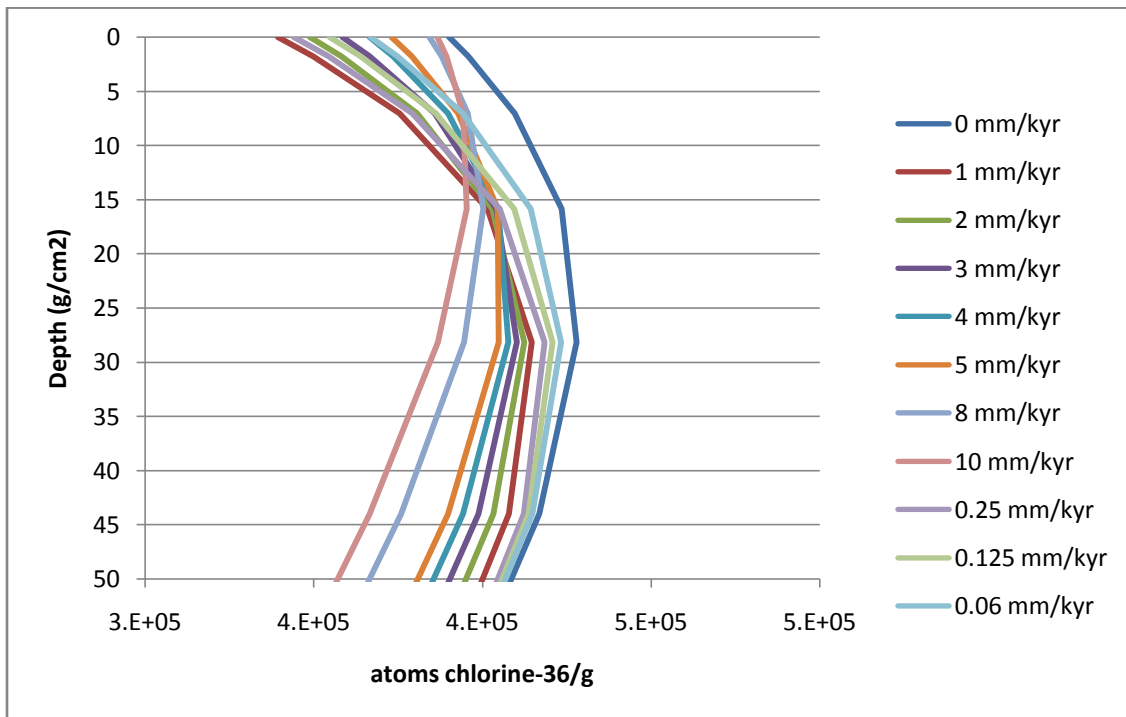


Figure 41-Depth profiles for sample 05TAB03 for varying erosion rates.

Although the depth profile sensitivity analysis does not directly show the effect of erosion on the production rate calibration, it is possible to infer that surface samples, which can be very sensitive to erosion, may not be the best method to calibrate the most

sensitive pathways, such as the thermal neutron absorption pathway. In this case, a sample from 15 cm depth may be a better option for at least some of the calibrated parameters. Based on the sensitivity studies, surface calibrated calcium and potassium rates seem to be more robust than the thermal neutron absorption pathway. A future calibration is planned using depth profile samples instead of surface samples for the  $P_f(0)$  pathway.

#### **5.4.2 Discussion**

The new production rates are similar enough to the other published values to be reasonable. In particular, the potassium rate is between the two preferred rates, Phillips and Stone. A rate between these two is probably close to the actual value of the production rate for this pathway. Overall, recent results are yielding calculated potassium production rates that appear to be converging toward a resolution of some of the discrepancy among the published production rates.

Another positive direction is the low value for  $P_f(0)$ . The original calculation of the Phillips, Stone, and Swanson rates depended on a specific formulation of each production pathway. It is possible that one of these pathways was calculated incorrectly or the samples were not sufficient to adequately constrain it. The most obvious choice is the thermal neutron absorption pathway. In this case, I believe that the sample 05PPT08 and its replicate constrains this pathway relatively well due to the low Ca and K concentrations. This low production rate seems to be in agreement with the Phillips rate. This is an area where a detailed calibration should still be performed in the future.

The new preliminary production rate described here used only the most recent methods and technology. The accuracy of the AMS has improved over the last decade

and this should improve all the chlorine-36 production rate calibration results. In this case, we do not have enough samples to accurately assess the effect of the better AMS results, or even better elemental analysis by XRF or ICP (Inductively Coupled Plasma), as contributing to better production rates. In general, it is safe to assume that better measurements will lead to better results.

In an area with more than 80 radiocarbon dates (OVIATT et al., 1992), it is clear that the independent age constraints are quite good at this location. Unfortunately, it is impossible to assess the independent age constraints used by each of the research groups to calculate the production rates based on the resulting production rates. This is still a possible source of discrepancy among production rates. It is more of a concern with the Swanson rate due to the single source of the independent ages. With both Phillips and Stone production rates, there are several sites with several independent ages from varying locations. The Swanson rates are based on a single location and a small error or incorrect assumption would propagate through into the production rates.

Scaling is another factor that may affect the Swanson rates more than the Phillips and Stone rates. If the geographic area for the Swanson production rate calibration, the Puget Lowlands, has some unrecognized systematic factor such as an atmospheric pressure anomaly, the scaling factor could be significantly different than the standard scaling factor that was used. In the case of both Phillips and Stone, this effect would be minimized by the use of several locations instead of a single location. This factor is a legitimate possibility because the production rate would be unique to that geographic location and Swanson is consistently able to correctly date exposure ages in the Puget

Lowlands region using the same production rates that provide such erroneous results at the Lake Bonneville sites.

Using these samples, resolution of the question of whether using mineral separates or whole rock is a significant source of the discrepancy in the calculated production parameters seems clear. Because Phillips and Swanson both use whole rock, while Stone uses mineral separates, any large discrepancies should follow the same pattern if it is the controlling factor. Because the division does not follow this pattern, the type of procedure used does not appear to have a primary effect on the production rate. However, smaller discrepancies may originate because of the different techniques.

Unfortunately, these results are based on a relatively small sample set and there were some problems with those samples. More samples of better quality are needed in order to truly calculate robust production rate parameters. The calculated production rates will improve as the Tabernacle Hill samples are redone and as mineral separates are performed on the Tabernacle Hill samples. The mineral separates will allow a specific pathway to be isolated and a production rate calculation performed based on that pathway alone. Eventually, as more sites are sampled by CRONUS-Earth members and more samples are processed, these production rates will be refined. Such an undertaking is beyond the scope of this work and will be pursued during my doctorate.

The goal of this study was not to create a new set of chlorine-36 production rates or to endorse only one of the published rates. It is clear, based on the information presented here, that none of the proposed production rates are entirely correct and that significant work will be needed to reconcile the different existing rates. Currently, the Phillips rate worked best for these particular samples, although the Stone rate is also

within uncertainty for many samples. The Swanson rate has been shown to not provide reasonable ages at this location. However, this work has also shown that with new geological calibration sites hand-picked by the CRONUS-Earth group, the production rates of chlorine-36 are beginning to agree. Hopefully, future studies at new sites and the processing of numerous samples will eventually produce cosmogenic production rates for each pathway that are generally accepted by the cosmogenic community.

## 6 CONCLUSIONS

The goal of this particular study was to assess the differences among published chlorine-36 production rates on a single surface of known age. The Phillips, Stone, and Swanson production rates were compared to two sampling sites at the first CRONUS-Earth geological calibration site: Lake Bonneville, Utah. At the first site, the Tabernacle Hill basalt, the Phillips and Stone production rates were the best fit to the radiocarbon bounds (16.6-17.4 cal ka), yielding weighted mean ages of  $17.6 \pm 0.2$  ka and  $16.9 \pm 0.2$  ka (erosion = 0.9 mm/kyr), respectively. The Swanson production rate gave a weighted mean age of  $12.7 \pm 0.2$  ka, which was significantly below the lowest radiocarbon bound. At the second site, the Promontory Point quartzite, the Phillips age was the only one that was close to the carbon-14 bounds (17.4-18.9 cal ka), even assuming zero erosion, yielding a weighted mean age of  $17.4 \pm 0.4$  ka. In this case, both Stone and Swanson rates produced ages that were considerably lower than the lowest carbon-14 bound, with weighted means of  $13.6 \pm 0.3$  ka and  $12.1 \pm 0.3$  ka, respectively. If the Bonneville sites are considered together, the Phillips rate was the most reasonable production rate. When new production rate parameters are established, the rates should be relatively close to the existing Phillips rate.

The three main pathways for chlorine-36 production do not contribute equally to the production in the rocks at these sites. The Stone rates produced ages that were in agreement with one location and disagreement at another, probably because the chemical compositions of the samples were different. In some lithologies, such as those with high Cl and low K and Ca concentrations, the thermal neutron pathway can dominate the production. The thermal neutron absorption pathway is the most complicated pathway and has the largest uncertainty. It is likely that this rate is too high in both the Stone and Swanson rates, causing the samples at Promontory Point, which are dominated by this pathway in several cases, to appear significantly too young. The eventual production rate for this pathway should be at the lower end of the range of currently published production rates.

By using the sample data and information about processing techniques, reasons for the discrepancy among production rates were examined in detail. While both the scaling of production rates to account for atmospheric anomalies and the lack of adequate independent age constraints at the original calibration site could have contributed to the variation in the Swanson production rate, these could not be assessed with this data. One factor that could be clearly assessed was the use of mineral separates versus whole rock during calibration. Mineral separates should provide the most precise answers due to the isolation of a specific production pathway. Ideally, if all pathways are quantified, mineral separate results should provide the same answers as whole rock for the age and inventory of a sample. Phillips and Swanson both calibrated production rates on whole rock, while Stone calibrated production rates on mineral separates. Since both Phillips and Stone were close to the correct age at Tabernacle Hill, while Swanson's ages were

significantly different, it was clear that the use of whole rock instead of mineral separates did not inherently cause any large discrepancies in the results.

The chlorine-36 results from this study were compared to all other available data from these samples. The results compared favorably with the other chlorine-36 data, although there was still concern over several of the samples that did not fall within the carbon-14 bounds. It was clear that sample procedures must be updated to take advantage of new techniques that will help with homogeneity and reproducibility. When these data were compared to other nuclides, both beryllium-10 and helium-3, the results were also encouraging. These data were in relative agreement among the different nuclides for our best samples. This agreement, with ages calculated with the Phillips and sometimes the Stone production rates, also shows the difference among the production rates and highlights the lack of agreement between the Swanson ages and the ages calculated by other nuclide systems. This supports the fact that the Swanson production rates did not yield reasonable results at either of the Lake Bonneville sites.

In order to assess the progress of this project, new preliminary production rates were calculated based on the reproducible data from both Tabernacle Hill and Promontory Point. The lithologies of these samples were very complementary, containing rocks with significant production from all three main pathways. The preliminary rates were  $67.1 \pm 2.3$  atoms  $^{36}\text{Cl}$  (gram Ca\* yr) $^{-1}$  for calcium,  $158 \pm 11$  atoms  $^{36}\text{Cl}$  (gram K\* yr) $^{-1}$  for potassium, and  $638 \pm 27$  neutrons (gram\*yr) $^{-1}$  for  $P_f(0)$ . This appears to be moving towards agreement because the potassium rate is between the rates for Phillips and Stone, the two best sets of production rates, and the value for  $P_f(0)$  is very similar to the lowest of the published production rates, as was expected based on the

production rate comparison performed at each site. However, it is important to note that this calibration was performed on a limited dataset and is not intended to be used as a new set of production rate parameters at this time.

After more samples from varying locations and lithologies are collected and processed, new production rate parameters will be produced. Future sites include Peru, Scotland, the Puget Lowlands in Washington state, and Hawaii. Also, the addition of new mineral separates from several of the other locations will allow a more thorough examination of each of the production pathways as well as processing techniques. The mineral separates will represent isolated pathways for the main reaction types, such as potassium-enriched samples, calcium-enriched samples, and those with only chlorine target minerals. A calibration of the thermal neutron absorption pathway using samples at depth is also planned. The combination of whole rock and mineral separates from a variety of geographical locations will contribute to the calculation of very robust production rates.

## 7 REFERENCES

- Aruscavage, P. J. and Campbell, E. Y., 1983. An ion-selective electrode method for determination of chlorine in geological materials. *Talanta* **30**, 745-749.
- Balco, G., 2007. CRONUS  $^{10}\text{Be}/^{26}\text{Al}$  Web Calculator. Version 2.  
<http://hess.ess.washington.edu/math/>.
- Bentley, H. W., Phillips, F. M., and Davis, S. N., 1986. Chlorine-36 in the terrestrial environment. In: Fritz, P. and Fontes, J. C. Eds.), *Handbook of Environmental Isotope Geochemistry*. Elsevier, New York. 427-480.
- Bevington, P. R. and Robinson, D. K., 1992. *Data Reduction and Error Analysis for the Physical Sciences*. McGraw-Hill, Inc. 328 pages.
- Bright, R. C., 1963. Pleistocene lake Thatcher and Bonneville, southeastern Idaho. Doctorate, University of Minnesota. 292 pages.
- Bull, W. B., 1996. Prehistorical earthquakes on the Alpine fault, New Zealand. *Journal of Geophysical Research* **101**, 6037-6050.
- Cas, R. A. F. and Wright, J. V., 1988. *Volcanic Successions: modern and ancient: A geological approach to processes, products and successions*. Unwin Hyman, London. 528 pages.
- Cerling, T. E. and Craig, H., 1994a. Cosmogenic  $^3\text{He}$  production rates from 39°N to 46°N latitude, western USA and France. *Geochimica et Cosmochimica Acta* **58**, 249-255.
- Cerling, T. E. and Craig, H., 1994b. Geomorphology and in-situ cosmogenic isotopes. *Annual Review of Earth and Planetary Sciences* **22**, 273-317.
- Condie, K. C. and Barsky, C. K., 1972. Origin of Quaternary Basalts from the Black Rock Desert Region, Utah. *Geological Society of America Bulletin* **83**, 333-352.
- Currey, D. R., Oviatt, C. G., and Plyler, G. B., 1983. Lake Bonneville stratigraphy, geomorphology, and isostatic deformation in west-central Utah, *Geologic Excursions in Neotectonics and Engineering Geology in Utah*. 63-82.
- Davis, R., Jr. and Schaeffer, O. A., 1955. Chlorine-36 in nature. *Annals of the New York Academy of Science* **62**, 105-122.
- DeGrey, L., Miller, M., and Link, P., 2008. Lake Bonneville Flood.  
[http://geology.isu.edu/Digital\\_Geology\\_Idaho/Module14/mod14.htm](http://geology.isu.edu/Digital_Geology_Idaho/Module14/mod14.htm).
- Desilets, D. and Zreda, M. G., 2001. On scaling cosmogenic nuclide production rates for altitude and latitude using cosmic-ray measurements. *Earth and Planetary Science Letters* **193**, 213-225.
- Desilets, D. and Zreda, M. G., 2003. Spatial and temporal distribution of secondary cosmic-ray nucleon intensities and applications to in situ cosmogenic dating. *Earth and Planetary Science Letters* **206**, 21-42.

- Desilets, D., Zreda, M. G., Almasi, P. F., and Elmore, D., 2006a. Determination of cosmogenic  $^{36}\text{Cl}$  in rocks by isotope dilution: innovations, validation and error propagation. *Chemical Geology* **233**, 185-195.
- Desilets, D., Zreda, M. G., and Prabu, T., 2006b. Extended scaling factors for in situ cosmogenic nuclides: New measurements at low latitude. *Earth and Planetary Science Letters* **246**, 265-276.
- Dethier, D. P., Fred Pessl, J., Keuler, R. F., Balzarini, M. A., and Pevear, D. R., 1995. Late Wisconsinan glaciomarine deposition and isostatic rebound, northern Puget Lowland, Washington. *GSA Bulletin* **107**, 1288-1303.
- Dunai, T. J., 2000. Scaling factors for production rates of in situ produced cosmogenic nuclides: a critical reevaluation. *Earth and Planetary Science Letters* **176**, 157-169.
- Dunbar, N. W., 1999. Cosmogenic  $^{36}\text{Cl}$ -determined age of the Carrizozo lava flows, south-central New Mexico. *New Mexico Geology* **21**, 25-29.
- Dunbar, N. W. and Phillips, F. M., 2004. Cosmogenic  $^{36}\text{Cl}$  ages of lava flows in the Zuni-Bandera volcanic field, north-central New Mexico, U.S.A. *New Mexico Bureau of Geology & Mineral Resources Bulletin* **160**, 309-318.
- Dunne, J., Elmore, D., and Muzikar, P., 1999. Scaling factors for the rates of production of cosmogenic nuclides for geometric shielding and attenuation at depth on sloped surfaces. *Geomorphology* **27**, 3-11.
- Easterbrook, D. J., 2003. Comment on the paper "*Determination of  $^{36}\text{Cl}$  Production Rates from the Well-Dated Deglaciation Surfaces of Whidbey and Fidalgo Islands, Washington*" by T. W. Swanson and M. C. Caffee. *Quaternary Research* **59**, 132-134.
- Elmore, D. and Phillips, F. M., 1987. Accelerator Mass Spectrometry for Measurement of Long-Lived Radioisotopes. *Science* **236**, 543-550.
- Elsheimer, H. N., 1987. Application of an Ion-Selective Electrode Method to the Determination of Chloride in 41 International Geochemical Reference Materials. *Geostandards Newsletter* **11**, 115-122.
- Evans, J. M., 2001. Calibration of the production rates of cosmogenic  $^{36}\text{Cl}$  from potassium. Doctorate of Philosophy, advised by Stone, J. O., The Australian National University. 142 pages.
- Evans, J. M., Stone, J. O. H., Fifield, L. K., and Cresswell, R. G., 1997. Cosmogenic chlorine-36 production in K-feldspar. *Nuclear Instruments and Methods in Physics Research B* **123**, 334-340.
- Fabryka-Martin, J., 1988. Production of radionuclides in the earth and their hydrogeologic significance, with emphasis on chlorine-36 and iodine-129. Doctor of Philosophy with a major in Hydrology, advised by Davis, S. N., Hydrology and Water Resources, University of Arizona. 400 pages.
- Felton, A., Godsey, H. S., Jewell, P. W., Chan, M., and Currey, D. R., 2002. Depositional models for tufa development in Pleistocene Lake Bonneville, Utah. *Geological Society of America, 2002 annual meeting* **34**, 368.
- Felton, A., Jewell, P. W., Chan, M., and Currey, D. R., 2006. Controls on Tufa Development in Pleistocene Lake Bonneville, Utah. *Journal of Geology* **114**, 377-389.

- Ford, T. D. and Pedley, H. M., 1996. A review of tufa and travertine deposits of the world. *Earth-Science Reviews* **41**, 117-175.
- Gaisser, T. K., 1990. *Cosmic Rays and Particle Physics*. Cambridge University Press, Cambridge. 279 pages.
- Gilbert, G. K., 1890. Lake Bonneville. *U.S. Geological Survey Monograph* **1**.
- Godsey, H. S., Currey, D. R., and Chan, M. A., 2005. New evidence for an extended occupation of the Provo shoreline and implications for regional change, Pleistocene Lake Bonneville, Utah, USA. *Quaternary Research* **63**, 212-223.
- Google, 2008. Google Earth. Version 4.3. <http://earth.google.com/>.
- Gosse, J. C. and Phillips, F. M., 2001. Terrestrial in situ cosmogenic nuclides: theory and application. *Quaternary Science Reviews* **20**, 1475-1560.
- Guyodo, Y. and Valet, J.-P., 1996. Relative variations in geomagnetic intensity from sedimentary records: the past 200,000 years. *Earth and Planetary Science Letters* **143**, 23-36.
- Guyodo, Y. and Valet, J.-P., 1999. Global changes in intensity of the Earth's magnetic field during the past 800 kyr. *Nature* **399**, 4.
- Handwerger, D. A., Cerling, T. E., and Bruhn, R. L., 1999. Cosmogenic <sup>14</sup>C in carbonate rocks. *Geomorphology* **27**, 13-24.
- Heisinger, B., Lal, D., Jull, A. J. T., Kubik, P., Ivy-Ochs, S., Knie, K., and Nolte, E., 2002. Production of selected cosmogenic radionuclides by muons: 2. Capture of negative muons. *Earth and Planetary Science Letters* **200**, 357-369.
- Idaho State University, 2006. Digital Geology of Idaho. <http://geology.isu.edu/nsf-isugeol/Modules/Module15/Module15.htm>.
- Korte, M. and Constable, C. G., 2005. Continuous geomagnetic field models for the past 7 millennia: 2. CALS7K. *Geochemistry, Geophysics, Geosystems* **6**, Q02H16.
- Lal, D., 1991. Cosmic ray labeling of erosion surfaces: In situ nuclide production rates and erosion models. *Earth and Planetary Science Letters* **104**, 424-439.
- Lal, D. and Peters, B., 1967. Cosmic Ray Produced Radioactivity on the Earth. In: Sitte, K. (Ed.), *Hanbuch der Physik*. Springer, Berlin. 551-612.
- Licciardi, J. M., Denoncourt, C. L., and Finkel, R., 2008. Cosmogenic <sup>36</sup>Cl production rates from Ca spallation in Iceland. *Earth and Planetary Science Letters* **267**, 365-377.
- Lifton, N., Smart, D. F., and Shea, M. A., 2008. Scaling time-integrated in situ cosmogenic nuclide production rates using a continuous geomagnetic model. *Earth and Planetary Science Letters* **268**, 190-201.
- Lifton, N. A., 2005. *Bonneville Sampling Plan*. (Unpublished)
- Lifton, N. A., Bieber, J. W., Clem, J. M., Duldig, M. L., Evenson, P., Humble, J. E., and Pyle, R., 2005. Addressing solar modulation and long-term uncertainties in scaling in situ cosmogenic nuclide production rates. *Earth and Planetary Science Letters* **239**, 140-161.
- Lifton, N. A., Jull, A. J. T., and Quade, J., 2001. A new extraction technique and production rate estimate for in situ cosmogenic <sup>14</sup>C in quartz. *Geochimica et Cosmochimica Acta* **65**, 1953-1969.
- Liu, B., Phillips, F. M., Fabryka-Martin, J., Fowler, M. M., and Stone, W. D., 1994. Cosmogenic <sup>36</sup>Cl accumulation in unstable landforms 1. Effects of the thermal neutron distribution. *Water Resources Research* **30**, 3115-3125.

- Masarik, J., 2002. Numerical simulation of in-situ produced cosmogenic nuclides. *Geochimica et Cosmochimica Acta* **66**, A491.
- Masarik, J. and Wieler, R., 2003. Production rates of cosmogenic nuclides in boulders. *Earth and Planetary Science Letters* **216**, 201-208.
- Merriam-Webster, 2001. Merriam-Webster's Atlas Online. [http://www.merriam-webster.com/maps/images/utah\\_map.gif](http://www.merriam-webster.com/maps/images/utah_map.gif).
- Nishiizumi, K., Winterer, E. L., Kohl, C. P., Klein, J., Middleton, R., Lal, D., and Arnold, J. R., 1989. Cosmic Ray Production Rates of  $^{10}\text{Be}$  and  $^{26}\text{Al}$  in Quartz From Glacially Polished Rocks. *Journal of Geophysical Research* **94**, 9.
- O'Brien, K., 1979. Secular Variations in the Production of Cosmogenic Isotopes in the Earth's Atmosphere. *Journal of Geophysical Research* **84**, 423-431.
- Oviatt, C. G., 1991. Quaternary geology of the Black Rock Desert, Millard County, Utah. *Utah Geol. Min. Surv. Spec. Stud.* **73**.
- Oviatt, C. G., 1997. Lake Bonneville fluctuations and global climate change. *Geology* **25**, 155-158.
- Oviatt, C. G., Currey, D. R., and Sack, D., 1992. Radiocarbon chronology of Lake Bonneville, Eastern Great Basin, USA. *Palaeogeography, Palaeoclimatology, Palaeoecology* **99**, 225-241.
- Oviatt, C. G. and Miller, D. M., 2005. *Lake Bonneville: Overview and geomorphic considerations*. (Unpublished)
- Oviatt, C. G. and Nash, W. P., 1989. Late Pleistocene basaltic ash and volcanic eruptions in the Bonneville basin, Utah *Geological Society of America Bulletin* **101**, 292-303.
- Phillips, F. M. and Plummer, M. A., 1996. CHLOE: A program for interpreting in-situ cosmogenic nuclide data for surface exposure dating and erosion studies. *Radiocarbon (Abstr. 7th Int. Conf. Accelerator Mass Spectrometry)* **38**, 98-99.
- Phillips, F. M., Stone, W. D., and Fabryka-Martin, J., 2001. An improved approach to calculating low-energy cosmic-ray neutron fluxes near the land/atmosphere interface. *Chemical Geology* **175**, 689-701.
- Phillips, F. M., Zreda, M. G., Flinsch, M. R., Elmore, D., and Sharma, P., 1996. A reevaluation of cosmogenic  $^{36}\text{Cl}$  production rates in terrestrial rocks. *Geophysical Research Letters* **23**, 949-952.
- Phillips, F. M., Zreda, M. G., Gosse, J. C., Klein, J., Evenson, E. B., Hall, R. D., Chadwick, O. A., and Sharma, P., 1997. Cosmogenic  $^{36}\text{Cl}$  and  $^{10}\text{Be}$  ages of Quaternary glacial and fluvial deposits of the Wind River Range, Wyoming. *GSA Bulletin* **109**, 1453-1463.
- Pigati, J. S. and Lifton, N., 2004. Geomagnetic effects on time-integrated cosmogenic nuclide production with emphasis on in situ  $^{14}\text{C}$  and  $^{10}\text{Be}$ . *Earth and Planetary Science Letters* **226**, 193-205.
- Povh, B., Rith, K., Scholz, C., and Zetsche, F., 2004. *Particles and Nuclei: An Introduction to the Physical Concepts*. Springer, Berlin. 396 pages.
- Press, F. and Siever, R., 2001. *Understanding Earth*. W. H. Freeman and Company. 121 pages.
- Rubin, M. and Berthold, S. M., 1961. U.S. Geological Survey radiocarbon dates VI. *Radiocarbon* **3**, 86-98.

- Sack, D., 1999. The Composite Nature of the Provo Level of Lake Bonneville, Great Basin, Western North America. *Quaternary Research* **52**, 316-327.
- Scott, W. E., 1988. Transgressive and high-shore deposits of the Bonneville lake cycle near North Salt Lake, Utah. *Utah Geol. Min. Surv. Misc. Publ.* **88**, 38-42.
- Stone, J., 2000. Air pressure and cosmogenic isotope production. *Journal of Geophysical Research* **105**, 23753-23760.
- Stone, J. O., 2005. Terrestrial chlorine-36 production from spallation of iron *10th International Conference on Accelerator Mass Spectrometry*, Berkeley, California.
- Stone, J. O., Allan, G. L., Fifield, L. K., and Cresswell, R. G., 1996. Cosmogenic chlorine-36 from calcium spallation. *Geochimica et Cosmochimica Acta* **60**, 679-692.
- Stone, J. O., Allan, G. L., Fifield, L. K., Evans, J. M., and Chivas, A. R., 1994. Limestone erosion measurements with cosmogenic chlorine-36 in calcite - preliminary results from Australia. *Nuclear Instruments and Methods in Physics Research B* **92**, 311-316.
- Stone, J. O. H., Evans, J. M., Fifield, L. K., Allan, G. L., and Cresswell, R. G., 1998. Cosmogenic chlorine-36 production in calcite by muons. *Geochimica et Cosmochimica Acta* **62**, 433-454.
- Stuiver, M. and Reimer, P. J., 1993. *Radiocarbon* **35**, 215-230.
- Stuiver, M., Reimer, P. J., and Reimer, R., 2005. CALIB radiocarbon calibration. Version 5.0. <http://radiocarbon.pa.qub.ac.uk/calib>.
- Swanson, T. and Caffee, M., 2005. Reply to Comment by D.J. Easterbrook on "Determination of <sup>36</sup>Cl Production Rates from the Well-Dated Deglaciation Surfaces of Whidbey and Fidalgo Islands, Washington. *Quaternary Research* **63**, 228-230.
- Swanson, T. W. and Caffee, M. L., 2001. Determination of <sup>36</sup>Cl Production Rates Derived from the Well-Dated Deglaciation Surfaces of Whidbey and Fidalgo Islands, Washington. *Quaternary Research* **56**, 366-382.
- Thomas, T. R., 2005. A method for preparation of rock samples for measurement of <sup>36</sup>Cl by isotope dilution accelerator mass spectrometry. Independent Study, Master of Science in Geochemistry, advised by Phillips, F. M., Earth and Environmental Science, New Mexico Tech.
- Utah Geological Survey, 2008. Where was Lake Bonneville, how large was it, and when did it exist? <http://geology.utah.gov/online/PI-39/pi39pg01.htm>.
- Zreda, M. G., 1994. Development and calibration of the cosmogenic <sup>36</sup>Cl surface exposure dating method and its application to the chronology of late Quaternary glaciations. Doctorate, advised by Phillips, F. M., Earth and Environmental Science, New Mexico Tech. 318 pages.
- Zreda, M. G. and Phillips, F. M., 1994. Cosmogenic <sup>36</sup>Cl accumulation in unstable landforms 2. Simulations and measurements on eroding moraines. *Water Resources Research* **30**, 3127-3136.
- Zreda, M. G. and Phillips, F. M., 2000. Cosmogenic Nuclide Buildup in Surficial Materials. In: Noller, J. S., Sowers, J. M., and Lettis, W. R. Eds.), *Quaternary Geochronology: Methods and Applications*. American Geophysical Union, Washington, D.C. 581.

Zreda, M. G., Phillips, F. M., Elmore, D., Kubik, P. W., Sharma, P., and Dorn, R. I., 1991. Cosmogenic chlorine-36 production rates in terrestrial rocks. *Earth and Planetary Science Letters* **105**, 94-109.

## 8 APPENDIX 1: SAMPLE CHLORINE-36 INFORMATION

### 8.1 Promontory Point Data

Table 15-Chemical data for Chlorine-36 Promontory Point samples.

Sample	05PPT01	05PPT02	05PPT03	05PPT04	05PPT05	05PPT08
<sup>a</sup> CO <sub>2</sub> (wt %)	0.60	0.60	0.20	0.01	0.40	0.10
<sup>a</sup> Na <sub>2</sub> O (wt %)	0.04	0.05	0.06	0.04	0.04	0.04
<sup>a</sup> MgO (wt %)	0.30	0.46	0.31	0.25	0.28	0.21
<sup>a</sup> Al <sub>2</sub> O <sub>3</sub> (wt %)	2.59	3.21	1.78	1.74	2.38	0.46
<sup>a</sup> SiO <sub>2</sub> (wt %)	92.90	91.40	94.20	94.40	93.70	96.50
<sup>a</sup> P <sub>2</sub> O <sub>5</sub> (wt %)	0.02	0.02	0.01	0.01	0.03	0.00
<sup>a</sup> K <sub>2</sub> O (wt %)	1.35	1.47	0.62	0.59	1.13	0.18
<sup>a</sup> CaO (wt %)	0.10	0.07	0.08	0.04	0.07	0.06
<sup>a</sup> TiO <sub>2</sub> (wt %)	0.09	0.18	0.09	0.13	0.16	0.06
<sup>a</sup> MnO <sub>2</sub> (wt %)	0.01	0.01	0.00	0.01	0.01	0.00
<sup>a</sup> Fe <sub>2</sub> O <sub>3</sub> (wt %)	1.60	1.91	1.84	2.75	1.07	0.87
<sup>d</sup> Cl (ppm)	67.06	42.12	45.06	44.41	48.86	119.95
<sup>c</sup> B (ppm)	11	11	8	12	7	3

<sup>c</sup> Sm (ppm)	< 2	1	1	1	1	1
<sup>c</sup> Gd (ppm)	< 2	1	1	1	1	1
<sup>b</sup> U (ppm)	6	<20*	<20*	<20*	<20*	<20*
<sup>b</sup> Th (ppm)	7	<20*	<20*	<20*	<20*	<20*
<b>First run</b>	<b>AMS</b>					
<sup>36</sup> Cl/Cl (x10 <sup>-15</sup> )	55.51	171.60	110.10	84.92	71.41	66.54
Error	3.74	6.70	15.21	5.06	5.05	4.53
<sup>35</sup> Cl/ <sup>37</sup> Cl	14.5000	7.0030	8.4360	8.7470	15.2400	8.0600
Error	0.0649	0.0350	0.0487	0.0437	0.0799	0.0403
<b>Second run</b>	<b>AMS</b>					
<sup>36</sup> Cl/Cl (x10 <sup>-15</sup> )	55.32	106.40	63.81	85.47	56.22	64.36
Error	2.95	4.67	3.20	5.15	2.92	2.94
<sup>35</sup> Cl/ <sup>37</sup> Cl	18.1300	8.8090	7.8550	8.3920	16.0400	8.1880
Error	0.1699	0.0509	0.0393	0.0485	0.0717	0.0409

A - determined by XRF at Michigan State University

B - determined by XRF at SGS Laboratories in Ontario, Canada; detection limits changed after measurement of 05PPT01

C - determined by NAA (neutron activation) at SGS Laboratories in Ontario, Canada

D - determined by calculations from the PRIME Lab data

E - assumed equal to measured Gd concentration

\*For the purposes of these calculations, the U & Th values from samples 05PPT01 were used in lieu of the <20 values until more accurate results can be obtained (expected August 2008)

**Table 16-Position and other data for Promontory Point samples.**

Sample	05PPT01	05PPT02	05PPT03	05PPT04	05PPT05	05PPT08
--------	---------	---------	---------	---------	---------	---------

Latitude	41.2637	41.2637	41.2636	41.2636	41.2639	41.2638
Longitude	112.475	112.475	112.476	112.477	112.475	112.475
Elevation (m)	1611	1611	1607	1604	1615	1616
Lithology	Quartzite	Quartzite	Quartzite	Quartzite	Quartzite	Quartzite
Shielding	0.975	0.992	0.884	0.982	0.981	0.884
Thickness (cm)	3	3	3	2.5	4	2.5

**Table 17-Promontory Point sample information – trial 1.**

Sample	05PPT01	05PPT02	05PPT03	05PPT04	05PPT05	05PPT08
Mass (g)	20.603	50.202	50.027	48.456	20.170	20.559
<sup>35</sup> Cl spike mass (g)	3.979	2.023	2.968	3.002	3.031	3.013
Spike concentration	0.999	0.999	0.999	0.999	0.999	0.999
Cl blank (mg Cl)	0.10	0.19	0.19	0.19	0.10	0.10
<sup>36</sup> Cl blank (at Cl-36)	957639	711541	830406	834760	838308	836093
Water content (wt %)	0.005	0.005	0.005	0.005	0.005	0.005

**Table 18- Promontory Point sample information – trial 2.**

Sample	05PPT01 B	05PPT02B	05PPT03B	05PPT04B	05PPT05B	05PPT08B
--------	--------------	----------	----------	----------	----------	----------

Mass (g)	20.029	38.968	41.610	49.408	20.054	20.077
<sup>35</sup> Cl spike mass (g)	3.992	2.990	3.007	3.003	3.004	2.993
Spike concentration	0.999	0.999	0.999	0.999	0.999	0.999
Cl blank (mg Cl)	0.11	0.19	0.19	0.19	0.11	0.10
<sup>36</sup> Cl blank (at Cl-36)	959250	833237	835326	834873	835024	833527
Water content (wt %)	0.005	0.005	0.005	0.005	0.005	0.005

## 8.2 Tabernacle Hill Data

Table 19-Chemical data for Cl-36 Tabernacle Hill samples.

Sample	05TAB01	05TAB02	05TAB03	05TAB04	05TAB05	05TAB06	05TAB07
<sup>a</sup> CO <sub>2</sub> (wt %)	0.07	0.78	0.00	0.00	0.41	0.74	0.00
<sup>a</sup> Na <sub>2</sub> O (wt %)	2.66	3.03	3.11	3.15	3.27	2.67	2.37
<sup>a</sup> MgO (wt %)	7.67	7.55	7.59	7.90	7.43	7.63	6.75
<sup>a</sup> Al <sub>2</sub> O <sub>3</sub> (wt %)	16.39	16.15	16.36	16.47	16.03	16.31	14.84
<sup>a</sup> SiO <sub>2</sub> (wt %)	49.38	48.91	48.99	49.11	49.26	49.08	46.13
<sup>a</sup> P <sub>2</sub> O <sub>5</sub> (wt %)	0.23	0.28	0.21	0.24	0.28	0.24	0.42
<sup>a</sup> K <sub>2</sub> O (wt %)	0.72	0.83	0.76	0.69	0.76	0.66	0.78
<sup>a</sup> CaO (wt %)	9.12	9.06	9.29	9.22	9.08	9.03	10.69

<sup>a</sup> TiO <sub>2</sub> (wt %)	1.59	1.54	1.63	1.57	1.58	1.58	1.42
<sup>a</sup> MnO <sub>2</sub> (wt %)	0.18	0.18	0.18	0.18	0.18	0.17	0.17
<sup>a</sup> Fe <sub>2</sub> O <sub>3</sub> (wt %)	11.93	11.65	12.17	12.00	11.68	11.82	11.65
<sup>d</sup> Cl (ppm)	78.59	83.80	105.15	70.69	182.09	82.81	149.16
<sup>c</sup> B (ppm)	0.00	0.00	0.00	0.00	0.00	0.00	0.00
<sup>c</sup> Sm (ppm)	3.00	2.00	3.00	2.00	3.00	3.00	3.00
<sup>c</sup> Gd (ppm)	3.00	2.00	3.00	2.00	3.00	3.00	3.00
<sup>b</sup> U (ppm)	0.00	0.00	3.00	0.00	2.00	4.00	0.00
<sup>b</sup> Th (ppm)	3.00	6.00	0.00	4.00	6.00	0.00	3.00
<b>First run</b>	<b>AMS</b>						
<sup>36</sup> Cl/Cl (x10 <sup>-15</sup> )	154.1	143.3	133.1	156	101.1	188.7	119
Error	5.2	5.7	5.6	6	3.6	5.7	7
<sup>35</sup> Cl/ <sup>37</sup> Cl	7.011	6.8211	6.11	7.48	4.863	6.8172	5.2545
Error	0.009	0.0041	0.012	0.037	0.007	0.0028	0.0050
<b>Second run</b>	<b>AMS</b>						
<sup>36</sup> Cl/Cl (x10 <sup>-15</sup> )	147.6	148.1	140.4	155.7	149.9	133.9	129.9
Error	6.57	5.073	5.642	7.13	5.4	4.52	4.283
<sup>35</sup> Cl/ <sup>37</sup> Cl	6.817	6.623	5.99	7.268	7.766	6.739	5.802

Error	0.0183	0.0533	0.0627	0.0118	0.024	0.0294	0.029
-------	--------	--------	--------	--------	-------	--------	-------

A - determined by XRF at Michigan State University  
B – determined by XRF at SGS Laboratories in Ontario, Canada  
C – determined by NAA (neutron activation) at SGS Laboratories in Ontario, Canada  
D – determined by calculations from the PRIME Lab data  
E – assumed equal to measured Gd concentration

**Table 20-Position and other data for Tabernacle Hill.**

Sample	05TAB01	05TAB02	05TAB03	05TAB04	05TAB05	05TAB06	05TAB07
Latitude	38.93	38.93	38.93	38.93045	38.92995	38.930067	38.930067
Longitude	112.522	112.522	112.523	112.522	112.51988	112.51897	112.51897
Elevation (m)	1458	1458	1461	1458	1455	1457	1457
Lithology	Basalt	Basalt	Basalt	Basalt	Basalt	Basalt	Basalt
Shielding	1	1	1	1	1	1	1
Thickness (cm)	3	3	3	3	3	3	3

**Table 21- Tabernacle Hill sample information – trial 1.**

Sample	05TAB01	05TAB02	05TAB03	05TAB04	05TAB05	05TAB06	05TAB07
Mass (g)	25.056	25.027	25.002	25.008	25.033	25.187	25.026
<sup>35</sup> Cl spike mass (g)	2.004	2.012	2.020	2.015	2.013	2.008	2.024
Spike concentration	0.982	0.982	0.982	0.982	0.982	0.982	0.982
Cl blank (mg Cl)	0.09	0.07	0.08	0.07	0.08	0.08	0.07

<sup>36</sup> Cl blank (at Cl-36)	704883	705810	706887	706293	705934	705390	707357
Water content (wt %)	0.005	0.005	0.005	0.005	0.005	0.005	0.005

**Table 22- Tabernacle Hill sample information – trial 2.**

Sample	05TAB01B	05TAB02B	05TAB03B	05TAB04B	05TAB05B	05TAB06B	05TAB07B
Mass (g)	24.893	25.732	25.389	25.332	25.337	25.072	25.033
<sup>35</sup> Cl spike mass (g)	2.015	2.107	2.018	2.018	2.085	2.044	2.026
Spike concentration	0.999	0.999	0.999	0.999	0.999	0.999	0.999
Cl blank (mg Cl)	0.08	0.08	0.08	0.08	0.08	0.08	0.09
<sup>36</sup> Cl blank (at Cl-36)	710559	722122	710849	710861	719379	714221	711931
Water content (wt %)	0.005	0.005	0.005	0.005	0.005	0.005	0.005

## 9 APPENDIX 2: FIELD SAMPLE PHOTOS AND FIELD SKETCHES

All sample photographs presented in this appendix were taken by Nishiizumi (personal communication, 2005) unless otherwise indicated.

### 9.1 *Tabernacle Hill photos and field data*

#### 9.1.1 05TAB01

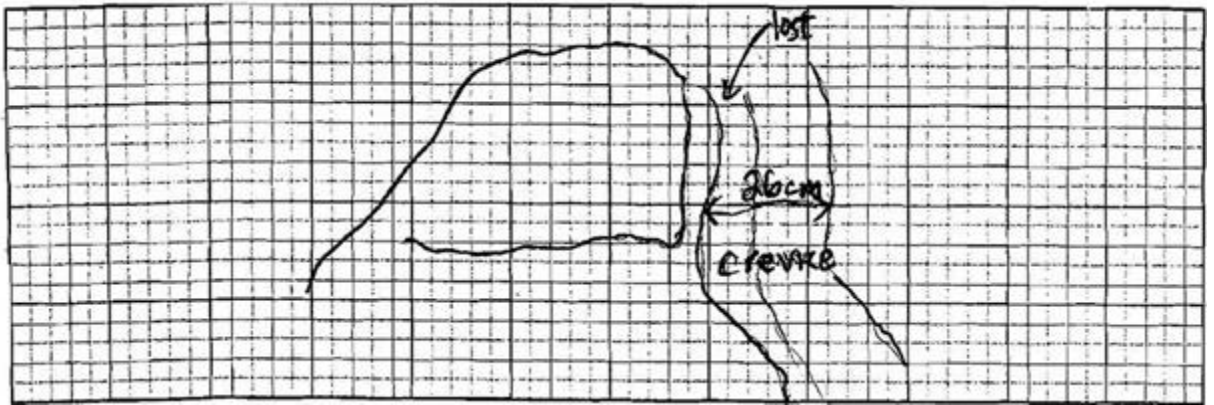


Figure 42-Official CRONUS field note sketch.

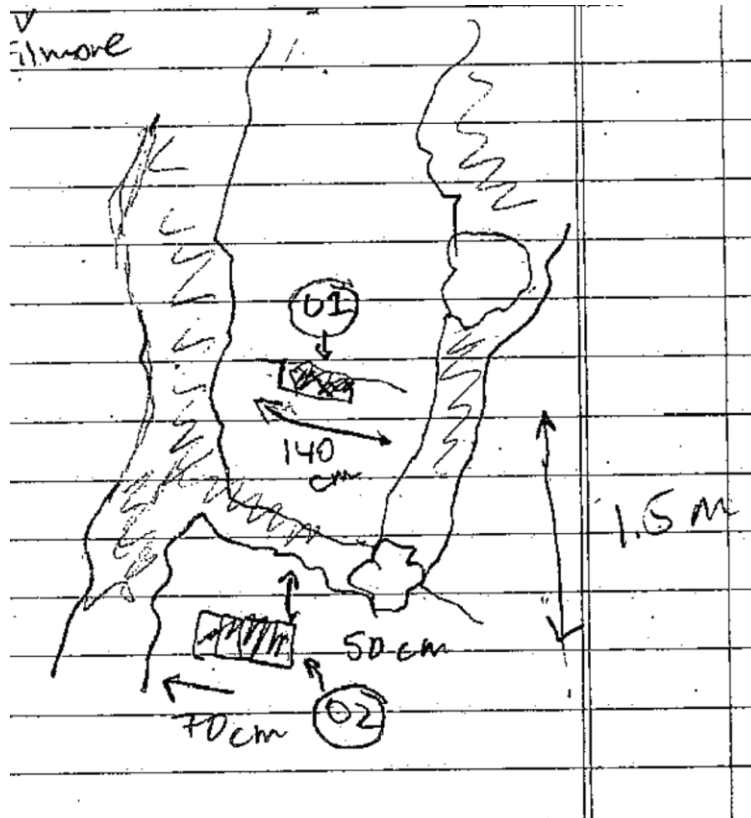


Figure 43- Same sketch for samples 05TAB01 & 05TAB02 (Kurz, personal communication, 2005).



Figure 44-05TAB01 prior to sample collection.



**Figure 45-05TAB01 prior to sample collection.**



**Figure 46-The horizon for 05TAB01.**



**Figure 47-Sample 05TAB01 after sample collection.**

### 9.1.2 05TAB02

“Before” pictures are the same as 05TAB01. Horizon pictures and the sketches are the same as well.



Figure 48-Sample 05TAB02 after collection.

### 9.1.3 05TAB03

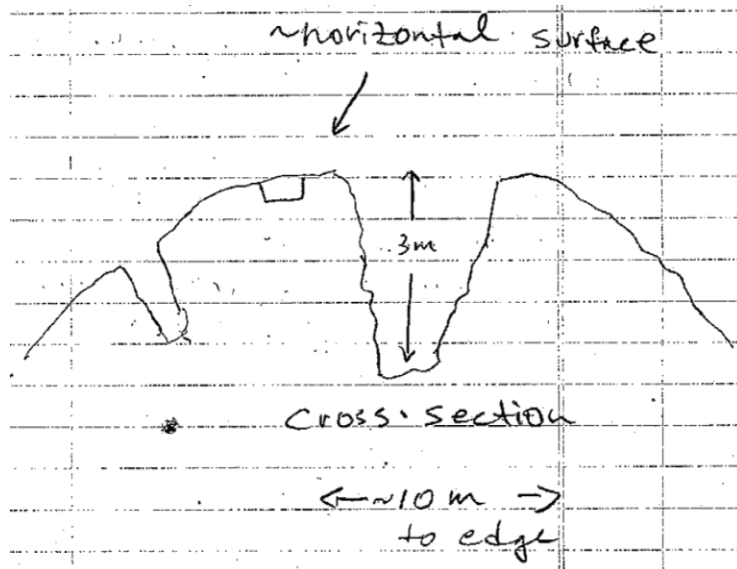
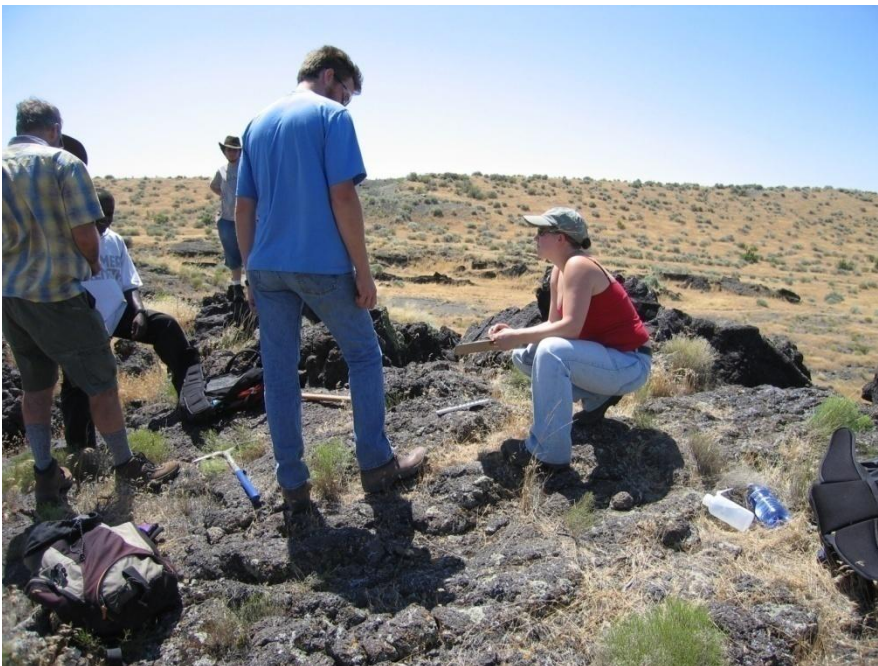


Figure 49-Sketch of 05TAB03 (Kurz, personal communication, 2005)



**Figure 50-Location of sample 05TAB03 at top of basalt tumulus.**



**Figure 51-Collection of sample 05TAB03.**



**Figure 52-Sample location for 05TAB03.**



**Figure 53-Horizon view for 05TAB03.**



**Figure 54-The sample location and sample 05TAB03 after collection.**



Figure 55-Sample 05TAB03 after sample collection.

#### 9.1.4 05TAB04

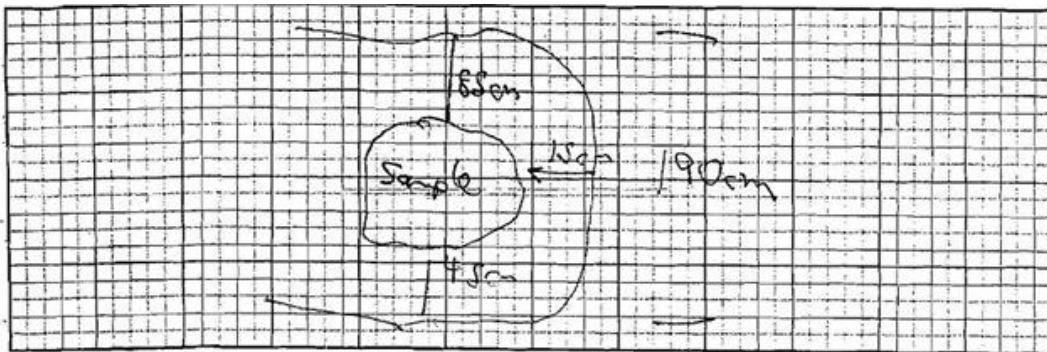


Figure 56-Official CRONUS field notes.

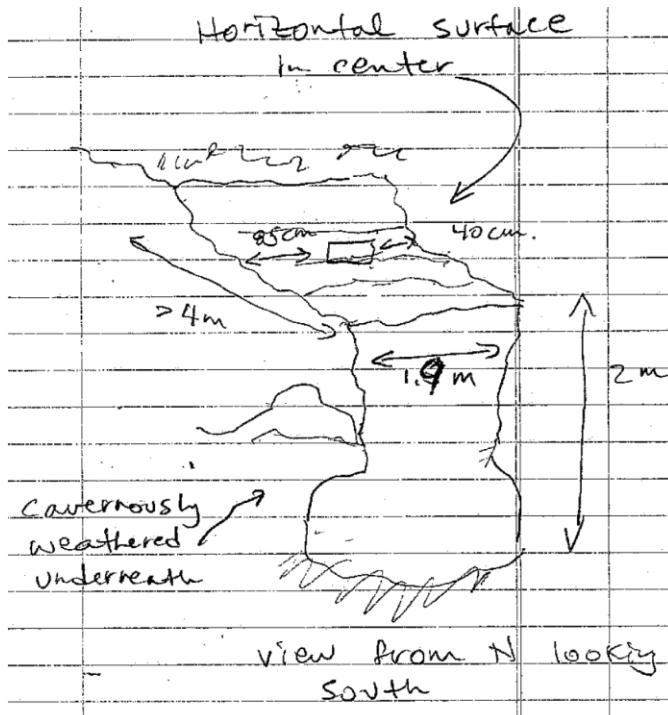


Figure 57-Sample sketch of 05TAB04 (Kurz, personal communication, 2005).



Figure 58-Sample location for 05TAB04.



**Figure 59-Sample location for sample 05TAB04.**



**Figure 60-Sample 05TAB04 after collection.**



Figure 61-Sample 05TAB04 after collection.

### 9.1.5 05TAB05

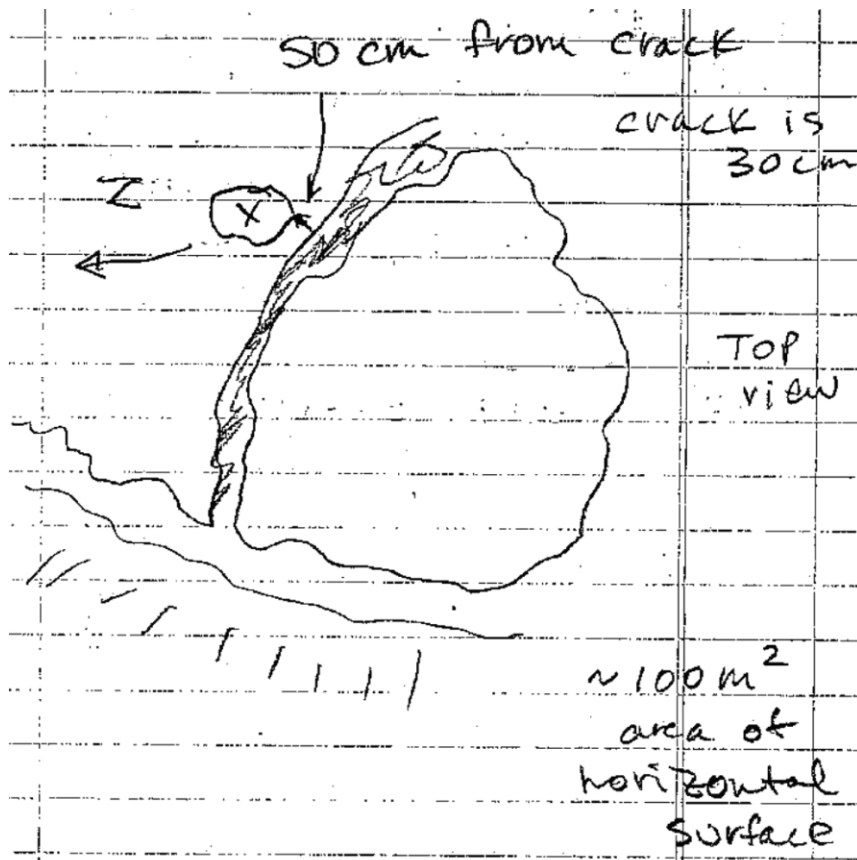


Figure 62-Sample sketch for 05TAB05 (Kurz, personal communication, 2005).



**Figure 63-Sample location for 05TAB05 at the top of the tumulus.**



**Figure 64-05TAB05 prior to sample collection.**



**Figure 65-05TAB05 prior to sample collection.**



**Figure 66-Horizon for sample 05TAB05.**



**Figure 67-Sample 05TAB05 after cutting but prior to collection.**



Figure 68-The sample location and sample 05TAB05 after collection.

### 9.1.6 05TAB06

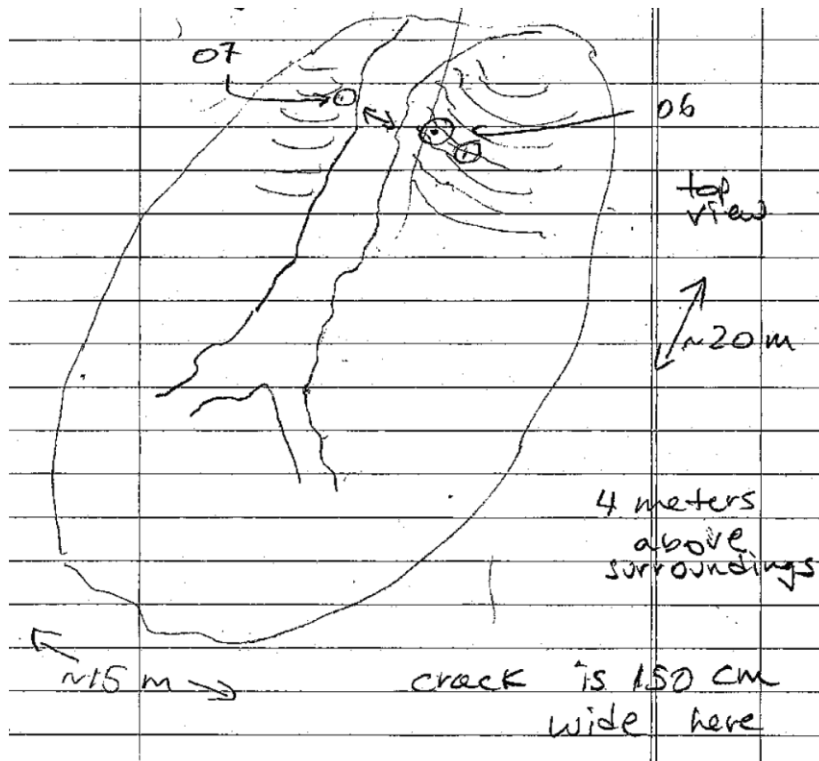


Figure 69-Sketch for both 05TAB06 & 05TAB07 (Kurz, personal communication, 2005).



**Figure 70-Sample location for 05TAB06.**



**Figure 71-Sample location for 05TAB06.**



Figure 72-Sample location for 05TAB06.



Figure 73-Horizon for samples 05TAB06 & 05TAB07.



Figure 74-Sample location for 05TAB06 after sample collection.

### 9.1.7 05TAB07

The panoramic view, before photos, and sketches are the same as 05TAB06.



**Figure 75-Left side is the 05TAB06 while the right side is 05TAB07.**



**Figure 76-Sample location for 05TAB07.**



Figure 77-Chipped out sample (in place) for 05TAB07.

## 9.2 Promontory Point Samples

### 9.2.1 05PPT01

Sketch rock (if desired):

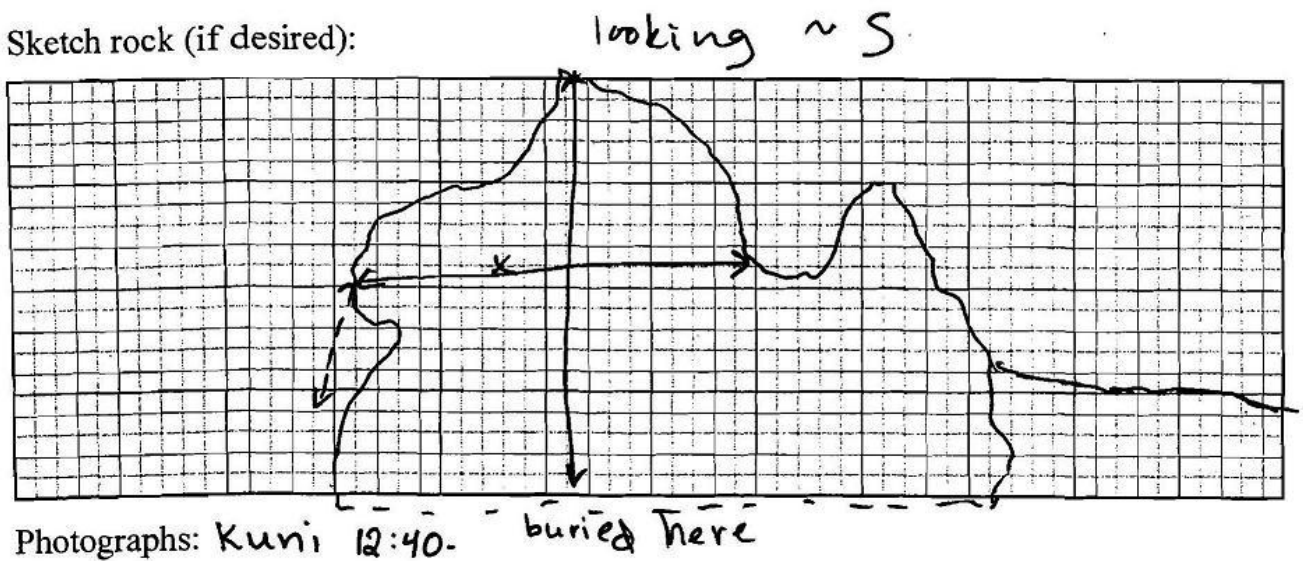


Figure 78-Official CRONUS field sketch.



**Figure 79-05PPT01 before sampling .**



**Figure 80-05PPT01 in profile before sampling.**



Figure 81-05PPT01 after sampling.

### 9.2.2 05PPT02

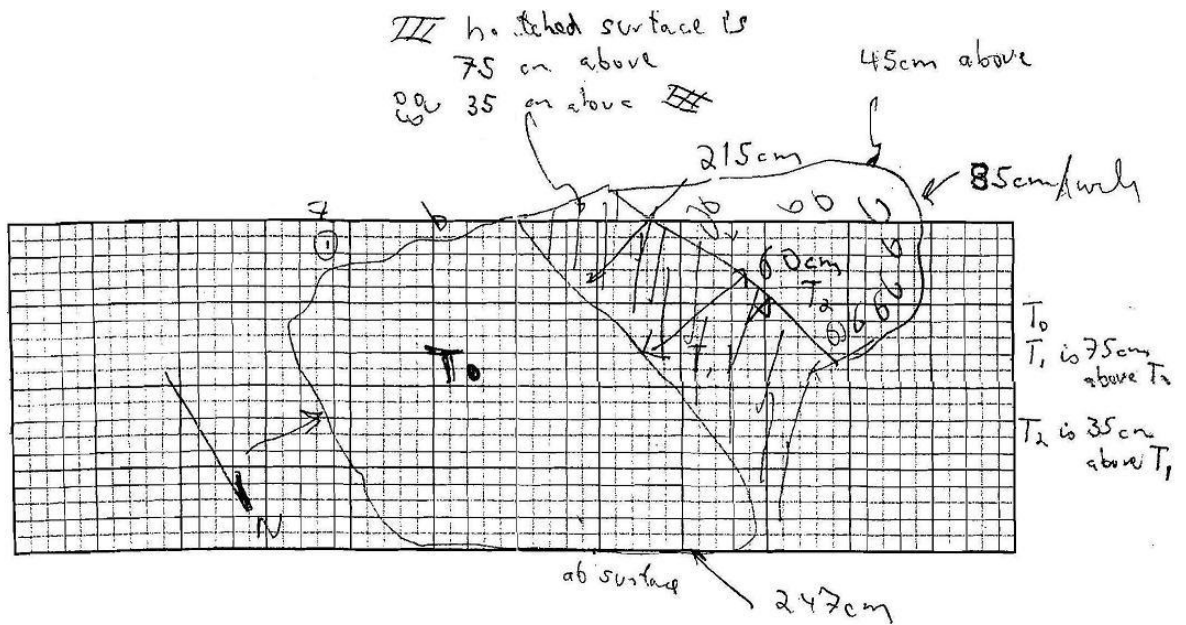


Figure 82-Official CRONUS field sketch.



**Figure 83-05PPT02 before sampling.**



**Figure 84-05PPT02 after sampling.**

9.2.3 05PPT03

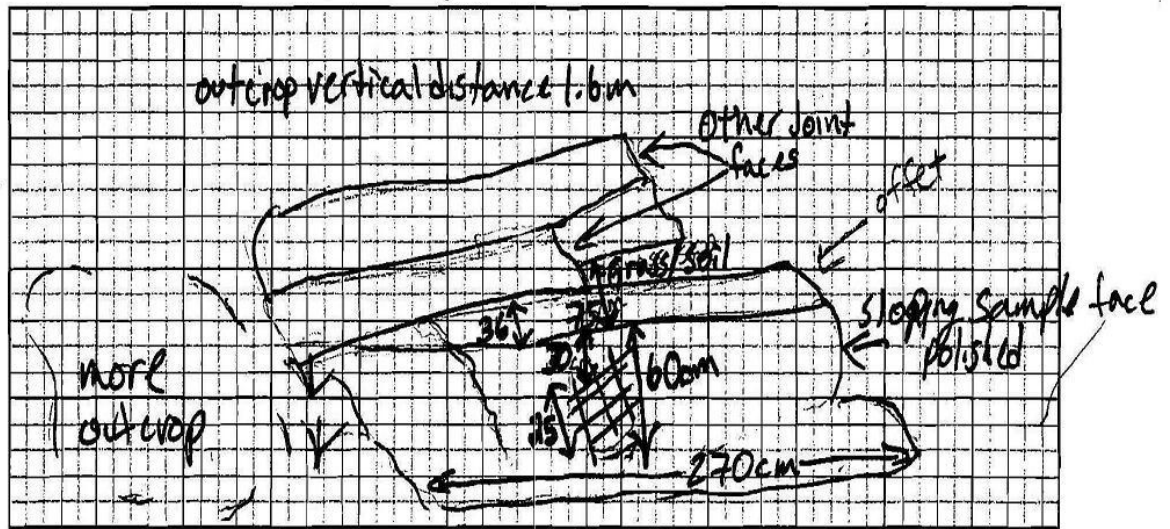


Figure 85-Official CRONUS field sketch.



Figure 86-05PPT03 before sampling.



**Figure 87-05PPT03 before sampling. Note blocky appearance of outcrop.**



**Figure 88-05PPT03 after sampling.**

## 9.2.4 05PPT04

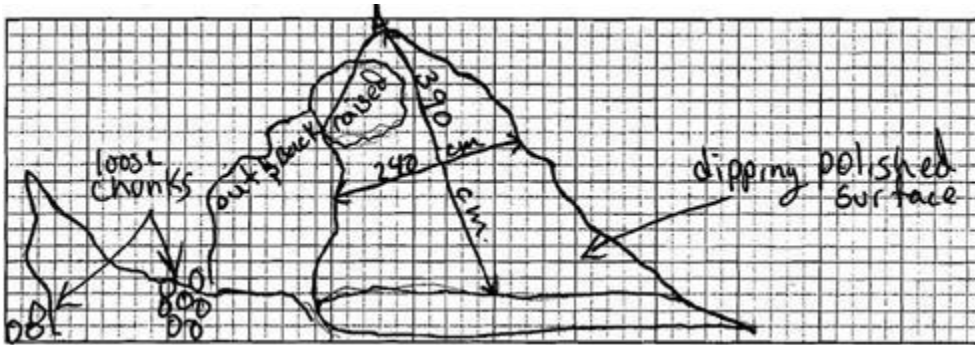


Figure 89-CRONUS field notes



Figure 90-05PPT04 before sampling.



**Figure 91-05PPT04 before sampling in profile.**



**Figure 92-Panorama around 05PPT04.**



**Figure 93-05PPT04 after sampling.**

9.2.5 05PPT05

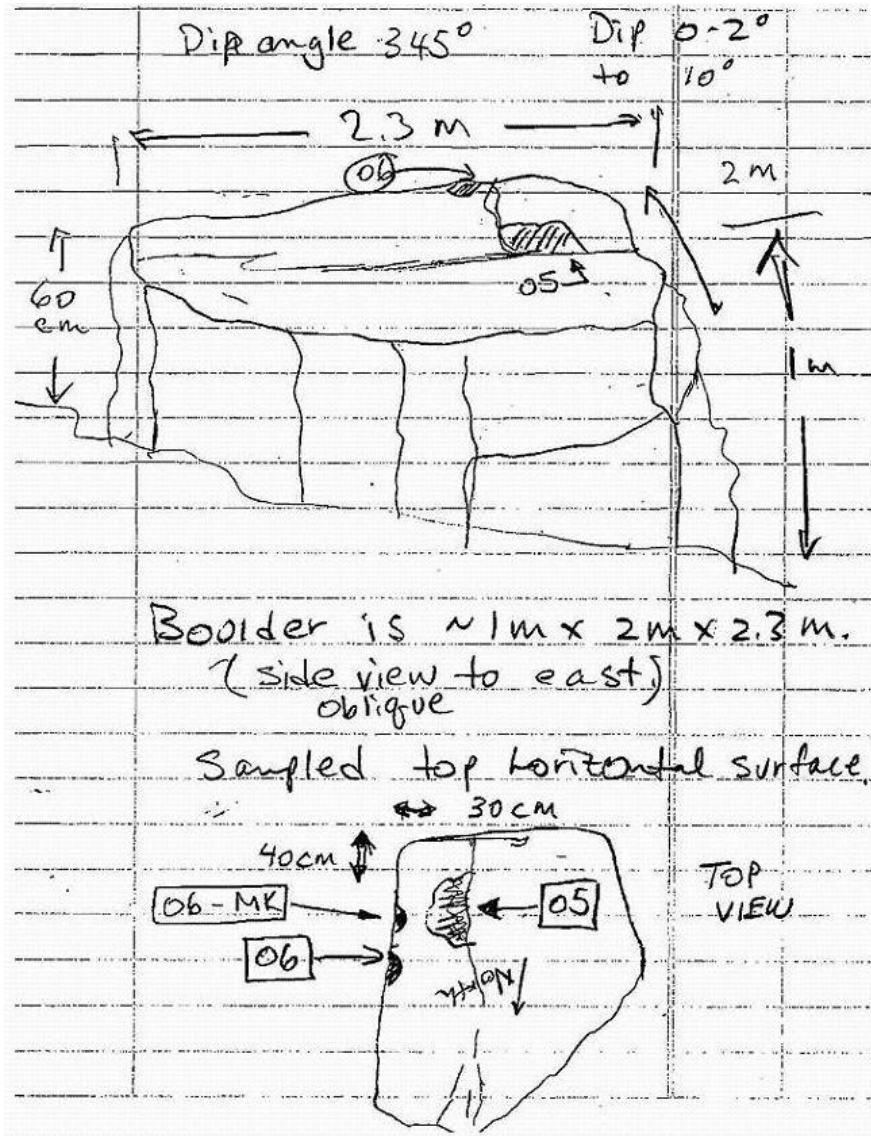


Figure 94-Sketch of samples 05PPT05 and 05PPT06 (not used in this study) (Kurz, personal communication, 2005).



**Figure 95-05PPT05 before sampling.**



**Figure 96-05PPT05 before sampling. Note profile of outcrop.**



Figure 97-05PPT05 after sampling. 05PPT05 and 05PPT06 were taken at the same location. 05PPT05 is the center piece while 05PPT06 was taken from an edge to examine edge effects.

### 9.2.6 05PPT08

Sketch rock (if desired):

looking S

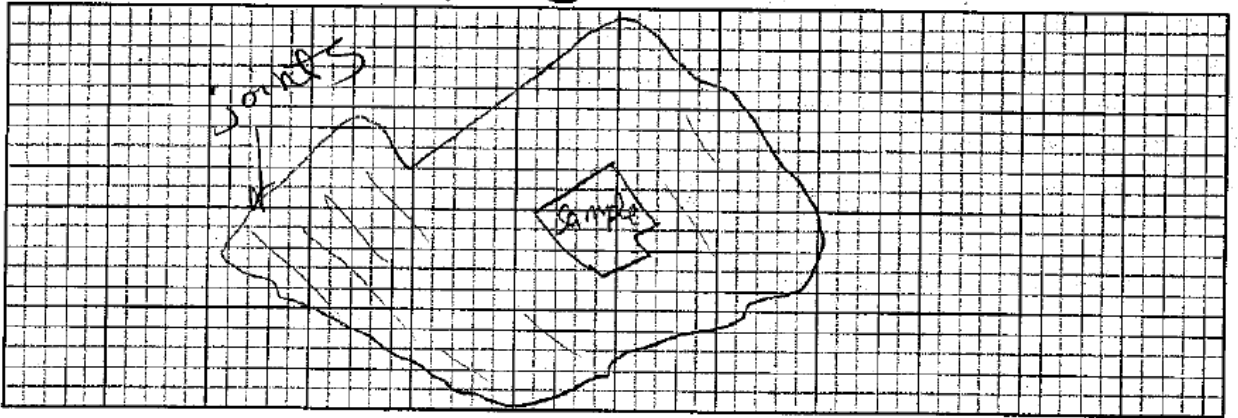


Figure 98-Official CRONUS field sketch.



Figure 99-05PPT08 before sampling.



Figure 100-05PPT08 in profile before sampling.



**Figure 101-05PPT08 panorama from sample.**



**Figure 102-05PPT08 after sampling.**

## **10 APPENDIX 3: CHLORINE-36 SAMPLE PREPARATION PROCEDURE**

### ***10.1 Sample splitting procedure***

The splitting procedure was from Clifton (personal communication, May 12, 2008). The samples were split into two parts repeatedly using a commercial sample splitter and aluminum pans. The splitting procedure was as follows:

- 1) Split the sample once into two parts: named 1 & 2.
- 2) Split the two samples into four parts and name them 1,2,3,4.
- 3) Combine parts 1 & 3, and 2 & 4.
- 4) Split 1 & 3 into two parts, and 2 & 4 into two parts.
- 5) Repeat this procedure until the sample has been split into an appropriately sized sample.

## **10.2 Rock preparation**

### **10.2.1 Initial cleaning**

**10.2.1.1** Using various wire brushes, dental picks and other tools, thoroughly clean the surface of the rock, removing any moss, lichen, dirt, or other organic matter.

### **10.2.2 Rock crushing**

**10.2.2.1** For all samples only the top 5-7 cm of the sample should be used. If the sample is thicker than this, trim off the lower part with a rock chisel or other necessary tools. This is usually necessary for lava flow samples. You will want to select a piece of the rock for thin section and grain size analysis. Preferably, this piece should not be taken from the surface and should be large enough for analysis (~1" x 1" x .5") (This is generally no problem with larger samples). If the sample is a composite, then no thin section is needed.

**10.2.2.2** Using a foxtail and/or compressed air, clean any box, table, or hammer that will be used in crushing the rocks.

**10.2.2.3** Place a piece of wax paper on the crushing surface.

**10.2.2.4** Place the thoroughly cleaned rock on the wax paper and, using a hammer, smash it into pieces of approximately 1-2 cm in size. Only crush enough to fill a small ziplock bag.

## **10.3 TEMA Mill: Grinding and Sieving**

### **10.3.1 TEMA Mill (Shatterbox)**

Final grinding of the sample should be done using a TEMA shatterbox or other similar machine. This machine consists of a circular metal case with a smaller hollow

metal circle and an inner solid piston. These inner circles shake around and crush the rocks.

**10.3.1.1** Clean the shatterbox vessel by grinding approximately 50 grams of OTTAWA quartz sand for 2 to 3 minutes, being sure to load some in each section of the vessel and that the rubber sealing gasket is in place. (The sound of the TEMA will change from a clanging sound to a high pitch, approximately 15-20 seconds).

**10.3.1.2** Place the vessel on the table and remove the inner piston and ring. Make sure the ventilation system is turned on. Dump this powder out and dispose of it and use compressed air to blow out any remaining material. Use alcohol and paper towel or lab paper to wipe the inside crushing surfaces. Do not use alcohol to wipe down the rubber O-ring. Make sure all surfaces are completely dry before adding sample. Use compressed air to dry if necessary.

**10.3.1.3** Set up the sieves so that the 1mm size sieve is on top, the 150 micron sieve is in the middle, with the pan underneath to collect the smallest fraction. The desired fraction is the one which rests between the 1mm sieve and 150 micron sieve.

**10.3.1.4** Load the TEMA vessel with the sample. Place the charge into the outer part of the vessel. A minimum “charge” for the TEMA is approximately 20 grams. Do not overfill the vessel, or it will not grind efficiently. Do not underfill the vessel or damage may occur. This takes practice. The sample will probably be ground in about 3-5 charges (for a typical 500g sample). Crush this sample briefly (approximately 3-15 seconds, depending on

rock type). Be careful not to overcrush as the sample becomes unusable if this happens.

**10.3.1.5** Dump this charge into the set of sieves and shake it briefly.

**10.3.1.6** Repeat these steps until all charges have been processed. Then take the largest size fraction from the sieve (the >1mm fraction) and recrush these briefly until the entire sample passes through the 1mm sieve. It may be useful to use scrap paper or wax paper to assist in transferring the fractions.

**10.3.1.7** If a sieve shaker is available, lace the entire set of sieves on the sieve shaker and allow it to shake for at least 10 minutes (or longer if possible). If not, then shake by hand for several minutes.

**10.3.1.8** Place the different size fractions into labeled Ziploc bags.

**10.3.1.9** Clean the vessel as described earlier between samples and before storing the vessel.

## **10.4 Leaching sample**

**The > 150-micron fraction of the sample should be leached in 3% nitric acid to remove meteoric chloride and secondary carbonate. If the sample material to be analyzed is carbonate, it should be leached in 18 MΩ DI water only and the carbonate procedure in section 6 should be followed.**

### **10.4.1 Sample leaching**

**10.4.1.1** Label large glass beakers (1 liter) (washed, then rinsed thoroughly in 18 MΩ DI water) with a permanent marker and transfer the ground samples to the beakers. If the samples are very large (i.e. greater than 300 g)

**you might consider using 2 separate beakers for the sample.**

**10.4.1.2 Add a volume of 3% HNO<sub>3</sub> about equal to the sample volume. (Add a very small amount of 3% nitric acid at first and note the reaction of the sample. Then add the rest to equal the sample volume). Stir the sample with a clean stir rod or swirl the sample around to assure that it is completely wetted. NOTE: Any bubbling behavior should be noted in your lab book (this is usually the result of a high concentration of carbonate in the rock sample and, if significant, may require a second leaching, or more). Safet note: Use all acid in the fume hood.**

**10.4.1.3 Directions on how to make acids: 3% nitric acid solution in a 1L container: Dilute 43mL stock (70%) nitric acid in a 1L container.**

**2.5 L container: Dilute 125 ml of stock 70% nitric in a 2.5L acid bottle. Use 18.2 MΩ DI water for dilution.**

**10.4.1.4 After stirring the sample, add additional 3% nitric acid equal to 3 - 4 times the sample volume. The acid should be added more slowly to samples that reacted or bubbled strongly when the first acid aliquot was added, in order to prevent bubbling over.**

**10.4.1.5 Stir each sample several times with a clean stir rod or swirl until the whole sample is wetted and cover the beaker with a clean watchglass.**

**10.4.1.6 The samples should be allowed to leach for 8 - 12 hours. If possible, stir the samples once or twice during leaching.**

**10.4.1.7 If a sample reacted particularly vigorously, add an additional small amount of**

**3% nitric acid about half way through leaching, in case the existing acid has been neutralized.**

## **10.4.2 Rinsing leached sample**

**10.4.2.1** When leaching is complete, carefully pour the solution, but not the sample, down the drain. **NOTE:** The fine powder on top can usually be rinsed down the drain. You typically just want the grains.

**10.4.2.2** Rinse the sample once with 18 M $\Omega$  DI water, pouring the rinse down the drain.

**10.4.2.3** After the first rinse, add a small volume of 3% nitric acid. If bubbling occurs, the sample will have to be leached again by following the steps in 3.1.

**10.4.2.4** For samples that do not react or bubble further, rinse the sample with a 1% sodium hydroxide (NaOH) solution. **Directions for making 1% NaOH solution:** Mix 10 g NaOH pellets with 18 M $\Omega$  DI water in a 1 L container, then swirl until dissolved.

**10.4.2.5** Add the NaOH in small (<10 mL) aliquots, stirring thoroughly between additions, until the pH of the solution is at least 7 (use pH paper). **NOTE:** You may want to only add one aliquot of 30-40ml of NaOH, and then small (~10 ml) aliquots until the pH of 7 is reached. Stir thoroughly between additions.

**10.4.2.6** Let stand for 10-30 minutes. Decant the NaOH down the drain, and then rinse the sample in 18 MΩ DI water 3 - 4 times (or more) until the pH is around 5 or 6 (neutral).

**10.4.2.7** Cover the beakers with watchglasses and place the rinsed samples in the oven until dry. This may take 12 hours to 3 days depending on the size of the sample and the temperature of the oven. Most dry in less than 24 hours. You do not want the sample to boil. If possible, stir the samples once or twice with a clean stir rod at some point during the drying process.

### **10.4.3 Weigh and bag samples**

**10.4.3.1** Remove the dried samples from the oven and allow them to cool.

**10.4.3.2** If the sample size allows, place about 30 grams of sample (obtained using the "cone and quarter" technique, see section 3.5) in a labeled whirlpack bag. This sample will later be ground in the TEMA mill to a fine powder for analysis by XRF, PGES, and total Cl. Put the rest of the sample in an additional labeled whirlpack bag.

**10.4.3.3** XRF needs a minimum of 1 gram but would like to have 3. PGES analysis of B and Gd as well as the XRF for U and Th (XRAL lab) needs a minimum of 6 grams but would like to have 12. Total Cl requires just a few milligrams, but it is nice to have 3 to 5 grams. So, set aside 30-40 grams if the sample size is large enough, otherwise all that you think you can spare, keeping the above minimum values in mind.

### **10.4.4 Cone and quarter technique**

**10.4.4.1** Dump the sample onto a clean piece of wax paper, forming a cone shaped pile.

**10.4.4.2** Mark the cone shaped pile with a clean spatula or scoopula dividing it into approximately equal quarters.

**10.4.4.3** Remove your sample from one of the quarters so as to have a general mix of the entire sample, not just what's on top.

**10.4.5 Grinding sample in TEMA mill for chemical analysis**

**10.4.5.1** Rinse an appropriate number of 20 ml scintillation vials and small glass vials with 18 MΩ DI water. (Usually 2 scintillation vials and 1 small glass vial per sample). Dry the vials in the oven at an appropriate temperature.

**10.4.5.2** Clean the TEMA Mill as described above. Add the entire sample (the 30 grams that was labeled to grind for analysis) to the clean vessel and grind until the sound changes from a clanking sound to a high pitched sound (~15s). The sample should now be a very fine powder.

**10.4.5.3** Weigh approximately 15 grams into one of the scintillation vials (for PGE and NAA), 5 grams into the other (for XRF) and place the remainder into a labeled small whirlpack or other bag (for total Cl). When transferring into the vials use the "cone and quarter" technique (section 3.5).

**10.4.5.4** Send these samples to other labs for XRF total element analysis, B and Gd PGES analysis, and XRF for U and Th.

***10.5 Determination of approximate chlorine concentration***

In this procedure an approximate total chlorine concentration is determined using a specific ion electrode in order to calculate the size of sample to be processed and the amount of <sup>35</sup>Cl carrier to be added. The

dissolution of the sample is accomplished by placing a small amount of sample in the outer ring of the Teflon cell and a reducing solution in the inner ring of the Teflon cell. An oxidizing solution is then placed in the outer ring of the cell being careful that the oxidizing solution and sample do not make contact until the lid has been securely placed on the cell. The equilibrium concentration of chlorine in the middle solution is measured and the concentration of chlorine in the sample (ppm in the rock) is computed using Labcalcs.

## **10.5.1 Cleaning the Teflon diffusion cells (two step process)**

**10.5.1.1 First solution: combine 300 ml (concentrated)  $\text{H}_2\text{SO}_4$  with 10.5 ml of saturated  $\text{K}_2\text{Cr}_2\text{O}_7$  solution in a 600 ml acid washed beaker. The  $\text{K}_2\text{Cr}_2\text{O}_7$  solution should be put in the beaker first, and then the acid should be added SLOWLY. This solution is dark brown when first prepared, and can be used until it becomes green.**

**10.5.1.2 Put the first solution on the hotplate until it is too hot to touch (~ 1/2 hour at a setting of 7 or 8, or high). When this is hot enough remove it from the hotplate and fill each diffusion cell with the hot solution until the center ring is completely covered. Place the lids on the cells. Make sure to keep the lids with their cells because the lids fit uniquely. While holding the lids on, invert the cells back and forth several times, then place them under the hood right side up and leave for 10-15 minutes. (NOTE: the lids fit easier if you place them on each cell immediately after filling the cell)**

**10.5.1.3 Second solution: heat 300 ml of stock (OK)  $\text{HNO}_3$  in a 500 ml beaker on the hotplate as above. When it is close to boiling, add 50 ml of  $\text{H}_2\text{O}_2$ . Add the hydrogen peroxide very slowly to prevent boil over.**

**10.5.1.4 Empty the first solution back into the beaker and rinse the cell and lid in 18 M $\Omega$  DI water very thoroughly. Place this rinse in a separate waste container.**

**10.5.1.5 After all the cells have been emptied and rinsed, fill each cell with the second solution, making sure the center ring is covered completely. While holding the lid on, invert**

each cell several times and place on the hood floor right side up for 10-15 minutes.

**10.5.1.6** Dump the second solution out of the cell into the beaker. When finished with all the cells, place the second solution in a waste container.

**10.5.1.7** Rinse each cell thoroughly in 18 M $\Omega$  DI water. Place the cells on a piece of clean lab paper on the counter.

### **10.5.2** Preparing the oxidizing and reducing solutions

**10.5.2.1** Reducing solution: Add 5.8 g of KOH pellets to a tared 50mL plastic test tube with a lid. Retare. Add 0.29 g of Na<sub>2</sub>SO<sub>3</sub> to the mixture. Retare. Add 31 g of 18 M $\Omega$  DI water. Replace the lid, shake the solution and put aside.

**10.5.2.2** Oxidizing solution: Use a 100-ml Teflon beaker. Place it on the balance and tare. Add 0.4 g of KMnO<sub>4</sub>. Retare. Carefully add 5.6 g of 18 M $\Omega$  DI water, trying to rinse the sides of the beaker as you do. Place the beaker on the orbital shaker. Add 1.85 ml of 50% H<sub>2</sub>SO<sub>4</sub>. Turn the shaker on and leave it for a few minutes. Remove the beaker and place it under the hood. Carefully add 32 ml of HF to the Teflon beaker. Make sure to measure the HF in the plastic graduated cylinder.

### **10.5.3** Loading the Cells (Do not turn on the hood!)

**10.5.3.1** Conditioning cell: The first cell is used to condition the electrode so it should have no sample loaded.

**10.5.3.2 Standards:** Standards are used to calibrate the electrode and determine a slope from which the concentration of the samples can be determined. The number and concentration of standards run with each sample set depends on the concentration of Cl in the samples. For complete unknowns, run a 10 ppm, 100 ppm, 250 ppm and a 500 ppm liquid standard. Note: Standards should be remade fresh every 3-4 months.

*10.5.3.2.1 Measure 0.2000 g ( $\pm 0.0004$  g) of standard solution into the outer ring of the diffusion cell and record the exact mass. The standard solution should form a bead in the outer ring of the cell.*

*10.5.3.2.2 Prop the cell on the hood shelf with the bead of standard on the uphill side. (You want to prevent premature mixing with oxidizing solution)*

**10.5.3.3 Samples:** Place the lid on the stainless hood shelf and place the diffusion cell on the balance. Write down the empty cell weight and tare the balance. Using an 18 M $\Omega$  DI water rinsed and dried spatula, add 0.2000 g ( $\pm 0.0004$  g) of leached, powder sample to the outer ring. With the spatula, spread the sample over ~160 degrees in the outer ring, and then record the exact final mass. Place the cell on the hood shelf with the sample on the uphill side.

**10.5.3.4 Adding Solutions:** When all of the standards and samples have been loaded, put 2.5 ml of reducing solution into the inner ring of the diffusion cells using an automatic pipette. Then, measure 3 ml of oxidizing solution into the downhill part of the outer ring using a Teflon dropper or other plastic dropper. You

**do not want the oxidizing solution to come into contact with the sample.**

**10.5.3.5 Shaker:** Place the lids on the cells and carefully place all of the cells on an orbital shaker, checking the lids occasionally by pressing down on them to make sure they are sealed properly. Tighten the bars, recheck the lids, set the speed of the orbital shaker ~ 100rpm and shake the cells for 16 to 20 hours. Mark the start time and date.

**10.5.3.6 Finally:** Using 18 M $\Omega$  DI water in the squeeze bottle, rinse the Teflon beaker containing the oxidizing solution and automatic pipette tip into the HF waste bucket. Place them both on the counter to dry. Dump any leftover reducing solution down the drain.

#### **10.5.4 Cl determinations**

We currently use a portable Beckman meter and an Orion model 96-17BN combination chloride electrode. It is important to remember that this method will only give an estimate of the total chloride present, which is sufficient for determining the amount of sample needed to be dissolved. AMS/IDMS is used for the actual chloride analysis.

**10.5.4.1 Preparation:** Locate the meter, specific ion electrode, and the electrode stand. Place the meter near a sink. **NOTE:** Wear gloves to prevent possible chloride contamination from the salts and oils on your hands.

*10.5.4.1.1 Remove the black protective cover on the tip of the electrode and rinse the outside of the electrode with 18 M $\Omega$  DI water.*

*10.5.4.1.2 Fill the inside of the electrode with 18 M $\Omega$  DI water and push down on the top of the*

*electrode allowing the water to drain out.  
Repeat.*

*10.5.4.1.3 Using the correct filling solution, fill the electrode about 1/2 full and push down on the top of the electrode allowing the solution to drain out.*

*10.5.4.1.4 Refill the electrode with filling solution about 3/4 full. Then, holding the electrode with both hands and your thumbs on either side of the top (white cap) press down firmly at the same time letting both thumbs slip off the cap allowing it to "snap" back quickly, thus sealing in the solution.*

*10.5.4.1.5 Refill the electrode with filling solution to about 1/2 inch below the fill hole.*

*10.5.4.1.6 Cover the fill hole with a gloved finger and rinse the outside of the electrode thoroughly with 18 M $\Omega$  DI water. Shake it off approximately 3 times using a quick flick of the wrist. Carefully wipe or blot up any water still adhering to the side of the probe being careful not to touch the tip of the electrode.*

*10.5.4.1.7 Check the tip of the electrode for any air bubbles or drops of water that may interfere with the readings, being careful not to invert the electrode. If air bubbles are present, repeat 10.5.4.1.3.*

*10.5.4.1.8 Place the electrode in the rack arm of the stand.*

**10.5.4.2 Electrode conditioning: Turn the orbital shaker off and note the time in your lab book. Carefully retrieve the conditioning cell and place it on the hood shelf. Open the lid of the cell and using 18 M $\Omega$  DI water in a squeeze bottle rinse the lid into the HF waste bucket. Use the fume hood for these steps.**

*10.5.4.2.1 Using a small Teflon/disposable plastic dropper carefully remove the droplets on the separation ring between the inner and outer portions of the cell, placing the removed droplets in the HF waste bucket.*

*10.5.4.2.2 With the small Teflon dropper, pipette off the purple solution in the outer ring and place in the HF waste bucket. Run the dropper around the outer wall of the inner ring and the inner wall of the outer ring removing any adhering droplets of the purple solution*

*10.5.4.2.3 Carefully rinse the outer ring of the cell with 18 M $\Omega$  DI water and pipette this solution off. Make sure not to get any small droplets of water in the center solution.*

*10.5.4.2.4 Carefully tip the cell until the solution in the inner ring is close to the top of the inner ring and rotate the cell allowing the solution to collect any adhering drops on the inner portion of the separation ring and incorporate them into the inner solution.*

*10.5.4.2.5 Carefully move the cell to the counter and place the electrode in the inner ring conditioning solution. The electrode should not touch the bottom of the cell, but should be completely immersed in solution. The electrode should be conditioned for 15-30 minutes (whenever the reading is stable after 15 minutes).*

**10.5.4.3 Determinations:** When the time is almost up for the conditioning cell, take the next cell off the shaker and move it to the hood. Rinse the lid and remove the purple solution as described above. (The procedure for standards and samples are the same). **NOTE:** The chlorine is in the inner reducing solution and the mass needs to be accurately measured.

*10.5.4.3.1 Remove the purple solution and rinse the cell as described above.*

*10.5.4.3.2 Take the cell to the balance and weigh it to determine the total mass.*

*10.5.4.3.3 While this cell is on the balance, take the final reading from the conditioning cell and **\*write it down\*** on the Cl log sheet or in a lab notebook.*

*10.5.4.3.4 Rinse the electrode in 18 M $\Omega$  DI water and dry with a small piece of lab paper.*

*10.5.4.3.5 Retrieve the cell from the balance, being sure to **record the final mass of the cell.***

*10.5.4.3.6 Place the electrode in the center solution as before.*

*Retrieve the next cell from the orbital shaker and repeat the process until all cells have been done being sure to **write the stable reading down before removing the electrode.** NOTE: Be consistent with the time between readings (i.e. the amount of time the sample or standard is exposed to the atmosphere (evaporation)).*

## **10.5.5 Calculation of Cl content**

**10.5.5.1 CHLOE:** On the input page fill in the appropriate data concerning the sample name and location. Also fill in the information received from XRF concerning major elements,

**U and Th. Also fill in the elevation, latitude and longitude information. On the shielding page fill in any appropriate information concerning shielding, if required. The ppm of Cl is determined using "Lab Calcs" (Sect. 4.5.3 part 4.5.3.1).**

*10.5.5.1.1 Go to the "theoretical" page of CHLOE, enter the estimated exposure age of the sample, and write down the estimated  $^{36}\text{Cl}/^{35}\text{Cl}$  ratio (R/S ratio) that is calculated by CHLOE.*

## **10.5.5.2 Saving the worksheet**

*10.5.5.2.1 On the input sheet of CHLOE select the "save data" button. A screen titled "Use the following workbook" will appear.*

*10.5.5.2.2 You will be prompted to "Open another workbook" or "Create a new workbook". If a workbook already exists that is appropriate for the sample you can open it by single clicking on "Open another workbook" and then selecting the workbook that you want to open from its location. Otherwise, create a new workbook by single clicking on "Create a new workbook". A screen will appear prompting the user to enter a title. Title the workbook so as to be able to readily identify it should you need to reopen it at a later date. Single click OK.*

*10.5.5.2.3 On the "Use the following workbook" screen, select the "down" arrow and then the name of the workbook you just created. Single click OK.*

*10.5.5.2.4 A "Enter name of sheet" screen will appear. Enter a name for the sheet. (Usually the sample name and number will automatically appear. This was entered in the Sample ID,*

Name box on the input sheet of CHLOE). Select OK and the workbook will be saved.

10.5.5.2.5 To Import data from a previously saved workbook, single click "Import data", select the down arrow if the workbook is already open, otherwise select open a workbook, and select the workbook from the location it is stored at. Select the sheet or sample that you wish to import data for. Single click OK.

**10.5.5.3 LABCALCS: On the FINAL MASS page, fill in the appropriate boxes concerning the ppm of the standards, initial and final masses and millivolt readings. Do the same for the samples.**

10.5.5.3.1 Try to select standards that are on either side of the sample in question by selecting and deselecting the appropriate boxes next to each. Observe the ppm concentration of each sample and record the appropriate concentration for each. (Also, look at the bottom of the graph and record the  $R^2$  value)

**10.5.5.4 On the SPIKE addition page: at the top of the page fill in the box concerning ppm concentration and the box concerning estimated  $^{36}\text{Cl}/\text{Cl}$  ratio (obtained from CHLOE). Read the information included on the side of the charts.**

10.5.5.4.1 The values highlighted in **green** meet all the constraints and will most often be used though they are not necessarily optimal for that parameter.

10.5.5.4.2 The values highlighted in **red** do not meet the constraints.

10.5.5.4.3 Basically, first you want the Stable/Stable ratio (S/S) to be above 3 (but under 100). Second, you want to maximize the

*<sup>36</sup>Cl/Cl ratio (R/S). Third, maximize the AgCl mass recovered, preferably at least 10 mg.*

## **10.6 Chloride extraction for $^{36}\text{Cl}$ analysis**

**10.6.1 Initial sample dissolution (For carbonates, follow the alternate procedure listed in section 10.8.1).**

**10.6.1.1 Large (1 liter) Teflon bottles are used for the initial stages of sample dissolution for most samples. Before using, these need to be rinsed in  $\text{NH}_4\text{OH}$ , 18 M $\Omega$  DI water, hot  $\text{HNO}_3$ , then thoroughly rinsed in 18 M $\Omega$  DI water.**

**10.6.1.2 The amount of sample dissolved and spike used will depend on the sample composition and age. Use the LabCalcs Excel Workbook to determine the appropriate masses of rock to dissolve and spike to add and record this information.**

**10.6.1.3 Exactly weigh the appropriate amount of sample into the Teflon bottle using the cone-and-quarter technique (section 10.4.4). Record the sample weight in your logbook. Add 18 M $\Omega$  DI water at a ratio of 1:1 with the sample weight. Swirl the sample.**

**10.6.1.4 Exactly weigh the amount of spike determined from the LabCalcs program into an acid-washed 10-ml plastic beaker. Record the mass, concentration, and the identification code of the spike in your lab book. Add the spike to the sample and rinse the beaker several times with 18 M $\Omega$  DI water, adding the rinse to the sample. Swirl the sample.**

**10.6.1.5 Prepare a cold water bath for each sample so that the following reaction can be slowed if it begins to proceed too rapidly.**

**(NOTE: All of the remaining steps in this section must be performed under the hood) HF is a very hazardous weak acid and caution should be exercised when using. Pay**

particular attention to inhalation of vapors and any spills and splashes should be cleaned up immediately. Always wear appropriate clothing including lab coat, goggles, and gloves when using HF.

**10.6.1.6** In a Teflon separatory funnel measure and add HNO<sub>3</sub> at a ratio of 1:2 of the sample weight (volume to weight), and add HF in a 2½:1 ratio to the sample weight. Add both solutions to the funnel and then drip them into the Teflon bottle containing the sample. This solution needs to be dripped into the Teflon bottle slowly because of the possibility of violent reaction with silicates. Position the separatory funnel and Teflon bottle so that the water bath may be added if needed. Example: For a 50g sample, add 25mL of 70% Nitric acid and 125mL of Hydrofluoric acid.

**10.6.1.7** Swirl the samples often. If lots of bubbling takes place, or if a bottle becomes hot enough for the Teflon to soften, place the bottle in the cold water bath for a few minutes. The drip rate must be very slow initially, but can be speeded up as more solution is added (watch the temperature). The drip rate may also depend on the sample type; i.e. the solution may need to be added to granite samples more slowly.

**10.6.1.8** Once all of the solution has been dripped into the samples, cap the bottles and then loosen the caps approximately 1/4 turn. Place the Teflon bottle on a hot plate under the hood at a low setting (the hot plate should be warm to the touch but not hot). Repeat this process for each sample. The dissolution may take as long as 48 to 72 hours but should be checked every 12 hours or so. The samples should be swirled periodically. Some samples dissolve overnight.

**10.6.1.9** If silica gel deposits on the walls of the bottle add an additional 10-20 ml aliquot of HF, depending on the sample size. Swirl the samples after the addition of HF.

**10.6.2 Separation of Cl from dissolved rock by precipitation of AgCl**

**10.6.2.1** After complete dissolution, transfer the solution and solid into 250-ml Teflon bottles that have been cleaned as described above for 1 liter bottles.

**10.6.2.2** Centrifuge the bottles at ~2500 rpm for at least 10 minutes.

**10.6.2.3** Decant the solution into a Teflon beaker that has been cleaned as described above for 1 liter bottles. NOTE: if the sample is small; transfer to a clean labeled 250 ml Teflon bottle instead of a Teflon beaker.

**10.6.2.4** Add 10 ml of 0.2 M  $\text{AgNO}_3$  to the solution in the Teflon beaker, or bottle, using an acid washed 10-ml beaker (this doesn't have to be exact). Cover the Teflon beakers with Teflon covers or loosely cap the bottles, place on a warm hot plate, and leave for approximately 12 hours (overnight). Longer if solution is not heated.

**10.6.3 Purification of AgCl**

**10.6.3.1** Transfer the solution and precipitate into 250-ml Teflon bottles, that have been cleaned as described above, and centrifuge each bottle. Transfer the liquid from the 250 ml bottles into an HF waste bucket and the precipitate into acid washed 50-ml centrifuge tubes, using 18 M- $\Omega$  DI water to facilitate the transfer.

- 10.6.3.2** Balance the tubes using 18 M- $\Omega$  DI water and cover with parafilm or cap. Centrifuge for at least 10 minutes at approximately 2000 rpm.
- 10.6.3.3** Decant the solution into the HF waste bucket used previously. Rinse the samples in 18 M- $\Omega$  DI water, balance the tubes, cover with parafilm, and centrifuge again.
- 10.6.3.4** Decant the water down the drain in the sink. Add enough  $\text{NH}_4\text{OH}$  (a few ml) to dissolve the white powder sample containing the  $\text{AgCl}$  (Strange looking precipitate may form here). Add the  $\text{NH}_4\text{OH}$  a small amount at a time, swirling the tube after each addition. Do not add more than you need to dissolve the powder. NOTE: you may need to use an acid washed, glass stir rod on some samples to assure that the chloride is in solution. All the chloride may be in solution even if all of the solid does not dissolve.
- 10.6.3.5** Balance the tubes using  $\text{NH}_4\text{OH}$ , cover with parafilm, and centrifuge for at least 10 minutes.
- 10.6.3.6** Decant the liquid containing the chloride into another 50-ml glass centrifuge tube (DO NOT USE PLASTIC TEST TUBES FOR THIS STEP!) that has been cleaned as described above. Add concentrated  $\text{HNO}_3$  slowly from the squeeze bottle (CAUTION: reaction may be violent at first) until  $\text{AgCl}$  precipitate begins to form (liquid turns milky white). The tube should be about  $\frac{1}{2}$  full when completed. Balance the tubes using  $\text{HNO}_3$  and let stand for 1-2 hours if time allows. Cover with parafilm and centrifuge for at least 10 minutes.
- 10.6.3.7** Decant the solution into a waste beaker being careful not to lose any precipitate. When

finished decanting all test tubes, dump the waste solution down the drain with the faucet running.

**10.6.3.8** Rinse the sample in 18 M- $\Omega$  DI water, balance, and centrifuge again.

#### **10.6.4 Sulfur removal**

**10.6.4.1** Pour off the solution and, as described in step 5.3.4, add enough  $\text{NH}_4\text{OH}$  to dissolve the  $\text{AgCl}$  sample (a few ml). Balance the tubes using  $\text{NH}_4\text{OH}$ , then add 1 ml of  $\text{Ba}(\text{NO}_3)_2$ , to precipitate  $\text{BaSO}_4$ . Cover the tubes with parafilm and leave the solution for at least 8 hours. (24 to 48 hours is preferable for the initial sulfur removal step if time allows).

**10.6.4.2** Centrifuge the sample for at least 10 minutes at approximately 2000 rpm (longer centrifuge times sometimes aids in removal of the solution). Carefully remove the solution with a clean glass pipette. (The pipettes should be rinsed in dilute nitric and then 18 M $\Omega$  DI water). If the “clump” of precipitate in the bottom of the tube begins to come apart, re-centrifuge the sample. Eventually it will stay in one coherent mass in the bottom of the tube. The solution may be placed in a 10 ml test tube that has been cleaned as described above if the sample is small, otherwise use 50-ml test tubes.

**10.6.4.3** Add enough  $\text{HNO}_3$  to precipitate  $\text{AgCl}$ , (CAUTION: reaction may be violent at first) balance the tubes using  $\text{HNO}_3$ , and cover with parafilm. Let stand for 2 hours, then centrifuge and pour off the acidic solution (down the drain). Rinse the  $\text{AgCl}$  sample in 18 M- $\Omega$  DI water and centrifuge again. If the sample is suspected of having a high sulfur content,

repeat the procedure 1-3 times. More times may be necessary if the sulfur content is extremely high. ( $^{36}\text{S}$  is an isobar of  $^{36}\text{Cl}$  and interferes with AMS analysis)

**10.6.4.4** When all the sulfur has been removed, rinse the sample (AgCl precipitate at this point) at least 3 times in 18 M- $\Omega$  DI water, centrifuging each time. The pH of the final solution should be about 7. Store the clean sample in 18 M- $\Omega$  DI water in a tightly covered test tube (parafilm) in a dark place until it needs to be sent away; however, drying the sample and packaging it for shipping is preferred (section 5.5).

#### **10.6.5 Preparation for shipping**

**10.6.5.1** Make sure all possible water has been decanted. Cover each test tube with a labeled piece of aluminum foil. Place the permanent marker-labeled test tubes in a glass beaker. Place samples in the oven for ~24 hours at a temperature of ~60 degrees Celsius.

**10.6.5.2** Send the finished samples to an AMS facility of your choosing, either wrapped in weigh paper or in a vial, depending on the current procedures at the AMS facility.

### **Alternate Procedures for Carbonates**

#### **10.7 Carbonate - Leaching sample**

##### **10.7.1 Sample leaching**

The > 150-micron fraction of the sample should be leached in 18 M $\Omega$  DI water.

**10.7.1.1** Label large glass beakers with permanent marker and transfer samples to beakers. Find

watch glasses to cover the beakers, and place in the hood.

**10.7.1.2** Add a volume of 18 MΩ DI water about equal to the sample volume. Swirl or stir (with a clean glass stir rod) the sample around until it is completely wetted.

**10.7.1.3** Add a volume of 18 MΩ DI water equal to 3-4x sample volume. Mix each sample several times, and cover beaker with a watchglass.

**10.7.1.4** The samples should be allowed to leach for about 8-12 hours. If possible, stir the sample once or twice during leaching.

**10.7.1.5** When leaching is complete, pour solution down drain and rinse sample several times with 18 MΩ DI water.

**10.7.1.6** Place rinsed samples in the drying oven for 6 -12 hours. The beakers should be covered with watchglasses. You do not want the sample to boil. If possible, stir the samples once or twice with a clean stir rod at some point during the drying process. At the same time, rinse one small, glass, black topped vial and one larger plastic vial with 18 MΩ DI water (only rinse the bottles, do not rinse the lids). Place these in the oven to dry.

## **10.8 Chloride extraction for <sup>36</sup>Cl analysis of Carbonates**

### **10.8.1 Initial sample dissolution**

**10.8.1.1** Large (4 liter) HDPE bottles are used for the initial stages of sample dissolution for carbonate samples. Before using, these need to be cleaned according to procedures outlined in “Teflon and glassware cleaning procedures”.

**10.8.1.2** The amount of sample dissolved and spike used will depend on the sample composition and age. Use the LabCalcs Excel Workbook to determine the appropriate masses of rock to dissolve and spike to add (Section 10.5.5.4).

**10.8.1.3** Exactly weigh the appropriate amount of sample into the 4L bottle using the cone-and-quarter technique and label the bottle twice, once with lab tape and once with a permanent marker. Record the sample weight in your log book. Add 18 M-Ω de-ionized water at a ratio of 2:1 with the sample weight. Swirl the sample.

**10.8.1.4** Weigh the appropriate amount of spike into an acid-washed 10-ml beaker. Record the mass, concentration, and the identification code of the spike in your lab book. Add the spike to the sample and rinse the beaker several times with de-ionized water, adding the rinse to the sample also. Swirl the sample.

**10.8.1.5** Clean small Teflon beakers (inside and out) using the procedure outlined above. These beakers must be small enough to fit through the opening of the 4L bottles used for the samples.

**10.8.1.6** (NOTE: All of the remaining steps in this section must be performed under the hood) Determine the total volume of acid required to dissolve the mass of carbonate in your sample. [You need a mole-to-2-mole ratio of carbonate to acid, e.g., 100 g or 1 mole of  $\text{CaCO}_3$  per 126 g or 2 mole of  $\text{HNO}_3$ .] For 50 g of carbonate, you need a total of 64 g of nitric. Also, this amount of acid must be placed in as small a container as possible so it should only be diluted after being placed in the larger container.

- 10.8.1.7** Place the acid calculated in the previous step into the small Teflon container and place this filled container into the 4L bottle with the sample, making sure not to spill any. Dilute the acid if necessary.
- 10.8.1.8** Place a household garbage bag around the mouth of the bottle and secure with a one or two large rubberbands tightly around the bottle lip. Make sure most of the air is out of the bag prior to its placement.
- 10.8.1.9** With the hood turned on, place a gloved hand into the sample bag, using the garbage bag as a second glove (but try not to get acid on the bag). Grab the small beaker, and flip it completely over, allowing the acid to react with the sample. Slowly remove your hand from the sample container being careful not to disturb the seal.
- 10.8.1.10** Once all the solution has finished reacting initially, swirl the sample. Repeat this process for each sample until acid has been added to all the samples. Let the samples stand until they are completely dissolved and come to equilibrium (approximately 3 days). The samples should be swirled periodically.
- 10.8.1.11** Remove the garbage bag from the sample bottle and carefully remove the Teflon beaker, rinsing it into the sample bottle with 18MΩ DI water.

## 11 APPENDIX 4: OTHER NUCLIDE DATA

Table 23- Original data from other laboratories for chlorine-36, helium-3, and beryllium-10. All results are shown in ka. The Phillips/Marrero data (no erosion) is shown for comparison. The Helium-3 analysis was performed at the Isotope Geochemistry Facility, under the supervision of Mark Kurz, at Woods Hole Oceanographic Institute. The Be-10 data is from the anonymous intercalibration study by CRONUS. The CRONUS Web calculator (BALCO, 2007) was used to calculate the results of the Be-10 data and the Lal (not time dependent) scaling was reported along with the external uncertainty. Be Lab 3 was not used in any analysis because the results were anomalous and probably due to incorrect calculation of age by the laboratory.

Source	Nuclide	05TAB01	05TAB02	05TAB03	05TAB04	05TAB05	05TAB06	05TAB07
Phillips/Marrero (run 1)	<sup>36</sup> Cl	18.2±0.6	16.5±0.7	15.8±0.7	18.0±0.0.7	13.1±0.6	22.1±0.7	14.0±0.8
Phillips/Marrero (run 2)	<sup>36</sup> Cl	17.7±0.8	17.5±0.6	16.6±0.7	17.9±0.9	16.9±0.6	15.6±0.6	14.7±0.6
Zreda	<sup>36</sup> Cl	19.0 ±1.5	16.6±1.5	14.8±0.9	18.9±1.5	18.9±2.3	21.5±4.4	16.9±1.5
Kurz	<sup>3</sup> He	17.6±0.3	17.1±0.4	17.4±0.3	17.7±0.3	17.9±0.3	18.2±0.4	17.4±0.3
Source	Nuclide	05PPT01	05PPT02	05PPT03	05PPT04	05PPT05	05PPT08	
Phillips/Marrero (run 1)	<sup>36</sup> Cl	14.7±1.2	19.4±0.8	22.9±3.7	17.1±1.2	18.9±1.5	13.9±1.2	
Phillips/Marrero (run 2)	<sup>36</sup> Cl	17.4±1.0	16.4±0.8	11.8±0.8	16.6±1.2	14.9±0.9	13.5±0.8	
Be lab 1	<sup>10</sup> Be	17.8±1.6	16.3±1.5	18.9±1.7	17.1±1.6	18.4±1.7	19.7±1.8	
Be lab 2	<sup>10</sup> Be	17.0±1.6	16.7±1.5	19.0±1.7	17.6±1.6	16.8±1.5	18.7±1.7	
Be lab 4	<sup>10</sup> Be	17.0±1.5	17.1±1.5	18.4±1.7	16.9±1.5	18.4±1.7	18.3±1.6	

## 12 APPENDIX 5: BLANK INFORMATION

**Table 24-Blank data for blanks run with the CRONUS samples. The R/S ratio is the Cl-36/total chloride ( $\times 10^{-15}$ ) and the S/S ratio is the Cl-35/Cl-37 ratio. Both the R/S and S/S are from the PRIME Lab. The blanks are labeled with the month and year they were started (BS0805 was the Blank Sample from August of 2005).**

Name	R/S	R/S Uncertainty	S/S	S/S Uncertainty
BS0805	14.2	2.9	4.098	0.009
BS0907	7.17	1.49	5.9110	0.0418
BS0107	11.37	2.73	4.7300	0.8212

**Table 25-Composition of Week's Island Halite solution from the analysis done by Thomas (2005). All values shown are in ppm.**

Weeks Island Halite	Cl	SO <sub>4</sub>	Na	Ca	Al	B	Cu
<i>Average</i>	69.7	0.27	45.3	0.011	0.014	0.075	0.002